MICROCOPY RESOLUTION TEST CHART

NATIONAL BUREAU OF STANDARDS-1963-A

REPORT DOCUMENTATION PAGE	READ INSTRUCTIONS BEFORE COMPLETING FORM
1. REPORT NUMBER 2. GOVT ACCESSION NO. Technical Report E-85-12 AD-A164392	RECIPIENT'S CATALOG NUMBER
4. TITLE (and Subtitle) ENTRAINMENT DESCRIPTIONS FOR MATHEMATICAL MODELING OF PUMPED-STORAGE INFLOWS IN RESERVOIRS	TYPE OF REPORT & PERIOD COVERED Final report 6. PERFORMING ORG. REPORT NUMBER
7. AUTHOR(s) Philip J. W. Roberts, Mark S. Dortch	8. CONTRACT OR GRANT NUMBER(s) Contract Nos. DACW39-81-M-2771, DACW39-82-M-3273
9. PERFORMING ORGANIZATION NAME AND ADDRESS Georgia Institute of Technology, School of Civil Engineering, Atlanta, Georgia 30331 and US Army Engineer Waterways Experiment Station, Hydraulics Laboratory, PO Box 631, Vicksburg, Mississippi 39180-0631	10. PROGRAM ELEMENT, PROJECT, TASK AREA & WORK UNIT NUMBERS CWIS No. 31593; EWQOS Work Unit IA.5 12. REPORT DATE October 1985
11. CONTROLLING OFFICE NAME AND ADDRESS DEPARTMENT OF THE ARMY US Army Corps of Engineers Washington, DC 20314-1000	13. NUMBER OF PAGES 118 15. SECURITY CLASS. (of this report)
14. MONITORING AGENCY NAME & ADDRESS(if different from Controlling Office) US Army Engineer Waterways Experiment Station Environmental Laboratory PO Box 631, Vicksburg, Mississippi 39180-0631	Unclassified 15a. DECLASSIFICATION DOWNGRADING SCHEDULE

16. DISTRIBUTION STATEMENT (of this Report)

Approved for public release; distribution unlimited.

DTIC
SELECTE
FEB 1 4 1986
E

17. DISTRIBUTION STATEMENT (of the abstract entered in Block 20, if different from Report)

18. SUPPLEMENTARY NOTES

Available from National Technical Information Service, 5285 Port Royal Road, Springfield, Virginia 22161.

19. KEY WORDS (Continue on reverse side if necessary and identify by block number)

Entrainment,
Inflow jets.
Mathematical models.
Pumped-storage reservoirs.

20. ABSTRACT (Continue on reverse side if necessary and identify by block number)

During hydropower generation and pumpback operations of pumped-storage projects, inflows are introduced into the reservoir system. These jetlike inflows often cause considerable entrainment of ambient water. The entrainment process can have a strong influence on the vertical distribution of reservoir water quality when pumped-storage inflow jets are discharged into a stratified reservoir. The objective of this study was to develop algorithms
(Continued)

DD FORM 1473   EDITION OF 1 NOV 55 IS OBSOLETE

20. ABSTRACT (Continued)

to describe the pumped-storage inflow entrainment process for use in reservoir water quality models. Pumped-storage inflow jets fall into two classes: strongly or weakly buoyant. The former class has been fairly extensively studied, and well-established mathematical models exist to predict their behavior. For this case, incorporation into a reservoir thermal model simply required adaptation of existing code. For the latter case, however, that of weakly buoyant jets, it was found that little information existed of either a theoretical or experimental nature. For that reason, an extensive series of experiments of a fundamental nature were performed on weakly buoyant jets into arbitrary stratification. The results were then reduced to a form suitable for inclusion into reservoir water quality simulation models. The developed algorithms were incorporated into an existing reservoir thermal simulation code, and a test application was made for Carters Lake, a Corps of Engineers pumped-storage project in Georgia.

PREFACE

The study reported herein was sponsored by the Office, Chief of
Engineers (OCE), US Army, as part of the Civil Works General Investiga-
tions, Environmental and Water Quality Operational Studies (EWQOS) Pro-
gram, under the work unit (CWIS No. 31593) entitled "Develop and Verify
Techniques for Describing Pumpback Mixing in Reservoirs." The EWQOS
Program is assigned to the US Army Engineer Waterways Experiment Station
(WES) under the management of the Environmental Laboratory (EL). The
OCE Technical Monitors for EWQOS were Mr. Earl E. Eiker, Dr. John Bush-
man, and Mr. James L. Gottesman.

The study was conducted during the period October 1980 to December
1983, principally by Dr. Philip J. W. Roberts of the School of Civil
Engineering, Georgia Institute of Technology (Ga. Tech). Mr. Reid
Matthews, a graduate student at Ga. Tech, conducted the experiments.
Mr. Mark S. Dortch, WES, directed the effort and was responsible for
the mathematical model modifications and applications. This report was
written by Dr. Roberts and Mr. Dortch. Through 21 May 1983, Mr. Dortch
was in the Hydraulics Structures Division (HSD) of the Hydraulics Labora-
tory (HL) under the general supervision of Mr. J. L. Grace, Jr., Chief,
HSD, and Mr. H. B. Simmons, Chief, HL. On 22 May 1983, Mr. Dortch be-
came Chief, Water Quality Modeling Group, Ecosystems Research and Simu-
lation Division (ERSD), EL, under the general supervision of
Mr. Donald L. Robey, Chief, ERSD, and Dr. John Harrison, Chief, EL.
Dr. Jerome L. Mahloch was Program Manager, EWQOS. The report was edited
by Ms. Jessica S. Ruff of the WES Publications and Graphic Arts Division.

During the preparation of this report, COL Tilford C. Creel, CE,
and COL Robert C. Lee, CE, were the Commanders and Directors of WES.
At the time of publication, COL Allen F. Grum, USA, was Director and
Dr. Robert W. Whalin was Technical Director.

This report should be cited as follows:

Roberts, P. J. W., and Dortch, M. S. 1985. "Entrainment
Descriptions for Mathematical Modeling of Pumped-Storage
Inflows in Reservoirs," Technical Report E-85-12, US Army
Engineer Waterways Experiment Station, Vicksburg, Miss.

1

CONTENTS

2

ENTRAINMENT DESCRIPTIONS FOR MATHEMATICAL MODELING
OF PUMPED-STORAGE INFLOWS IN RESERVOIRS

PART I: INTRODUCTION

Background

1. Pumped-storage (PS) hydropower is a well established means of
storing large amounts of energy for subsequent power generation. Pumped-
storage projects pump water to an upper reservoir during periods of low
energy demand when power can be bought at a reduced price. The water
stored in the upper reservoir is later released during periods of peak
power demand to generate high-value power.

2. Prior to construction of a PS project, the impact of the proj-
ect upon existing water quality should be assessed. The PS inflows and
outflows cause mixing that can significantly alter thermal stratifica-
tion and the water quality parameters within the reservoir. Conse-
quently, distributions within the reservoir affect the temperature and
quality of downstream releases. The effect of PS inflows is well demon-
strated by the temperatures observed at Allegheny Reservoir, Pa., for
pre- and post-PS hydropower (Dortch 1981).

3. Comprehensive modeling of PS projects necessitates simulation
of a complex dual reservoir and/or riverine system. The quality of in
situ and release water from conventional reservoirs is dependent upon
meteorology, hydrology, internal mixing processes, morphometry, regu-
lating structures, and operational methodology. The PS system is more
complex. One of the reservoirs of a PS system is usually much larger
than the other and normally goes through a thermal stratification cycle,
whereas the smaller reservoir usually does not stratify vertically.
Relatively large amounts of water are passed between the two reservoirs
during generation and pumpback, thus causing mixing and redistribution
of thermal and water quality characteristics.

4. When the PS flow enters the larger stratified reservoir

3

(Figure 1), a jet is often produced that entrains ambient water. The
entrained ambient water combines with the entering flow and causes an
increase in the volume flux of the jet. Density stratification of the
ambient pool eventually causes the jet to collapse and change into a
tranquil density current without additional entrainment. This entrain-
ment process can significantly alter the temperature (Figure 2) and
water quality parameters in the water column. Previous studies (i.e.
Dortch 1981) have demonstrated that the entrainment description can be
one of the most important inputs to a PS reservoir simulation model.
Therefore, adequate entrainment descriptions are necessary for realistic
models of PS projects.
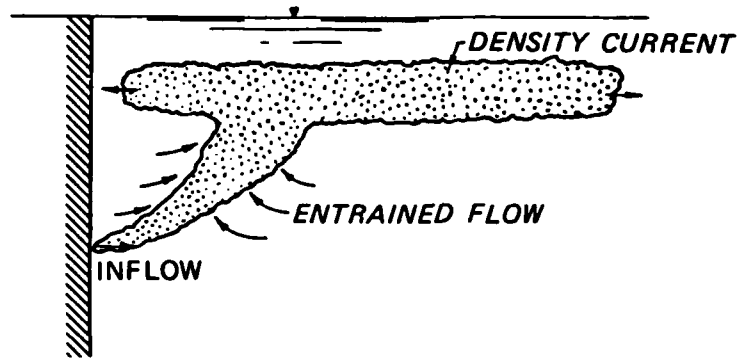
Figure 1.   Schematic of pumped-storage inflow jet
and entrainment

Past Experience

5.   A hybrid technique has been used successfully at the US Army
Engineer Waterways Experiment Station (WES) to model PS hydropower proj-
ects on a variety of existing and proposed PS projects including
Richard B. Russell Reservoir (Smith et al. 1981, Fontane and Bohan
1974), Marysville Lake (Fontane et al. 1977, Dortch 1978), Dickey-
Lincoln School Lakes (Dortch et al. 1976), and Kinzua Reservoir (Dortch
1981). This approach employs a one-dimensional (1-D) (vertical) reser-
voir simulation model that includes algorithms for the pumped-storage
mixing process. The algorithms were developed on a site-specific basis
from observed PS inflow characteristics produced in physical models.
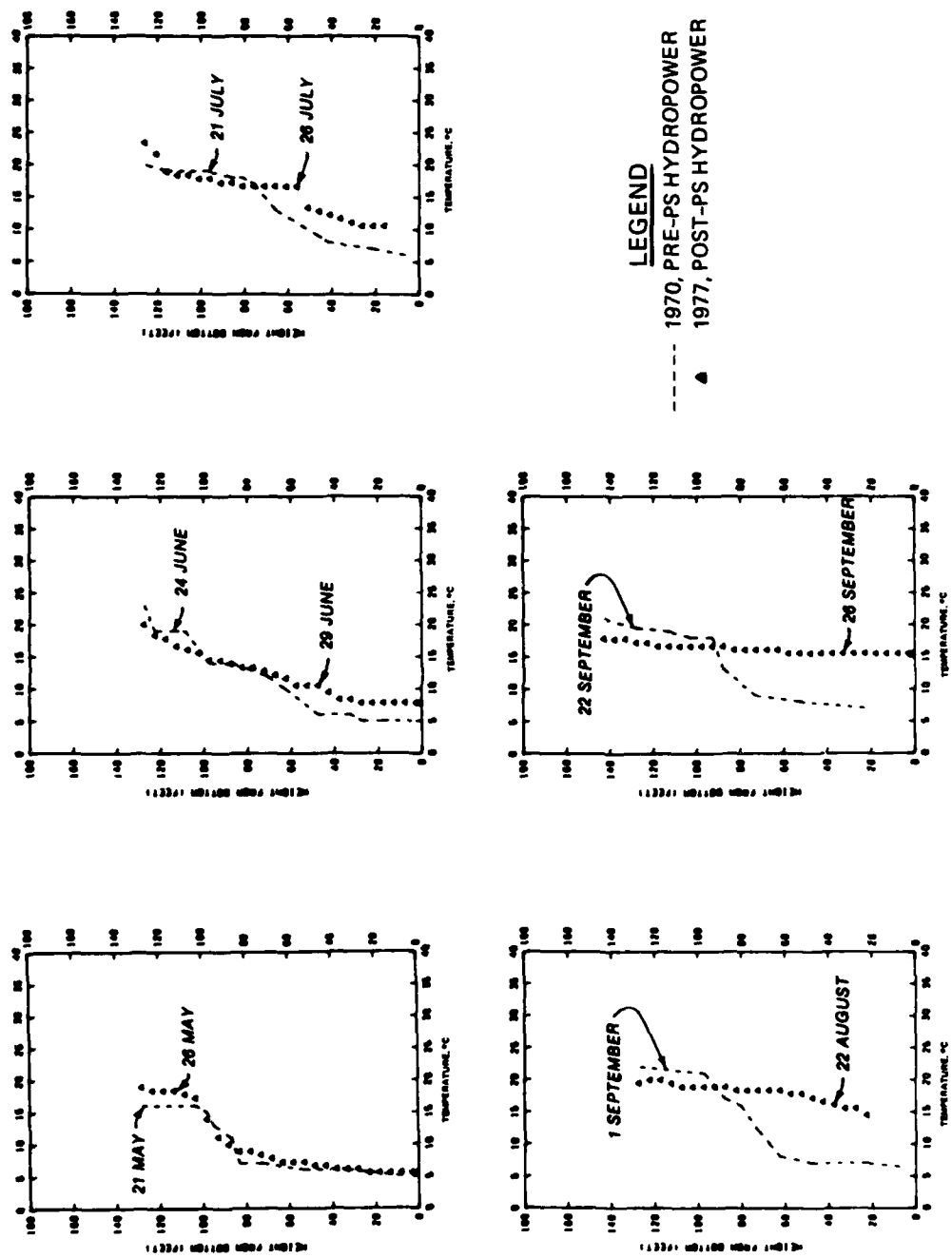
Figure 2. Observed temperature profiles, Allegheny Reservoir

6. The primary information obtained from physical models regarding PS inflows was the entrainment description. The entrainment description prescribes the total entrainment rate E (as a multiple of inflow rate) and the vertical distribution of entrained flow $Q_e(z)$. These parameters were obtained from the physical model for a typical set of flow and stratification conditions, and the values were used throughout the numerical simulations. This procedure did yield fairly accurate temperature simulations, as demonstrated by Figure 3 from the Allegheny Reservoir Study (Dortch 1981).

7. However, the entrainment parameters are actually not constant over a simulation period. These parameters are dependent upon the source geometry, buoyancy, momentum, and volume flux and the ambient stratification. Therefore, entrainment can vary from day to day at a particular project for different stratification and flow conditions. The temperature distribution is certainly influenced by the entrainment description, but the simulated distribution has been found to be mildly sensitive to variations in the entrainment parameters, especially E. For example, for the Allegheny Reservoir Study, the temperature results were found to be relatively insensitive to variations in E of up to about 50 percent. However, it was important to use the correct proportions of entrainment from the epilimnion and hypolimnion. Other parameters that are less continuous in the water column than temperature may be more sensitive to the prescribed amount of entrainment and dilution.
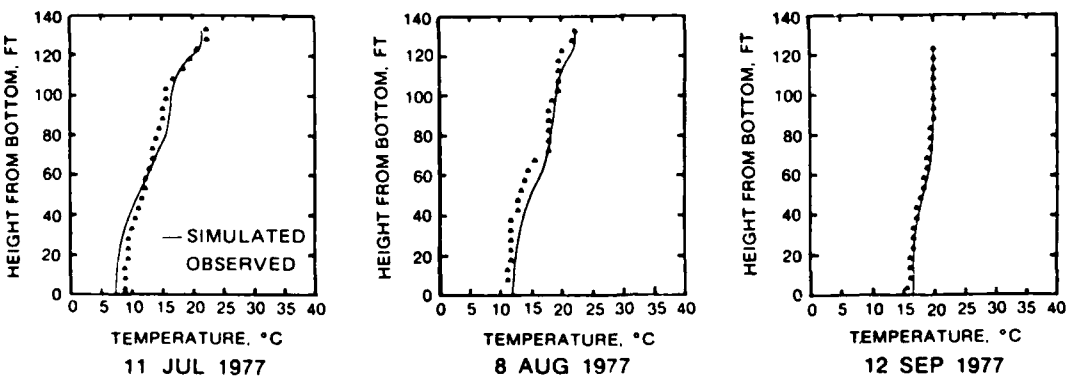
Figure 3. Comparison of simulated and observed temperature profiles at Allegheny Reservoir (Note: 1 ft = 0.3048 m)

6

Thus, for reservoir water quality simulations of PS projects, it seems desirable, if not necessary, to have entrainment algorithms that are functionally dependent on time-varying flow and stratification conditions.

Purpose and Scope of Study

8. The purpose of this work was to develop general-purpose algorithms to predict the entrainment parameters for varying types of PS inflows with varying conditions. The algorithms had to fit into the framework of 1-D reservoir water quality models, such as CE-QUAL-R1 (Environmental Laboratory 1982). It should be realized that general-purpose entrainment algorithms cannot be used for every project without some adjustments. For example, local topography and unusual source geometries can influence entrainment and mixing. In such instances, the hybrid (physical-numerical models) approach discussed earlier is recommended either to select and/or calibrate the most appropriate entrainment descriptions or, if necessary, to develop alternate descriptions. In either case, a general-purpose algorithm is more expedient for defining the appropriate description.

9. Following a literature study by Roberts (1981), it was concluded that existing jet models could be used to describe most of the highly buoyant types of PS inflows that might be encountered. However, little or no information was available for the prevailing cases of weak buoyancy. Pumped-storage inflow often takes the form of a jet of fairly high momentum but small buoyancy discharging into a density-stratified ambient. There are few experimental data available on this class of jet flows. As part of this study, a comprehensive series of experiments on jet configurations typical of PS inflows was performed. These include horizontal and inclined jets of neutral or small positive or negative buoyancy discharging into stratified ambients. These experiments and the resulting algorithm for weakly buoyant jets are described herein.

10. Along with the weakly buoyant jet algorithm, a jet model for strongly buoyant' inflows was selected and incorporated into the 1-D reservoir simulation code. In addition to the discussions of the weakly

and strongly buoyant jet algorithms, the 1-D modeling approach for PS projects is discussed, and application results are presented.

8

PART II: MODELING FRAMEWORK

11. Mathematical models have been used in the past (Dortch et al. 1976, Dortch 1981, Holland et al. 1982) to simulate thermal stratification and release temperatures in PS (as well as conventional) reservoirs. Previous studies had indicated that for PS reservoirs, the PS inflow was a dominant mixing process. Therefore, these models, which included natural stratifying and mixing mechanisms such as surface heat inputs, inflow, outflow, wind mixing, and internal diffusion, were modified to include mixing mechanisms for PS operations.

12. A 1-D (vertical) reservoir thermal simulation code (WESTEX), which was developed by WES, was modified to account for PS inflows and entrainment. The code also allows simulation of an afterbay, which often is a part of a PS project. The larger, stratified reservoir of the system is conceptualized as a number of homogeneous horizontal layers stacked vertically, and the heat sources and sinks to a general layer are represented as shown in Figure 4. If a dual-reservoir system is used, then the other reservoir must be modeled, too. In all previous studies, the smaller reservoir was not expected to stratify; thus, fully mixed conditions were used to budget heat and water.

13. The solution for the temperature history of a general layer is obtained through conservation of mass and energy and an equation of state for density as a function of temperature. The energy equation is stated as:

$$\frac{\partial \theta_L}{\partial t} = \frac{\theta_i Q_i}{A_L \Delta z} - \frac{\theta_L Q_o}{A_L \Delta z} + \frac{1}{A_L} \frac{\partial}{\partial z} \left(DA_L \frac{\partial \theta_L}{\partial z} \right) - \frac{1}{A_L} \frac{\partial (Q_v \theta_L)}{\partial z}$$

$$+ \frac{1}{\rho C_p A_L} \frac{\partial H}{\partial z} + \frac{\theta_p Q_p}{A_L \Delta z} - \frac{Q_e \theta_L}{A_L \Delta z} \qquad (1)$$

where

θ_L = temperature of layer, deg

t = time, T

θ_i = inflow temperature, deg

9

Q_i = tributary flow rate into layer, L^3/T

A_L = horizontal area of layer, L^2

Δz = layer thickness, L

Q_o = outflow rate from layer for reservoir releases, L^3/T

z = elevation, L

D = vertical diffusion coefficient, L^2/T

Q_v = net vertical flow into or out of layer, L^3/T

ρ = density of water, M/L^3

C_p = specific heat of water, $\dfrac{\text{heat energy}}{\text{degrees} \cdot M}$

H = external heat source (surface heat exchange H_s and short wave penetration H_i), heat energy/T

θ_p = pumped-storage inflow temperature including entrainment, deg

Q_p = pumped-storage layer inflow rate after all entrainment, L^3/T

Q_e = pumped-storage layer entrained flow rate, L^3/T
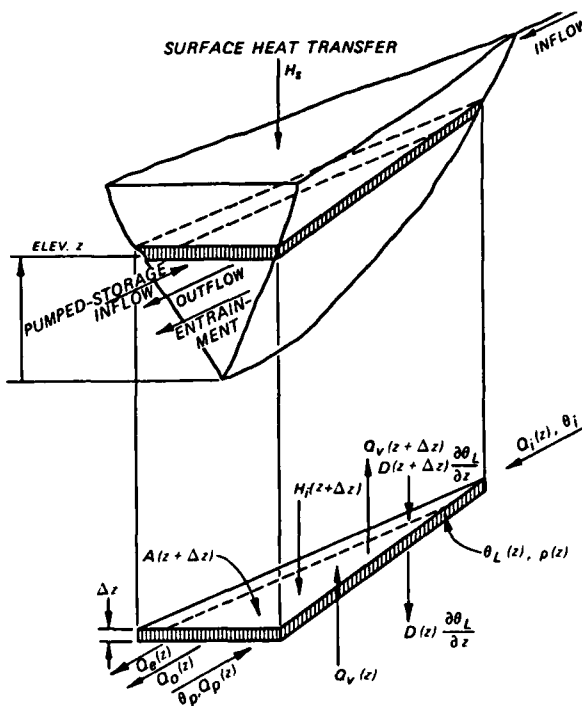
Figure 4. Typical layer of 1D model

10

An equation similar to Equation 1 would exist for each water quality constituent.

14. The pumped-storage inflow Q_p is the sum of entrained flow $Q_e(z)$ from all layers and the PS initial jet inflow rate Q_j. The PS inflow temperature θ_p is a flow-weighted average of the inflow jet at its temperature and all the entrainment flows at their respective layer temperatures. The temperature of the inflow jet is obtained from the heat budget of the afterbay or the smaller reservoir of dual-reservoir systems.

15. The entrained flow is treated as withdrawal of specified amounts from specified layers. It is important to realize that entrainment withdrawal results in vertical flows downward. The PS inflow, Q_p, is handled in the same manner as the upstream inflow; it is placed into the layer of neutral, or closest to neutral, buoyancy. The inflows cause vertical upward flow. The entrainment distribution and rate, which are affected by source geometry, buoyancy, volume, and momentum fluxes and ambient stratification, must be specified. The total entrained flow rate, Q_E, can be expressed in terms of the jet volume flux through a total entrainment coefficient, E,

$$Q_E = EQ_j = \sum_{\text{all layers}} Q_e(z) \tag{2}$$

resulting in

$$Q_p = (1 + E)Q_j \tag{3}$$

If the shape of the entrainment distribution is known or specified, the entrained flow to be withdrawn from each layer ($Q_e(z)$) can be determined.

16. A daily time step for the simulations has been found to be adequate. However, the PS inflow rates must be used to obtain entrainment flows that are functionally dependent on momentum and volume fluxes. Additionally, outflow rates are required to predict the withdrawal zone. Since PS hydropower outflow and inflow rates can vary significantly during a daily time step, actual release and pumpback rates should be used with the durations of these flows to account for changes in daily water budget.

11

PART III: JET-INDUCED ENTRAINMENT

Introduction

17. In a literature survey of methods of predicting entrainment in the types of jets expected in PS reservoirs, Roberts (1981) identified 16 possible jet configurations that could arise. Of these, some had been well studied and were well understood, and some had not been studied at all. Subsequently, it was decided to investigate further the types of jets that would be expected to occur most often in PS reservoirs. These are horizontal or inclined discharges of positive, negative, or neutral buoyancy into an arbitrarily stratified environment. Even with this broad range of variables it was found that the jets fell into two classes: strongly or weakly buoyant. The former class has been fairly extensively studied, and well-established mathematical models exist to predict their behavior. For this case, incorporation into a reservoir thermal model simply required adaptation of an existing code. However, for weakly buoyant jets, it was found that little information existed of either a theoretical or experimental nature. For that reason an extensive series of experiments of a fundamental nature were performed on weakly buoyant jets discharged into arbitrary stratification. The results were then reduced to a form suitable for inclusion into reservoir simulation models.

18. The development of the algorithms for predicting jet-induced entrainment is outlined in the following sections. First, the general problem is discussed and analyzed by dimensional and length scale arguments, and criteria for separation into weakly and strongly buoyant jets are presented. Next, the algorithms for predicting strongly buoyant and weakly buoyant jet dynamics are presented. Also, the results of the experiments on weakly buoyant jets (discussed in detail in Appendix A) are summarized, and the empirical formulas used to incorporate the results into the reservoir thermal model (WESTEX) are presented. Finally, the approach is summarized, and flowcharts for the entrainment subroutines are given.

12

Analysis

19. The problem under consideration is shown in Figure 5. A jet inclined upwards at an angle θ to the horizontal discharges into a stagnant reservoir of arbitrary stratification denoted by $\rho(z)$, where ρ is water density as a function of vertical position z. The jet entrains ambient water as it rises or falls and may eventually reach a height at which its density is equal to that of the ambient water. Near this height, the jet collapses vertically and intrudes as a horizontally flowing density current. This study was particularly concerned with the amount of flow entrained into the jet and the vertical distribution of the entrained flow. Because of the large number of parameters involved and the arbitrary shape of the ambient density profile, an unreasonably large number of dimensionless parameters and experiments would be needed to describe all possible situations. The problem can be made tractable, however, by making some simplifying assumptions for the ambient stratification, which when combined with judicious dimensional analysis will yield results of an accuracy consistent with modeling requirements.

20. The idealized problem is shown in Figure 6. A jet of area A is discharged at an angle θ into a stagnant ambient fluid. The ambient stratification is characterized by a well-mixed surface layer separated by a density jump of magnitude $\Delta\rho$ from a linearly stratified lower layer. This stratification is an idealization of that occurring in reservoirs. The idealized problem incorporates several other problems. For example, the density interface, if strong enough, approximates a nearby solid boundary. If the interface is far removed from the jet, it has no effect, and the flow is the same as that induced in a completely linear stratification. By linearizing the ambient stratification over the extent of jet influence, the results for linear stratification can be used; this approximation will be utilized later.

21. The problem is analyzed by dimensional and length scale arguments in Appendix A (Analysis section). It is shown that the problem can be characterized by the relative magnitudes of five length scales that can be formed from the parameters involved. These length scales

13
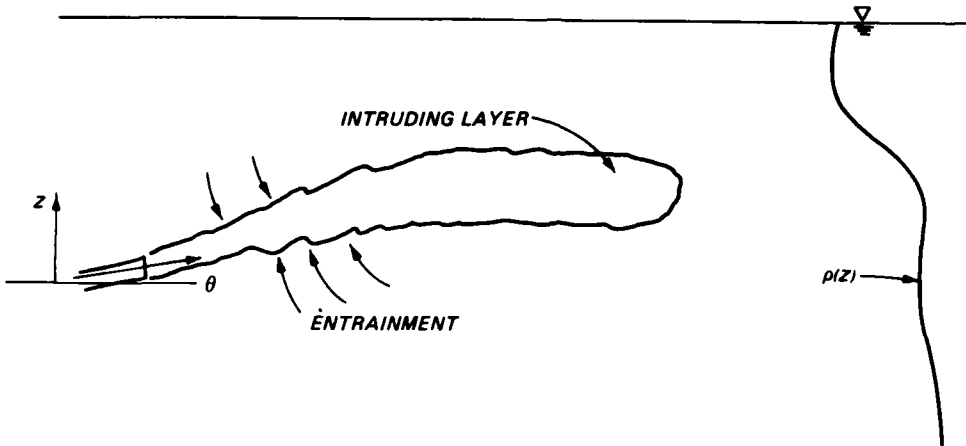
Figure 5.   Generalized problem
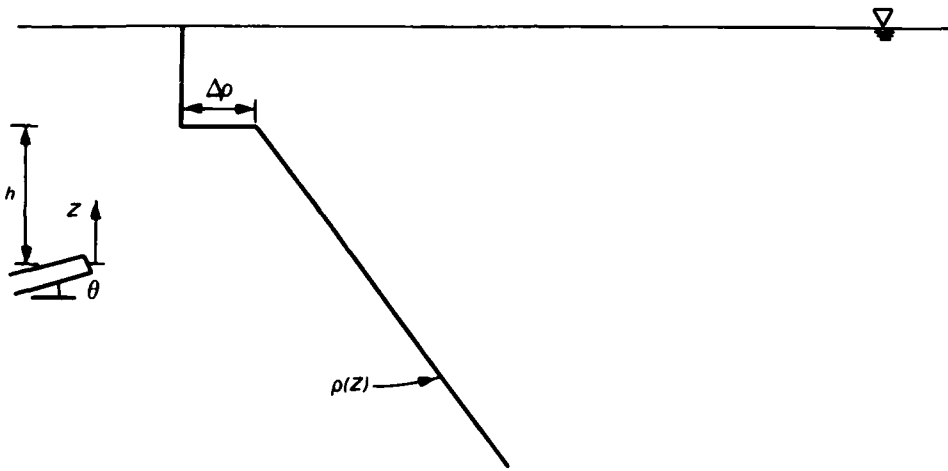
Figure 6.   Idealized problem

$(\ell_Q, \ell_M, \ell_\varepsilon, \ell_\Delta)$ and   h , and their physical significances, are discussed in Appendix A.

22.   Consider first the case where   h , the jet submergence below the interface, is much larger than the other length scales, i.e., $h \gg \ell_Q$, ℓ_M , ℓ_ε , ℓ_Δ .   In this case, the jet and its extent of influence are far removed from the interface, and the presence of the interface should not affect the flow field.   The only length scales are

14

now ℓ_Q , ℓ_M , and ℓ_ε . If ℓ_Q is not large relative to ℓ_M or ℓ_ε , the nozzle geometry should exert only a secondary influence on the flow field and not affect its gross characteristics (Wright 1977b). This leaves only ℓ_M and ℓ_ε , which characterize the relative effects of the ambient stratification and the buoyancy and momentum fluxes. If $\ell_M \ll \ell_\varepsilon$, then the effects of the source momentum flux are confined to the region near the nozzle. The flow is predominantly buoyancy driven, similar to that of a sewage discharge in a stratified ocean. On the other hand, if $\ell_M \gg \ell_\varepsilon$, the buoyancy is small and the flow is momentum dominated. For the former case ($\ell_M \ll \ell_\varepsilon$), mathematical (integral) models have been developed and applied (Koh and Brooks 1975). These models break down, however, as ℓ_M/ℓ_ε becomes large, and there is little information available on these flow types.

23. It is shown in Appendix B (see Figure B2) that the following ranges apply: for $\ell_M/\ell_\varepsilon <$ ~0.8 , the flow is buoyancy dominated, i.e. plumelike; for $0.8 < \ell_M/\ell_\varepsilon < 2$, both momentum and buoyancy are important; and for $\ell_M/\ell_\varepsilon > 2$, the momentum is dominant. The integral models work reasonably well so long as momentum does not dominate; therefore, they are proposed for the PS modeling when $\ell_M/\ell_\varepsilon < 2$. The adaptation of the integral models to WESTEX is described in the following section. For $\ell_M/\ell_\varepsilon \geq 2$, the experimental studies that were performed as part of the present effort (described in Appendix A) are used. The adaptation of these experimental results to WESTEX is described in paragraphs 34-38.

Strongly Buoyant Jets

Integral buoyant jet model

24. These jets are defined as having $\ell_M/\ell_\varepsilon < 2$. Several models have been used to predict these flows; the well-established model of Fan and Brooks (1969) and Koh and Fan (1970) are used here. The formulation of this model is described in Appendix C.

Adaptation of integral buoyant jet model to reservoir thermal model

25. The integral buoyant jet model requires several modifications

15

for use in a thermal model for a PS reservoir. These include choice of
nozzle size, choice of model coefficients, and prediction of the en-
trained flow distribution. These adaptations are discussed below. No
assumptions on linearity of the density profile are required, as the
model will accommodate arbitrarily shaped ambient density profiles. The
integral buoyant jet model, as adapted to the reservoir simulation code,
is referred to as subroutine SBJET (Strongly Buoyant JET).

26. Fan and Brooks' model assumes a round nozzle and a radially
symmetric flow field around the trajectory of the jet center line. For
a noncircular nozzle, the flow field will not be radially circular near
the discharge. However, as discussed in Appendix A, for distances from
the nozzle much longer than its characteristic size, the nozzle size
will not explicitly affect the flow field. At this point, the flow
field will be radially symmetric. Therefore, we can approximate the
flow as being equivalent to one discharged from a round nozzle with the
same momentum and buoyancy fluxes as the noncircular nozzle. This re-
quires that the equivalent round nozzle has the same cross-sectional
area A , as the actual nozzle, or:

$$\ell_Q = \sqrt{A} \tag{4}$$

and
$$d = \sqrt{\frac{4A}{\pi}} \tag{5}$$

where d is nozzle diameter. These approximations are used in SBJET.
In practice, the approximations will be better the closer the discharge
is to being round. Thus, a square nozzle would be a better approxima-
tion to the equivalent round nozzle than would be a long slot.

27. Use of the integral model requires specification of the en-
trainment coefficient α and turbulent Schmidt number λ (see Appen-
dixes B and C). It is well known that the entrainment coefficient of a
plume is greater than that of a jet, and that the entrainment coeffi-
cient of a jet which makes a transition to a plume will vary along its
trajectory. The entrainment coefficient will increase, being close to
that of a jet near the nozzle and approaching that of a plume far away.

16

The values of the two coefficients are given in Appendix B, Equations B21 and B22. For PS reservoir jets, the density differences are small, and it is unlikely that the flow will ever approach that of a plume. The momentum will usually dominate, and so it is appropriate to use jet entrainment coefficients. (For further discussion of this, see Appendix B.) Therefore, α from Equation B21 is:

$$\alpha = 0.0535 \tag{6}$$

The term λ is the same for jets and plumes; the value is given by Equation B23 as:

$$\lambda = 1.2 \tag{7}$$

28. The most difficult adaptive problem is the specification of the vertical distribution of entrained volume flux into the jet, essential for use in a reservoir simulation model. This problem has received almost no discussion in the literature; the experiments performed as part of the present studies (Appendix A) are apparently the first in which the entrained flow rate and its vertical distribution have been directly measured. These experiments do not cover the more buoyant jets for which the integral model is used, however, and some assumptions are necessary to predict the distribution.

29. The entrainment into the jet is given by the well-known assumption (Equation C6 and Table C1) that the entrained flow velocity is proportional to the local jet center-line velocity. For a round jet, that is:

$$\frac{dQ}{ds} = 2\pi\alpha ub \tag{8}$$

where

   Q = jet volume flux, L^3/T

   s = distance along jet trajectory, L

   u = local jet center-line velocity, L/T

   b = local jet half-width, L

17

30. It is assumed that the flow is entrained uniformly around the jet perimeter. The method of solution for the jet in SBJET is a numerical space integration proceeding along the trajectory outwards from the nozzle. The length of the step is specified in the program as DS . The flow entrained during one integration step from each model layer into the jet is therefore proportional to the fraction of the total jet perimeter lying in that layer. This is illustrated in Figure 7, where it is assumed that the jet radius r is proportional to two standard deviations of the assumed Gaussian distribution of velocity

$$r = C_w \ \sqrt{2}b \qquad (9)$$

where C_w is a constant specified by the user.
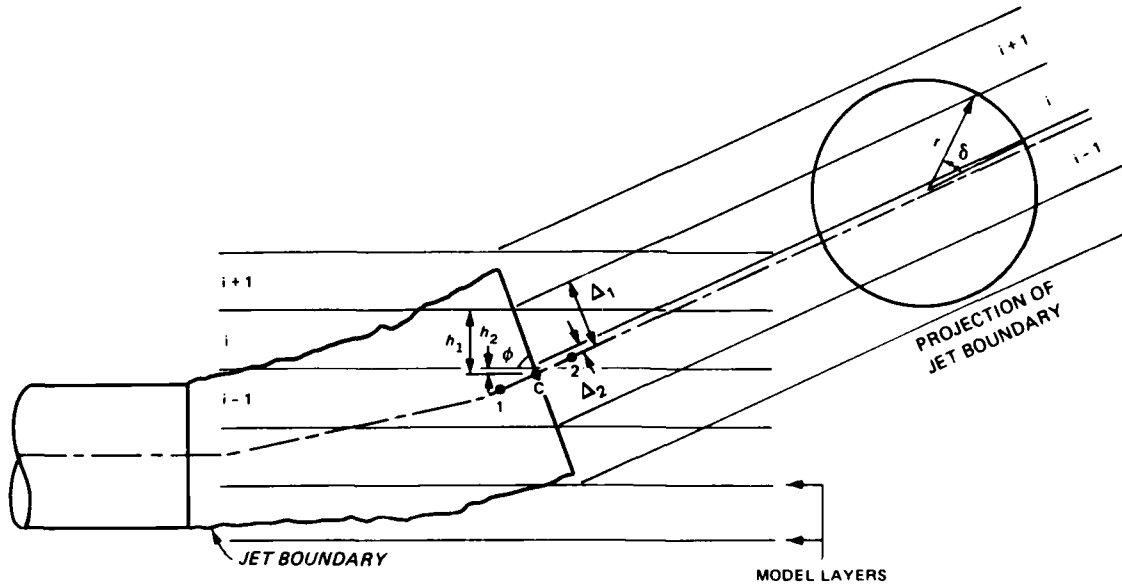
Figure 7. Method for predicting entrained flow distribution from integral buoyant jet model

31. Consider the ith model layer. The intersection of the jet perimeter subtends an angle δ (denoted by ALPHA in SBJET) at the center. The perimeter P of the jet contained within layer i is:

$$P = 2\delta r \qquad (10)$$

18

and the entrainment from layer i $[q_e(i)]$ is

$$q_e(i) = \frac{P}{C} Q_{ep} \tag{11}$$

where Q_{ep} is the total entrainment around the jet perimeter (see Appendix C) and C is the jet circumference $2\pi r$. From the geometry shown in Figure 7, the following relationships can be shown:

$$\delta = \sin^{-1}\left(\frac{\Delta_1}{r}\right) - \sin^{-1}\left(\frac{\Delta_2}{r}\right) \tag{12}$$

$$\Delta_1 = \frac{h_1}{\sin\phi} \tag{13}$$

$$\Delta_2 = \frac{h_2}{\sin\phi} \tag{14}$$

32. To evaluate $q_e(i)$ from Equation 11, the total entrainment Q_{ep} and the local geometry of the jet must be known. These are computed within SBJET as shown in Appendix C. The numerical solutions of the equations in Appendix C are performed in SBJET by integrating forward in space along the jet trajectory from, for example, point 1 to point 2 in Figure 7. The coordinates of the disk center for this space step are given by

$$x_c = \frac{x_1 + x_2}{2} \tag{15}$$

and

$$y_c = \frac{y_1 + y_2}{2} \tag{16}$$

and ϕ by

$$\phi = \tan^{-1}\frac{x_2 - x_1}{y_2 - y_1} \tag{17}$$

19

x_1 , x_2 , y_1 , and y_2 and the volume entrained are computed at each space step.

33. The entrained flow distribution for each layer is computed for each space step by Equations 10-17 and added to those computed in the previous step. This is continued until the terminal rise height of the jet is reached. The procedure is shown in the flowchart, Figure 8.

Weakly Buoyant Jets

Experimental study

34. Weakly buoyant jets are defined as those having $\ell_M/\ell_\varepsilon \geq 2$. The extensive experimental program to investigate these jets is described in Appendix A. Adaptation of these results to the thermal model is discussed below.

Adaptation to reservoir thermal model

35. The experiments performed on weakly buoyant jets were of a fundamental nature, and some adaptations of these results were necessary to put them in a form suitable for a reservoir thermal simulation model. In the experiments, several parameters were measured, including the total volume flux entrained into the jet. For the present purpose, however, it is more convenient to fit an empirical equation to the measured distribution of volume flux into the jet. The parameters of the equation are chosen to maintain consistency between the total measured flux and that computed from the empirical distribution.

36. The basic equation is (Equation A56):

$$\frac{q_e}{M^{1/2}} = \frac{q_{em}}{M^{1/2}} \exp\left[-\left(\frac{\eta - \eta_o}{b}\right)^2\right] \tag{18}$$

where

q_e = the entrained flow rate per unit depth

$\eta = z/\ell_\varepsilon$, the nondimensional height

η_o = parameter to account for asymmetry of entrained volume flux distribution about the jet axis

20
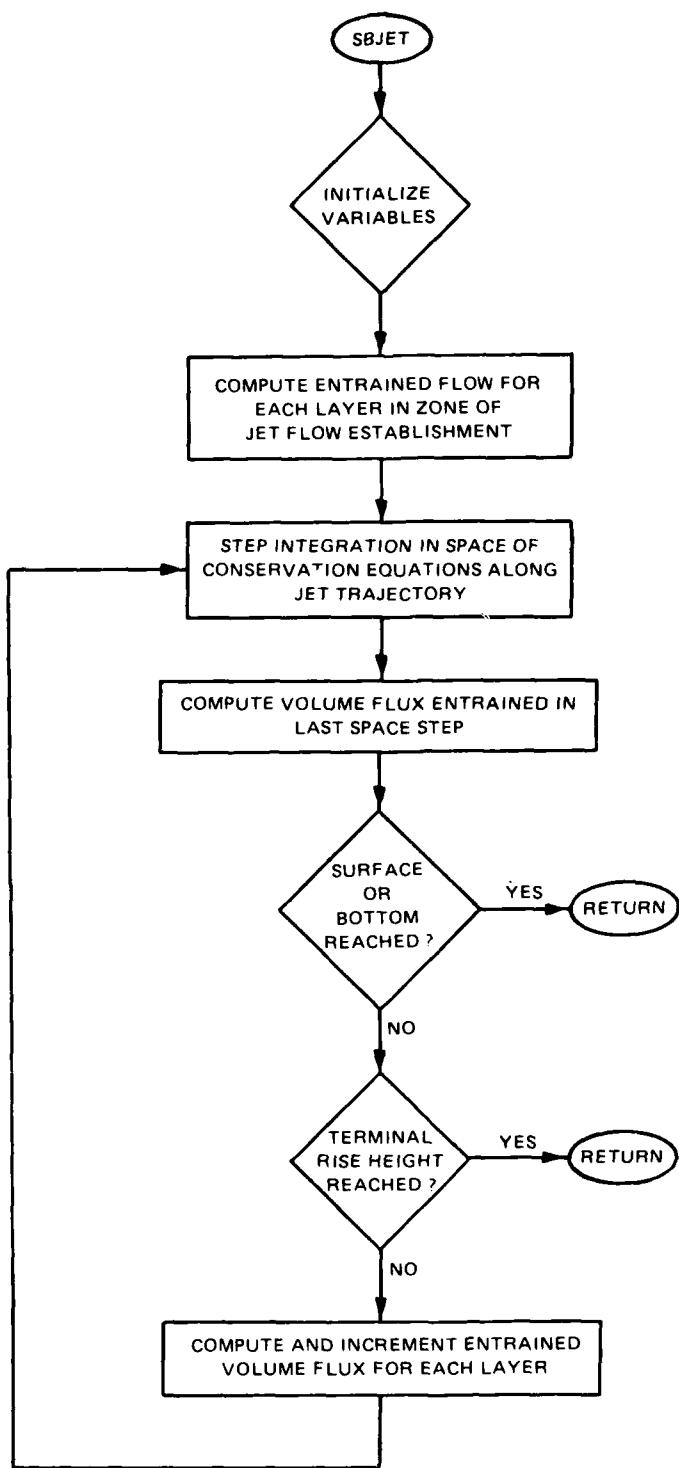
Figure 8. Flowchart for subroutine SBJET

21

b = parameter to account for width of the entrained distribution

q_{em} = maximum of q_e ; occurs at $\eta = \eta_o$

The choice of empirical equations to predict the parameters of Equation 18 is discussed in Appendix A (section, Entrained Volume Flux Distribution), and the equations are summarized in Table A10. Comparisons of the volume flux distribution predicted by these equations with the actual measured distributions are shown in Figures A11, A12, and A22-A27. The fit in all cases is sufficiently close for the present modeling purposes, and the total entrained volume flux computed from these equations is within 11 percent of that measured. The entrained volume flux is withdrawn selectively from a vertical zone of finite thickness (see Figure A1). The limits of this zone are z_e and $z_e + W_e$, as computed from Equations A43 and A44 (Table A10).

37. The entrainment from a zone whose bottom height is z_1 and top height is z_2 is:

$$Q_e = \int_{z_1}^{z_2} q_e dz \tag{19}$$

substituting Equation 18 into Equation 19 and integrating yields:

$$Q_e = M^{1/2} q_o \sigma \sqrt{\frac{\pi}{2}} \left[erf(a_2) - erf(a_1) \right] \tag{20}$$

where q_o is $q_{em}/M^{1/2}$, σ is the standard deviation of the assumed Gaussian distribution, Equation 18, i.e.,

$$\sigma = \frac{\ell_\varepsilon b}{\sqrt{2}} \tag{21}$$

$$a_1 = \frac{z_1 - z_o}{\sqrt{2}\sigma} \tag{22}$$

22

$$a_2 = \frac{z_2 - z_0}{\sqrt{2}\sigma} \qquad (23)$$

$$z_0 = \eta_0 \ell_\varepsilon \qquad (24)$$

and erf is the error function:

$$\text{erf}(t) = \frac{2}{\sqrt{\pi}} \int_0^t e^{-s^2} \, ds \qquad (25)$$

38. The entrainment distribution is computed in the subroutine WBJET in a manner shown in the flowchart of Figure 9. As the experimental results apply to linear stratifications, the first step is to linearize the ambient density profile. This is done by a least squares fit over the depth corresponding to the top and bottom of the jet outlet, and the stratification parameter ε (see Appendix A) is computed using this depth. The length scales ℓ_Q, ℓ_M, and ℓ_ε are calculated from Equations A6, A7, and A8. The vertical extent of the jet influence, z_e to $z_e + W_e$, is calculated from Equations A43 and A44, and the stratification parameter ε is then recalculated over this height. This procedure is repeated until the calculation of ε is within 1 percent of the previously calculated value. The entrained flow rate is then computed for each layer from Equation 20 where the parameters are calculated from the equations of Table A10 and Equations 21-24.

Summary and Entrainment Subroutine Flowcharts

39. Flow parameters are first computed in the subroutine ENTRAIN. The stratification parameter ε is first computed by linearizing the stratification profile over the depth corresponding to the top and bottom of the jet outlet. The length scales ℓ_Q, ℓ_M, ℓ_ε, and the ratios ℓ_Q/ℓ_ε and ℓ_M/ℓ_ε are then computed. As discussed in Appendixes A and B, jets for which $\ell_M/\ell_\varepsilon < 2$ are strongly buoyant. For

23

WBJET

COMPUTE ℓ_Q, ℓ_m

COMPUTE ℓ_ϵ, ℓ_Q/ℓ_ϵ, ℓ_m/ℓ_ϵ

COMPUTE W_e, z_e, FROM EQS. A43, A44

COMPUTE NEW VALUE OF STRATICATION
PARAMETER ϵ BY LEAST SQUARES
FIT OVER DEPTH OF JET INFLUENCE:
z_e TO $z_e + W_e$

NEW
ϵ WITHIN 1%
OF OLD ?

NO

YES

COMPUTE ENTRAINED VOLUME FLUX
PER LAYER

RETURN
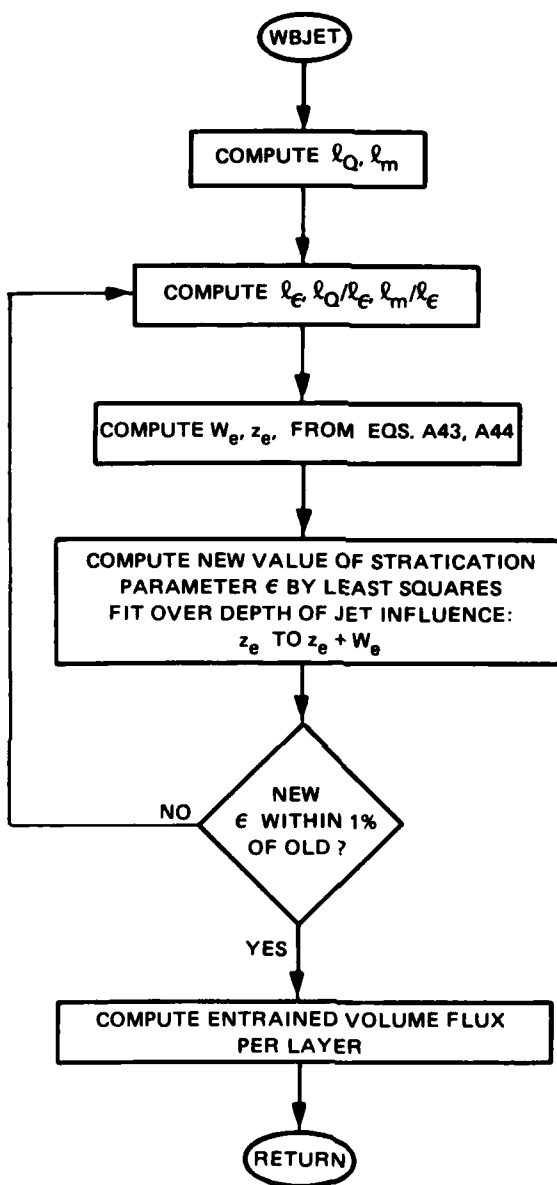
Figure 9. Flowchart for subroutine WBJET

this case, the subroutine SBJET is called. If $\ell_M/\ell_\varepsilon \geq 2$, the jet is momentum dominated, and the subroutine WBJET (W̲eakly B̲uoyant J̲E̲T̲) is called. The flow diagram for ENTRAIN is shown in Figure 10.

40. The entrainment distribution is computed in SBJET by a modified version of Fan and Brooks' (1969) integral model. The method of solution used in their model is given in Appendix C; the adaptation to WESTEX is described in paragraphs 25-33. (The flow diagram for SBJET is shown in Figure 8.)

41. The entrainment distribution for weakly buoyant jets is computed in WBJET by use of experimental results obtained during the present study. These results are presented in Appendix A, and their adaptation to WESTEX is described in paragraphs 35-38. (The flow diagram for WBJET is shown in Figure 9.)

42. One final modification is required to account for the presence of the free surface or, as in the case of Carters Lake, Ga., a nearby solid lower boundary. If $z_e + W_e$ is above the free surface, entrainment above is cut off; if the location of z_e is below a solid boundary, entrainment below is cut off. This assumption will generally reduce the total flow entrained into the jet and is used in both SBJET and WBJET.
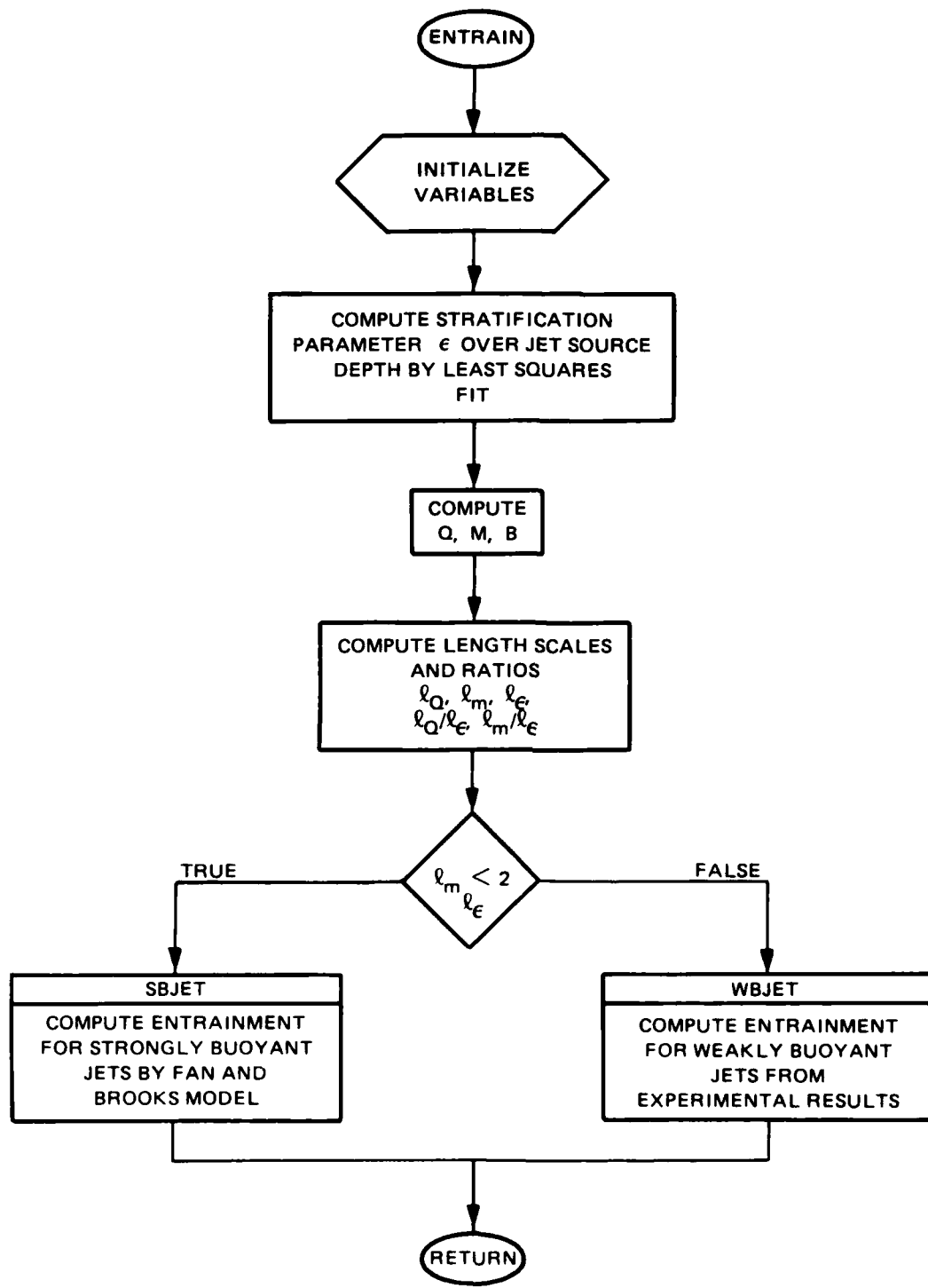
Figure 10. Flowchart for subroutine ENTRAIN

26

PART IV: APPLICATION TO CARTERS LAKE, GEORGIA

43. The general-purpose entrainment algorithms presented herein
were incorporated into the reservoir thermal simulation code (WESTEX).
The WESTEX code already contained the algorithms to simulate the effects
of PS operations, as discussed in Part II. To test the capability of
the general purpose entrainment algorithms within the thermal modeling
framework, the revised code was tested with a site-specific application.
A Corps of Engineers PS reservoir, Carters Lake, Ga., was selected for
the test case.

44. Carters Lake is a 500-MW PS project located on the Coosawattee
River (Figure 11). At normal summer pool elevation (327 m mean sea
level (msl)), Carters Lake contains 473×10^6 m^3 of water with a maximum
depth of 124 m. A reregulation dam located about 2.9 km below Carters
Dam impounds about 21.6×10^6 m^3 at a maximum pool depth of approxi-
mately 15.2 m.

45. The maximum generation and pumpback flow rates at Carters Dam
are 611.6 and 213.2 m^3/sec, respectively. With these flows and the
reservoir depths and volumes noted above, the upper reservoir maintains
a strong thermal stratification, while the lower reservoir is practi-
cally fully mixed. The heat budget of the afterbay (reregulation pool)
was modeled by assuming the afterbay was fully mixed.

46. The four penstocks for the four turbines are located at invert
elevation 299 m at the bottom and end of a rock-cut channel in the right
abutment. The entrance channel is approximately 488 m long and a mini-
mum of 61 m wide. Two of the turbines are reversible pump-turbines that
discharge into the upper reservoir through two penstocks. The dimen-
sions of each penstock intake are 6.25 m high by 4.27 m wide. The length
scale relationships (Equations A6-A8) and ratios $(\ell_Q/\ell_\varepsilon$ and $\ell_M/\ell_\varepsilon)$
were computed for the Carters Lake pumped inflows. During periods of
upper-lake stratification, the PS inflow jet was found to be within the
range of applicability of the results of Appendix A (high momentum and
low buoyancy, $\ell_M/\ell_\varepsilon \geq 2$; negligible effects of nozzle size, ℓ_Q/ℓ_ε
≤ 0.5). During periods of little or no upper-lake stratification,

Figure 11. Carters Lake project features

buoyancy was expected to be more important $(\ell_M/\ell_\varepsilon < 2)$, thus requiring the use of the integral buoyant jet model, SBJET.

47. The two pumpback outlets were modeled as one outlet with a discharge area of 26.7 m^2 for $Q < 113$ m^3/sec and 53.4 m^2 for $Q > 113$ m^3/sec . The pumpback capacity of each pump-turbine is about 113 m^3/sec. The pumpback jet was expected to collapse before reaching the end of the rock-cut channel; thus, entrainment of ambient reservoir water was not expected below the channel bottom elevation. The entrainment algorithms were modified to not allow any entrainment below the channel invert, elevation 298 m.

48. Hydrological, meteorological, and operational data for 1979 were used for the simulation. Vertical profiles of temperature had been measured biweekly at Carters Lake between May and December 1979. The model simulation was started for 1 January 1979, with isothermal conditions of 10° C. A time step of a day was used. Predicted and observed temperature profiles are compared in Figure 12. In general, the predicted profiles exhibit too much mixing. It appeared that too much entrainment took place in the simulation.

49. Considering the constriction of the approach channel, it seemed quite reasonable that the channel sidewalls (as well as the bottom, as discussed above) could restrict the amount of entrainment. All of the results presented herein are based on wall jets issuing into an unconfined fluid.

50. The geometry shown in Figure 11 definitely does not satisfy this criterion, as the jet is confined by the sidewalls. Based on the experiments conducted on nonbuoyant jets in two-layer stratification, the bottom boundary will probably not affect the total entrainment much, but the entrained flow distribution becomes unsymmetrical, with the peak shifted toward the bottom (see Roberts and Matthews 1984). To compensate for this, the coefficient of 0.8 in Equation A60 was gradually reduced, and the effect on predicted temperature profiles was investigated. The agreement between predicted and observed profiles was best with a coefficient of zero rather than 0.8.

51. The sidewall effect of the narrow entrance channel is

29
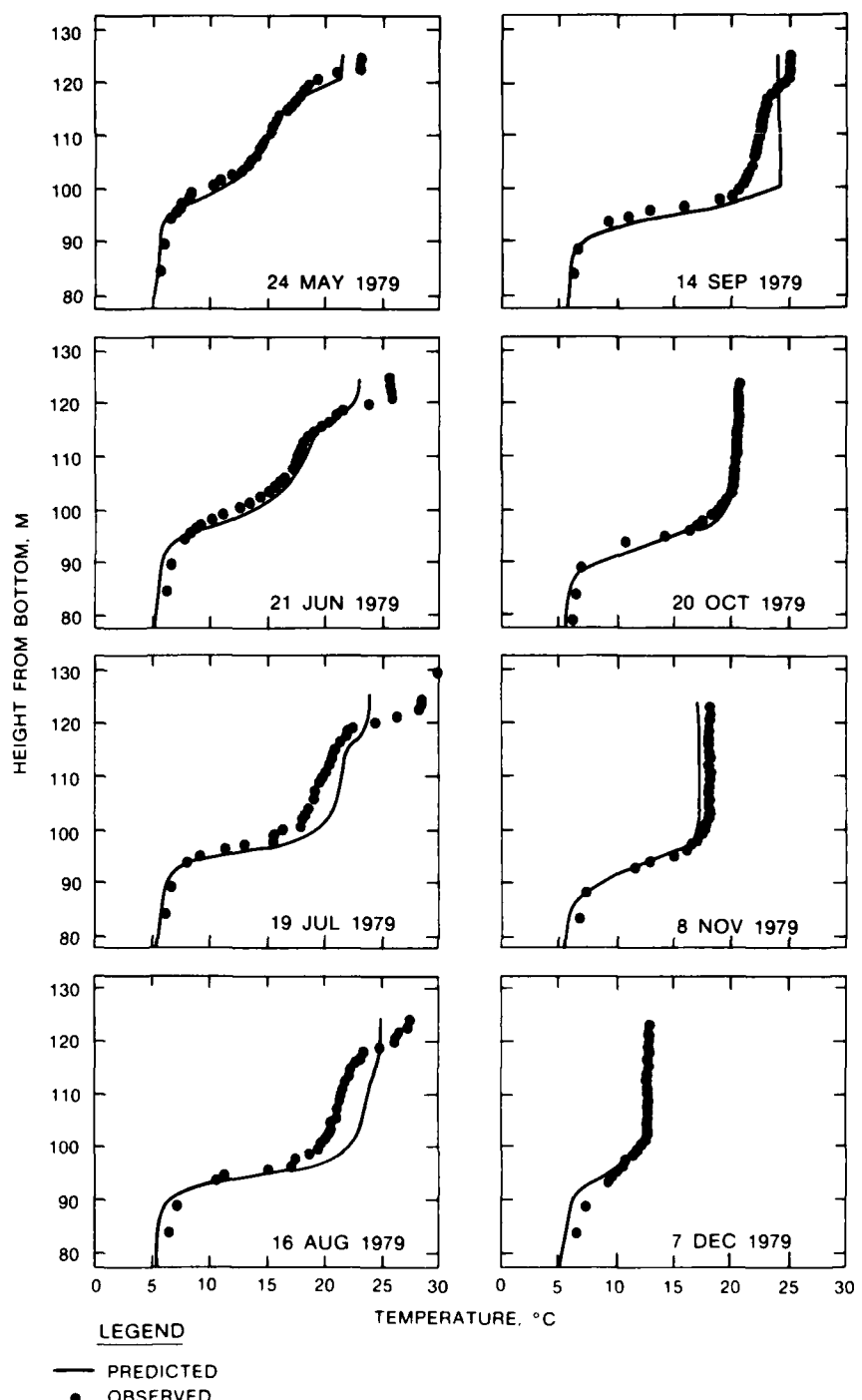
Figure 12. Carters Lake predicted and observed temperature profiles with developed entrainment algorithms

difficult to estimate. It is logical that the entrainment is reduced. The maximum entrainment per unit depth was reduced 50 percent by using a coefficient of 0.52 rather than 1.04 in Equation A62. These two changes to Equations A60 and A62 resulted in about a 60-percent decrease in total entrainment. The favorable results of these changes are shown in Figure 13.

52. The entrainment algorithms functioned very satisfactorily except for the site-specific changes discussed above. Subroutine SBJET was called from simulation day 1 (1 January 1979) through day 58 (27 February). After day 58, subroutine WBJET was called every day through the rest of the simulation (end of simulation was day 341), except for a couple of days in the spring. This indicates that at Carters Lake for 1979, the stratification was strong enough by early March to cause the jet to be weakly buoyant.
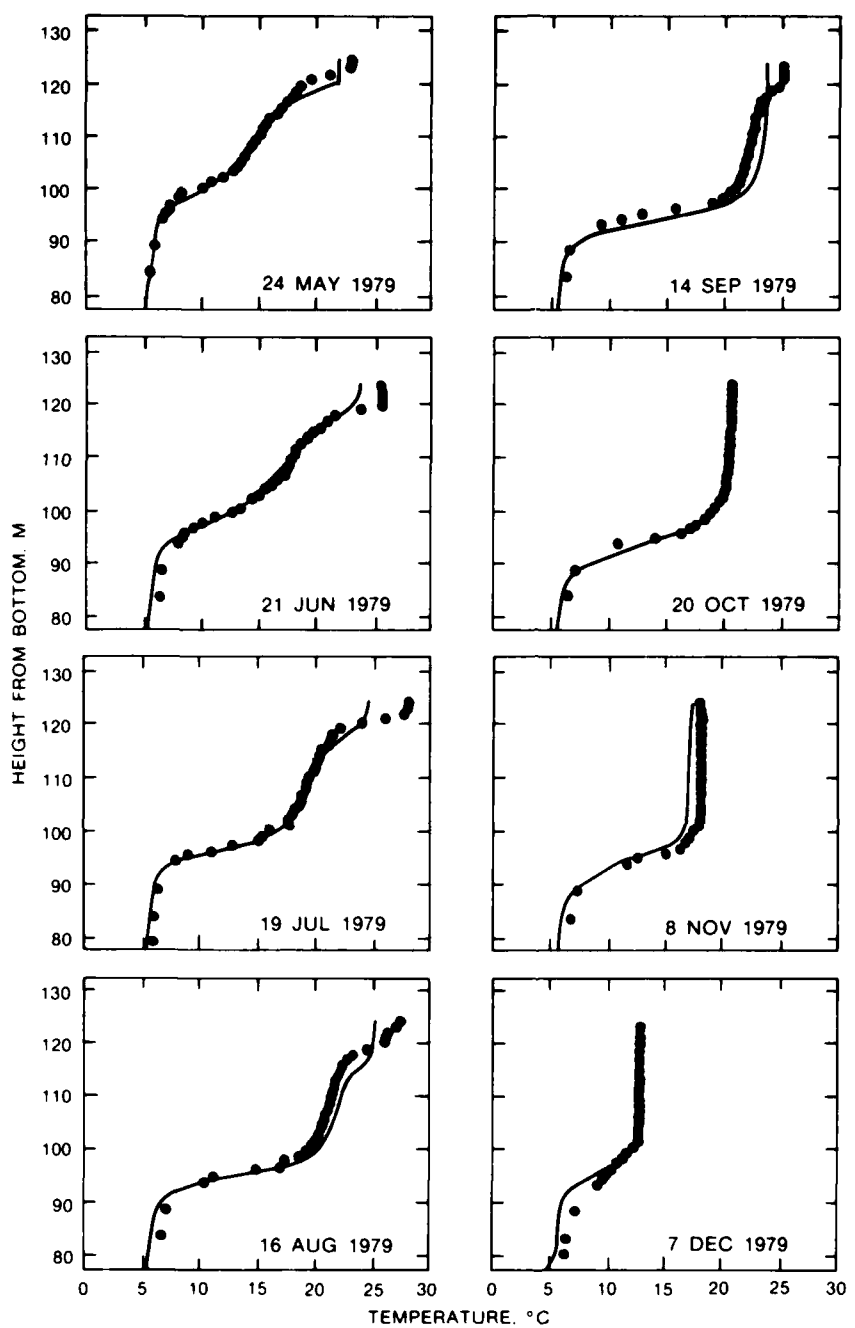
Figure 13. Carters Lake predicted and observed
temperature profiles with site-specific modifi-
cations to entrainment equations

PART V: SUMMARY AND RECOMMENDATIONS

53. Pumped-storage inflows can have a significant impact on reservoir thermal stratification. In the case of Carters Lake, the epilimnion and metalimnion were deepened to a depth of about 30 m, compared with about 10 m which is typical of most lakes in the region. This mixing and deepening of the thermocline have been accompanied by a substantial increase in the total heat in the reservoir.

54. The entrainment process must be modeled in order to simulate the mixing that occurs with PS inflows. To illustrate this, a simulation was conducted for Carters Lake without any entrainment. The results of this simulation are shown in Figure 14, along with the observed data and the predictions with entrainment. The differences in the predictions without entrainment and those with entrainment (and the observed) indicate that significant mixing occurs due to the entrainment process and that this process must be modeled to provide realistic predictions.

55. The research described herein provided a general-purpose entrainment algorithm. The algorithm should be applicable to most PS inflow jets, provided that the inflow is a horizontal or inclined ($\theta \leq 45$ deg) wall jet issuing into an unconfined fluid. Lateral and vertical restrictions in the fluid surrounding the jet impose site-specific considerations as with the Carters Lake application presented here. The Carters Lake intake channel geometry was restrictive, but it did not preclude the use of the algorithm, although it did require three modifications. One modification was made to prevent any entrainment below the channel bottom (see Part IV). The other two were made to reduce the total amount of entrainment and to modify the location of peak entrained flow, as these parameters were affected by sidewall and bottom boundaries, respectively. Permanent coding changes were implemented to account for the bottom effects. The effects of sidewall restrictions must be handled on a site-specific basis.

56. If sidewall interference is questionable, then the collapse length can be used as a first approximation for the nonrestrictive zone.
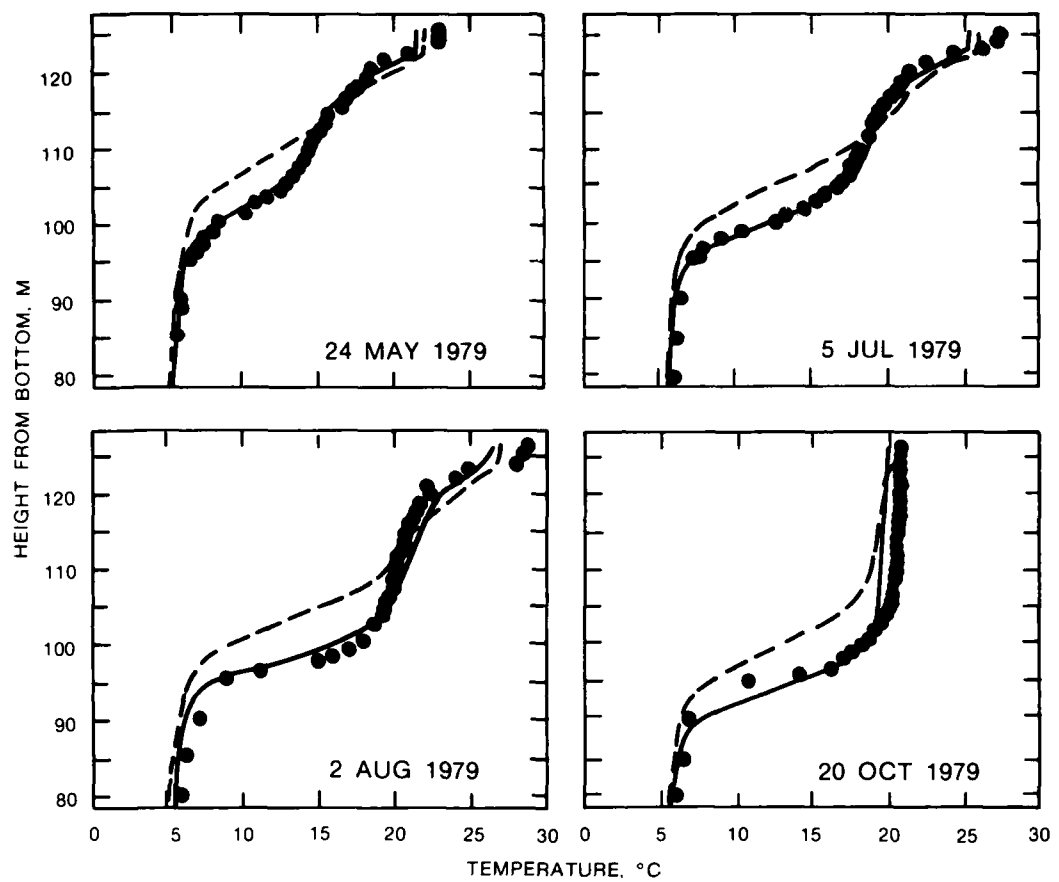
Figure 14. Carters Lake observed and predicted temperature profiles
with and without entrainment

The collapse length X_m can be estimated by $3\ell_\varepsilon$ (see Table B1). If either sidewall is closer than about $x_m/3$, or ℓ_ε, from the jet center line, lateral restriction will probably occur. If lateral restriction is anticipated, then the coefficient in Equation A62 must be reduced. The amount of reduction must be calibrated with observed profiles. If observed profiles do not exist, it would be advisable to examine the sensitivity of this coefficient and to try to place some bounds on the predictions. An undistorted, near-field physical model could be used to measure the entrainment as influenced by local geometry (e.g., sidewalls). The physical model results would be used to adjust coefficients in the entrainment algorithm.

REFERENCES

Albertson, M. L., et al. 1950. "Diffusion of Submerged Jets," Trans-
actions of the American Society of Civil Engineers, Vol 115, Paper No.
2409.

Dortch, M. S. 1978. "Marysville Lake Hydrothermal Study; Report 2:
2250 MW-Project; Hydraulic and Mathematical Model Investigation," Tech-
nical Report H-77-5, US Army Engineer Waterways Experiment Station,
Vicksburg, Miss.

_____. 1981. "Investigation of Release Temperatures for Kinzua
Dam, Allegheny River, Pennsylvania," Technical Report HL-81-9, US Army
Engineer Waterways Experiment Station, Vicksburg, Miss.

Dortch, M. S., et al. 1976. "Dickey-Lincoln School Lakes Hydrothermal
Model Study," Technical Report H-76-22, US Army Engineer Waterways Ex-
periment Station, Vicksburg, Miss.

Environmental Laboratory. 1982. "CE-QUAL-R1: A Numerical One-
Dimensional Model of Reservoir Water Quality; User's Manual," Instruc-
tion Report E-82-1, US Army Engineer Waterways Experiment Station,
Vicksburg, Miss.

Fan, L. N., and Brooks, N. H. 1969. "Numerical Solutions of Turbulent
Buoyant Jet Problems," Report No. KH-R-18, W. M. Keck Laboratory of
Hydraulics and Water Resources, California Institute of Technology,
Pasadena, Calif.

Fischer, H. B., et al. 1979. Mixing in Inland and Coastal Waters,
Academic Press, New York.

Fontane, D. G., and Bohan, J. P. 1974. "Richard B. Russell Lake Water
Quality Investigation; Hydraulic Laboratory Investigation," Technical
Report H-74-14, US Army Engineer Waterways Experiment Station, Vicksburg,
Miss.

Fontane, D. G., et al. 1977. "Marysville Lake Hydrothermal Study;
Report 1: 900-MW Project; Hydraulic and Mathematical Model Investi-
gation," Technical Report H-77-5, US Army Engineer Waterways Experiment
Station, Vicksburg, Miss.

Holland, J. P., et al. 1982. "Norfolk Lake, Arkansas, Temperature
Analysis; Mathematical Model Investigation," Technical Report HL-82-12,
US Army Engineer Waterways Experiment Station, Vicksburg, Miss.

Jirka, G. H., et al. 1977. "Ocean Thermal Energy Conversion Plants:
Experimental and Analytical Study of Mixing and Recirculation," Report
No. 231, Ralph M. Parsons Laboratory for Water Resources and Hydro-
dynamics, Massachusetts Institute of Technology, Cambridge, Mass.

Koh, R. C. Y., and Brooks, N. H. 1975. "Fluid Mechanics of Wastewater
Disposal in the Ocean," Annual Review of Fluid Mechanics, Vol 7,
pp 187-211.

Koh, R. C. Y., and Fan, L. N. 1970. "Mathematical Models for the Prediction of Temperature Distributions Resulting from the Discharge of Heated Water in Large Bodies of Water," US Environmental Protection Agency Water Pollution Control Research Series, Report No. 16130DWO10/70.

List, E. J., and Imberger, J. 1973. "Turbulent Entrainment in Buoyant Jets and Plumes," Journal of the Hydraulics Division, American Society of Civil Engineers, Vol 108, No. HY4, pp 1461-1474.

Roberts, Philip J. W. 1981. "Jet Entrainment in Pumped-Storage Reservoirs," Technical Report E-81-3, prepared by School of Civil Engineering, Georgia Institute of Technology, for the US Army Engineer Waterways Experiment Station, Vicksburg, Miss.

Roberts, Philip J. W., and Matthews, P. R. 1984. "Dynamics of Jets in Two-Layer Stratified Fluids" in press, Journal of Hydraulic Engineering.

Roshko, A. 1976. "Structure of Turbulent Shear Flows: A New Look," American Institute of Aeronautics and Astronautics Journal, Vol 14.

Schneider, H. H. 1980. "Laboratory Experiments to Simulate the Jet-Induced Erosion of Pycnoclines in Lakes," paper presented at the June 1980 Second International Symposium on Stratified Flows held at Trondheim, Norway, pp 697-706.

Smith, D. R., et al. 1981. "Evaluation of In-Reservoir Cofferdam on Richard B. Russell Reservoir and Hydropower Releases; Hybrid Model Investigation," Technical Report HL-81-12, US Army Engineer Waterways Experiment Station, Vicksburg, Miss.

Turner, J. S. 1973. "Buoyancy Effects in Fluids," 1st ed., Cambridge University Press, Cambridge, England.

Wright, S. J. 1977a. "Mean Behavior of Buoyant Jets in a Cross Flow," Journal of the Hydraulics Division, American Society of Civil Engineers, Vol 103, p 499.

_____. 1977b. "Effects of Ambient Cross Flows and Density Stratification on the Characteristic Behavior of Round, Turbulent Buoyant Jets," Technical Report KH-R-36, W. M. Keck Laboratory of Hydraulics and Water Resources, California Institute of Technology, Pasadena, Calif.

APPENDIX A: RESULTS OF EXPERIMENTS ON WEAKLY BUOYANT JETS

Introduction

1.   Investigation of the literature on weakly or neutrally buoyant jets discharging into a stratified ambient revealed little information. Experiments were therefore conducted to study this situation.   As even the restricted idealized problem, shown in Figure A1, represents a large number of experiments when all possible combinations of jet geometries, angles, density stratifications, and buoyancies are considered, emphasis was placed on the following categories:

   a.   <u>Series 1.</u> Horizontal neutral and slightly buoyant discharges into a linear stratification. The nozzle size was also varied to investigate the effects of this parameter. Results are presented in paragraphs 20-22.

   b.   <u>Series 2.</u> Inclined jets discharging at 22.5 or 45 deg to the horizontal into a linear stratification. Buoyancies were neutral, slightly positive, or slightly negative. The nozzle size was maintained small to eliminate effects of this parameter. Results are presented in paragraphs 23-26.

   c.   <u>Series 3.</u> Horizontal neutrally buoyant jets discharging into the lower layer of a two-layer fluid. The upper layer is well mixed and separated from the linearly stratified lower layer by a finite density jump. The depth of discharge below the interface was varied, but the nozzle size was kept small. Results are presented in paragraphs 27-29.

2.   The dynamics of nonbuoyant jets in uniform density fluids have been extensively studied (i.e., the review in Fischer et al. 1979)* and their gross characteristics are well known. Such a jet grows linearly with distance from the source, and its total volume flux continuously grows with distance. Schneider (1980) performed experiments on horizontal nonbuoyant jets discharging into the lower layer of a stagnant fluid consisting of two homogeneous layers of different densities. He measured the entrainment rate across the interface and showed that this

---

* Bibliographic information is given in the References section of the main text, page 36.
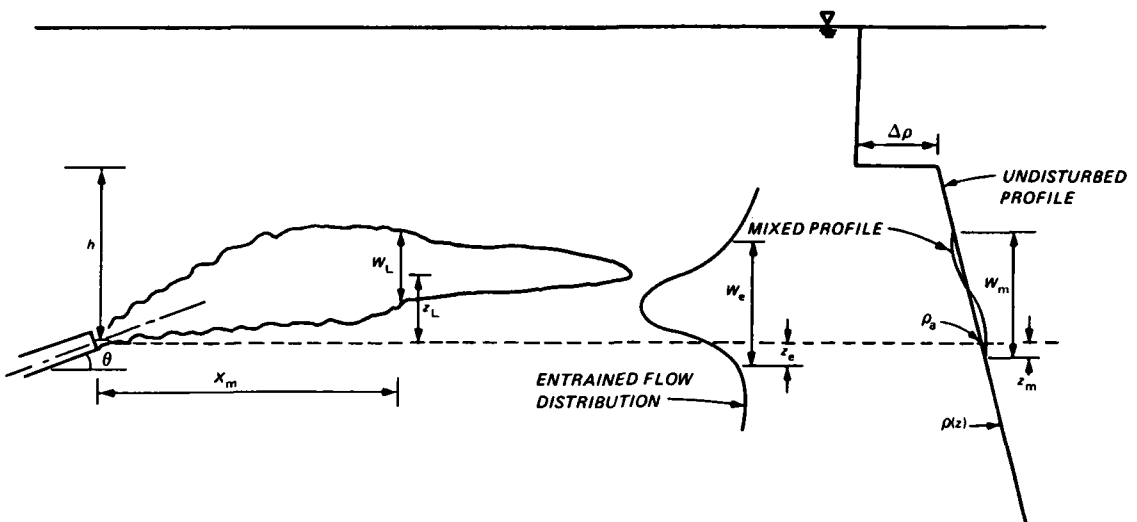
Figure A1. Definition sketch of idealized problem

rate is a function of a form of the Richardson number based on the depth of the discharge below the thermocline, the density jump across the thermocline, and the jet momentum flux. Jirka et al. (1977) reported experiments on jet discharges from ocean thermal energy conversion plants into the upper layer, which, although similar to the present situation, cannot be compared directly due to their emphasis on flows in the uniform upper layer.

3. When a jet is discharged into a continuously stratified medium, its behavior changes completely from one discharged into a homogeneous fluid. Near to the source, the jet growth is unaffected by stratification, but further away the initial jet velocity decays and the width grows until the local gradient Richardson number becomes large enough that the stratification removes the turbulent kinetic energy and the jet collapses vertically, causing entrainment to essentially cease. The entrained flow is selective due to the ambient stratification. Following collapse, the inflow moves upstream as a tonguelike density current.

4. In the following section a general dimensional analysis of the problem is presented in terms of length scales. The experimental procedure is discussed in paragraphs 14-19, and the results are given in paragraphs 20-29. A brief discussion of the results and equations to

describe them are presented in paragraphs 30-37. The distribution of
entrained volume flux for all the experiments and equations suitable
for inclusion into the pumped-storage (PS) model are given in paragraphs
38-43. Concluding remarks are given in paragraphs 44-45.

Analysis

5. The problem under consideration is shown in Figure A1. It is
most easily analyzed and discussed by means of the characteristic length
scales involved, following Fischer et al. (1979). Assuming the jet to
be fully turbulent so that Reynolds number effects are negligible, the
jet can be characterized by its kinematic fluxes of volume Q , momentum
M , and buoyancy B , where:

$$Q = uA \qquad (A1)$$

$$M = u^2 A \qquad (A2)$$

and

$$B = uA\left(\frac{\rho_a - \rho_o}{\rho_a}\right) g \qquad (A3)$$

where

    u = jet nozzle velocity

    A = nozzle area

    ρ_a = ambient density at the discharge depth

    ρ_o = jet density

    g = acceleration due to gravity

6. By making use of the Boussinesq assumption (Turner 1973), one
can characterize the ambient stratification by g' and ε where

$$g' = g \frac{\Delta\rho}{\rho_a} \qquad (A4)$$

$$\varepsilon = - \frac{g}{\rho_a} \frac{d\rho}{dz} \qquad (A5)$$

A3

and $\Delta\rho$ is the density jump across the interface. The square root of ε is the Brunt-Väisälä, or buoyancy, frequency.

7. Many characteristic length scales can be formed from the six parameters involved. This study is concerned with situations in which the momentum flux is always important and the volume and buoyancy fluxes less so. Five independent length scales can be formed, the most convenient of which are:

$$\ell_Q = \frac{Q}{M^{1/2}} = \sqrt{A} \qquad (A6)$$

$$\ell_M = \frac{M^{3/4}}{B^{1/2}} \qquad (A7)$$

$$\ell_\varepsilon = \left(\frac{M}{\varepsilon}\right)^{1/4} \qquad (A8)$$

$$\ell_\Delta = \left(\frac{M}{g'}\right)^{1/3} \qquad (A9)$$

8. The problem is characterized by the relative magnitudes of h (distance from elevation of jet source to density jump) and these five length scales, each of which has a physical significance. The term ℓ_Q is the square root of the nozzle area; it characterizes the distance from the origin for which the nozzle geometry affects the flow field. For distances from the origin much greater than ℓ_Q, the properties of the jet depend only on M and distance and are independent of the nozzle geometry (Fischer et al. 1979, p 324). The term ℓ_M is the characteristic distance from the nozzle over which the source momentum flux is important relative to the source buoyancy flux. In an unstratified environment, for distances from the origin much less than ℓ_M, the momentum flux dominates and the flow is jetlike; for distances much greater than ℓ_M, the buoyancy flux dominates and the flow is plumelike. For distances of the order of ℓ_M, both momentum and buoyancy fluxes are important. The term ℓ_ε characterizes the strength of the jet relative to the ambient linear stratification. The same length scale

A4

arises in vertically discharged jets in a linearly stratified ambient (Fischer et al. 1979), in which case the terminal rise height is directly proportional to ℓ_ε . The term ℓ_Δ characterizes the relative strengths of the jet momentum to the interfacial density jump.

9. There are several parameters of interest for the present study (see Figure Al). These include the collapse length X_m of the jet; the location of the neutrally buoyant collapsed layer Z_L ; the collapsed layer thickness W_L ; the location Z_e and width W_e of the entrained flow; the mixed layer thickness W_m , defined as the thickness of the ambient fluid where the density profile is altered by the jet after the inflow ceases; and Z_m , the location of the bottom of this layer. It is also desirable to know whether fluid is mixed into the jet from the upper layer in the two-layer case. This will be termed stability, where stable signifies no entrainment from the upper layer and unstable signifies that entrainment from the upper layer does occur.

10. The dependent variables can be expressed as:

$$X_m, \ W_L, \ W_e, \ Z_e, \ W_m, \ Z_m, \ Z_L = f(Q, \ M, \ B, \ h, \ \varepsilon, \ g', \theta) \qquad (A10)$$

and

$$\text{stability} = f(Q, \ M, \ B, \ h, \ \varepsilon, \ g', \ \theta) \qquad (A11)$$

Following dimensional analysis, Equations A10 and A11 can be written in terms of the length scales as:

$$\frac{X_m}{\ell_\varepsilon}, \ \frac{W_L}{\ell_\varepsilon}, \ \frac{Z_L}{\ell_\varepsilon}, \ \frac{W_e}{\ell_\varepsilon}, \ \frac{Z_e}{\ell_\varepsilon}, \ \frac{W_m}{\ell_\varepsilon}, \ \frac{Z_m}{\ell_\varepsilon}, \ = \ f\left(\frac{\ell_Q}{\ell_\varepsilon}, \ \frac{\ell_M}{\ell_\varepsilon}, \ \frac{h}{\ell_\varepsilon}, \ \frac{h}{\ell_\Delta}, \ \theta\right) \qquad (A12)$$

and

$$\text{stability} = f\left(\frac{\ell_Q}{\ell_\varepsilon}, \ \frac{\ell_M}{\ell_\varepsilon}, \ \frac{h}{\ell_\varepsilon}, \ \frac{h}{\ell_\Delta}, \ \theta\right) \qquad (A13)$$

11. The total volume flux in the jet becomes finite following collapse and does not increase continually with distance as in the unstratified case. Defining this total volume flux as μ , we have:

$$\mu = f(Q, M, B, h, \varepsilon, g', \theta) \tag{A14}$$

which, following dimensional analysis becomes:

$$\frac{\mu \varepsilon^{1/4}}{M^{3/4}} = f\left(\frac{\ell_Q}{\ell_\varepsilon}, \frac{\ell_M}{\ell_\varepsilon}, \frac{h}{\ell_\varepsilon}, \frac{h}{\ell_\Delta}, \theta\right) \tag{A15}$$

The term ℓ_ε is chosen as the normalizing length scale as this will always be important for the present class of problems.

12. The entrainment distribution can be derived by similar arguments. Suppose that q_e is the entrained volume flow rate per unit depth, so that the total entrained flow rate Q_e is:

$$Q_e = \int_{Z_e}^{Z_e + W_e} q_e \, dz \tag{A16}$$

then:

$$q_e = f(Z, M, B, Q, h, \varepsilon, g', \theta) \tag{A17}$$

which, following dimensional analysis and expression in terms of length scales, becomes:

$$\frac{q_e}{M^{1/2}} = f\left(\frac{Z}{\ell_\varepsilon}, \frac{\ell_Q}{\ell_\varepsilon}, \frac{\ell_M}{\ell_\varepsilon}, \frac{h}{\ell_\varepsilon}, \frac{h}{\ell_\Delta}, \theta\right) \tag{A18}$$

and the maximum value q_{em} is:

$$\frac{q_{em}}{M^{1/2}} = f\left(\frac{\ell_Q}{\ell_\varepsilon}, \frac{\ell_M}{\ell_\varepsilon}, \frac{h}{\ell_\varepsilon}, \frac{h}{\ell_\varepsilon}, \theta\right) \tag{A19}$$

13. Equations A12, A13, A15, A18, and A19 are based on dimensional analysis only and could be expressed in terms of the fundamental variables Q, M, B, h, ε, and g'. It is more convenient to express them in terms of the length scales, however, due to their physical significance and aid to interpretation.

Experimental Procedure

14. A sketch of the experimental configuration is shown in Figure A2. The experiments were performed in a Plexiglas-walled tank 8 ft (2.4 m) long, 4 ft (1.2 m) wide, and 2 ft (0.6 m) deep. The discharge was from a round nozzle. The stratification was obtained with salt by means of a two-tank filling method similar to that used by Wright (1977a). The fluid was introduced to the tank by a floating spreader. Salt concentrations, and hence density profiles, were measured by a two-wire conductivity probe mounted on a vertically traversing probe on an instrument carriage. A Sanborn recorder was used to monitor the conductivity probe; the probe and circuitry were very similar to those used by Wright (1977a). The jet fluid was dyed to make it visible, and photographs of the flow field were obtained by an overhead motor-driven 35mm camera. A mirror placed at the side of the tank enabled simultaneous side and overhead views to be obtained in the same photograph.

15. Due to the small velocities involved, it is quite difficult to measure the entrained volume flux. It was done by taking advantage of the entrainment-induced flow field in the tank. Prior to commencement of the experiment, potassium permanganate dye crystals were dropped into the tank along a straight line perpendicular to the jet axis, and beyond the point at which the jet would collapse. The subsequent movement of the dye streaks was photographed, and the entrained flow was computed.

16. As not all of the entrainment-induced flow is actually entrained into the jet, it was necessary to measure independently the width of the entrained flow W_e and its location Z_e . This was done by placing the conductivity probe within the jet, first, near its top and, second, near its bottom to record the salinity fluctuations. As material entrained into the jet is not immediately mixed (Roshko 1976), the maxima and minima of the salinity fluctuations at any level correspond to the upper and lower depths from which the fluid was entrained.

17. Salinity extremes were calculated and, from the measured density profile, the heights corresponding to these concentrations were computed. This gives the limits of the entrainment width and its location,
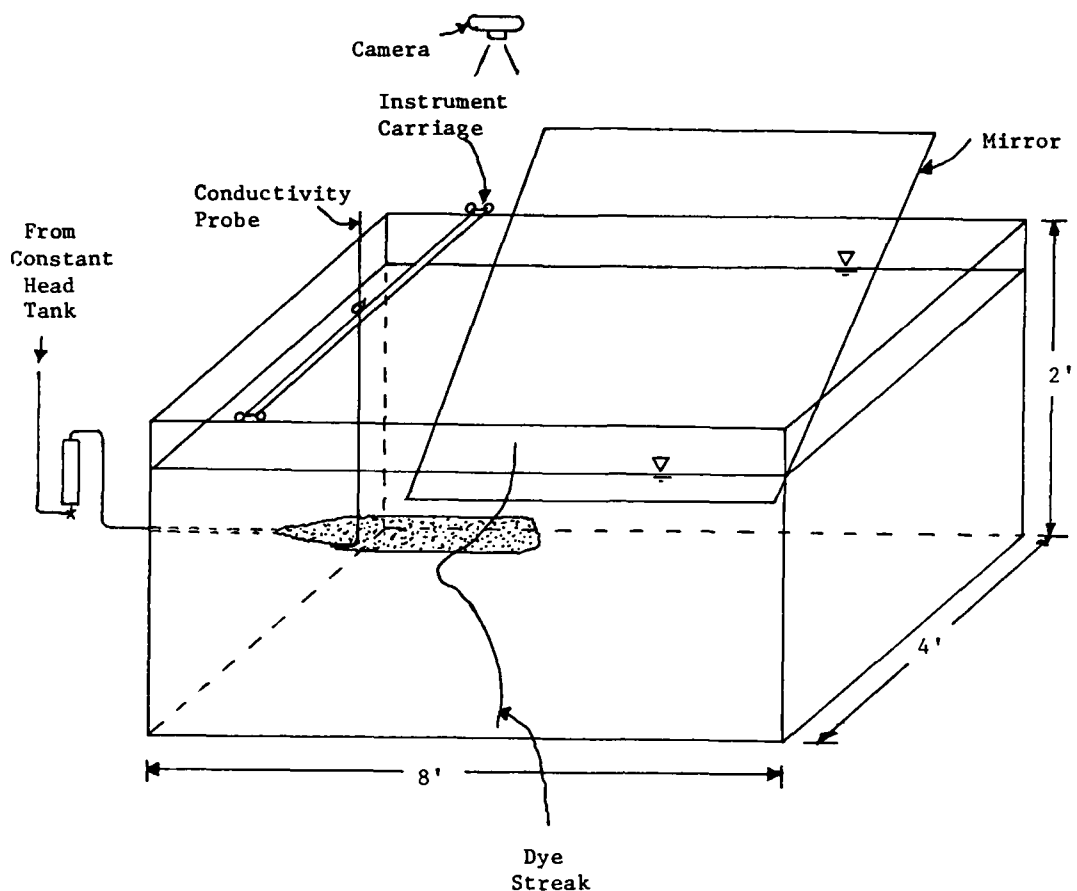
Figure A2. Experimental configuration

which were computed for each experiment. The volume flux was then found
by first computing the area A_f under each dye streak where

$$A_f = \int_{Z_e}^{Z_e + W_e} X(z) \, dz \tag{A20}$$

and X is the horizontal distance along the displaced dye streak at
height z measured from some datum. The area was computed on the digi-
tizing pad of an Apple microcomputer.

18. The area of each dye streak was plotted versus time, and a
straight line was fitted through the data. The slope of the line is the

A8

entrained flow rate per unit horizontal width, and the total entrained flow Q_e is

$$Q_e = \text{slope} \times w \qquad\qquad (A21)$$

where w is the horizontal width of the entrained flow field that was estimated from the overhead photographs. The flow field was found to be very uniform across the tank width beyond the jet boundaries. Finally, the total volume flux μ in the jet is computed by conservation of volume as:

$$\mu = Q_e + Q \qquad\qquad (A22)$$

19. The thickness of the collapsed layer W_L and the approximate length X_m were measured from the photographs.

Results

Horizontal buoyant and nonbuoyant jets into linear stratification

20. For these experiments there is no interfacial density jump; thus, ℓ_Δ (Equation A9) and h are not parameters. Experiments were performed for the following parameter ranges:

$$0.08 < \frac{\ell_Q}{\ell_\varepsilon} < 1$$

and

$$\frac{\ell_M}{\ell_\varepsilon} = 2 \text{ or } \infty$$

For these experiments W_m and Z_m, the mixed layer thickness and location, were not measured. For $\theta = 0$ deg, Equations A12, A15, A18, and A19 become:

A9

$$\frac{X_m}{\ell_\varepsilon}, \frac{W_L}{\ell_\varepsilon}, \frac{Z_L}{\ell_\varepsilon}, \frac{W_e}{\ell_\varepsilon}, \frac{Z_e}{\ell_\varepsilon} = f\left(\frac{\ell_Q}{\ell_\varepsilon}, \frac{\ell_M}{\ell_\varepsilon}\right) \qquad \text{(A23)}$$

$$\frac{\mu \varepsilon^{1/4}}{M^{3/4}} = f\left(\frac{\ell_Q}{\ell_\varepsilon}, \frac{\ell_M}{\ell_\varepsilon}\right) \qquad \text{(A24)}$$

$$\frac{q_e}{M^{1/2}} = f\left(\frac{Z}{\ell_\varepsilon}, \frac{\ell_Q}{\ell_\varepsilon}, \frac{\ell_M}{\ell_\varepsilon}\right) \qquad \text{(A25)}$$

and

$$\frac{q_{em}}{M^{1/2}} = f\left(\frac{\ell_Q}{\ell_\varepsilon}, \frac{\ell_M}{\ell_\varepsilon}\right) \qquad \text{(A26)}$$

21. Side-view photographs of neutral $(\ell_M/\ell_\varepsilon = \infty)$ and slightly buoyant $(\ell_M/\ell_\varepsilon = 2)$ jets are shown in Figures A3 and A4, and a simultaneous overhead and side view is shown in Figure A5 for a neutrally buoyant case. Many of the characteristics of all the jets studied are apparent in these photographs, including the initial unimpeded jet growth, the sudden vertical collapse and sideways spreading, the tongue-like horizontal intrusion, and the entrainment dye streak. Experimental parameters for this series of experiments are given in Tables A1 and A2.

22. Results for collapsed layer thickness W_L, entrainment width W_e, entrainment location Z_e, and rise height Z_L for the buoyant case are shown in Figures A6-A9, expressed in the form of Equation A23. The total entrained volume flux, Equation A24, is shown in Figure A10. The distribution of entrained volume flux is shown plotted in the form of Equation A25 in Figure A11 for nonbuoyant jets $(\ell_M/\ell_\varepsilon = \infty)$ and Figure A12 for buoyant jets $(\ell_M/\ell_\varepsilon = 2)$. The implications of these results are discussed in paragraphs 30-37.

Inclined buoyant and nonbuoyant
jets into linear stratification

23. The results of the previous section show the effects of the nozzle size ℓ_Q to be negligible for $\ell_Q/\ell_\varepsilon < \sim 0.2$. Even for larger values of ℓ_Q/ℓ_ε, the results for W_L, W_e, Z_e, and Z_L (Figures A6 through A9) are essentially independent of this parameter. Only the

A10
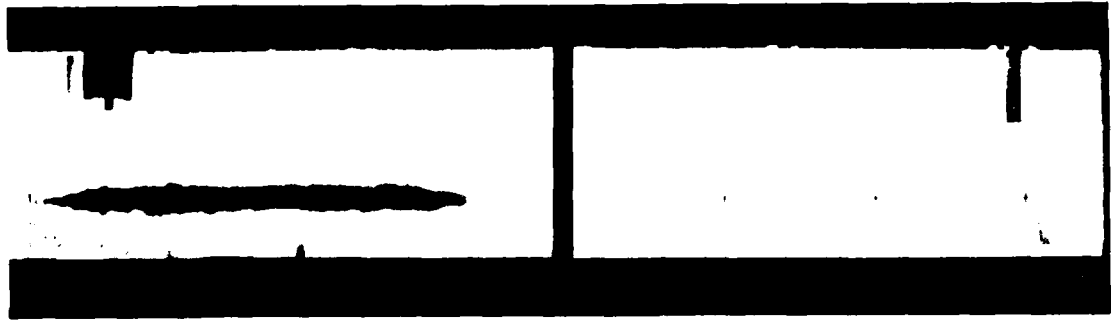
Figure A3. Side-view photograph of horizontal neutrally
buoyant jet ($\ell_M/\ell_\varepsilon = \infty$)
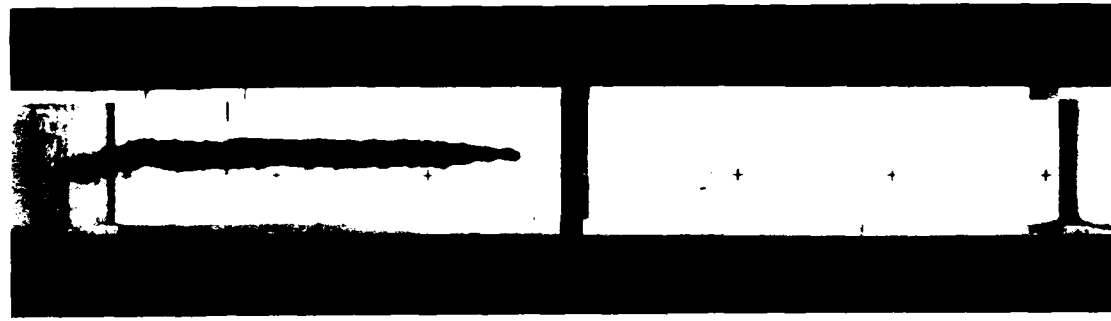
Figure A4. Side-view photograph of horizontal slightly
buoyant jet ($\ell_M/\ell_\varepsilon = 2$)

A11
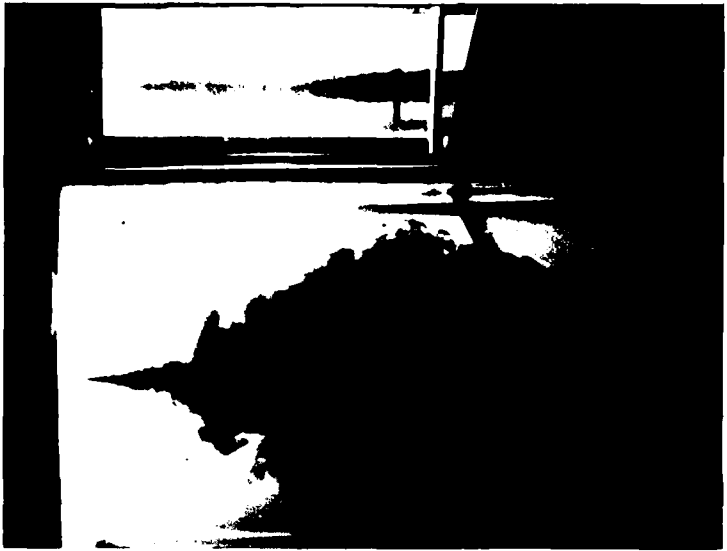
a. Side and top view of jet
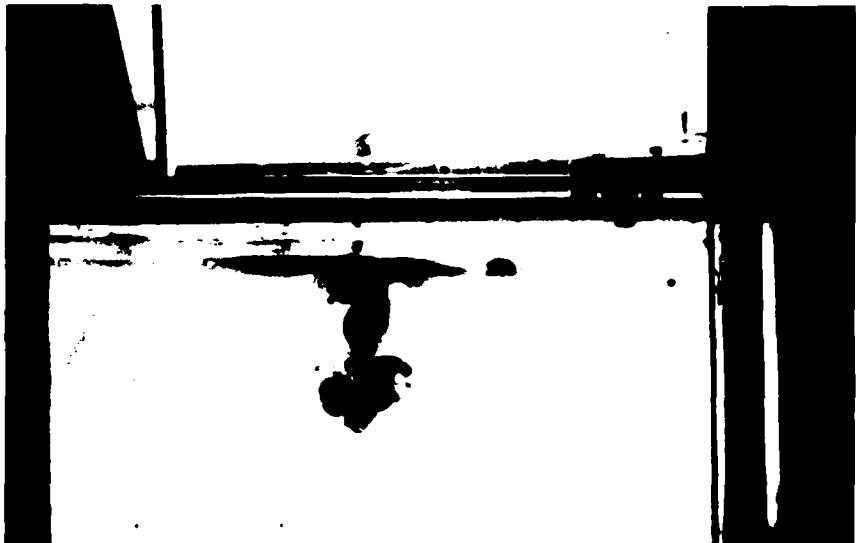
b. Entrainment dye streak

Figure A5. Simultaneous overhead and side view (in mirror at top) of horizontal neutrally buoyant jet

A12
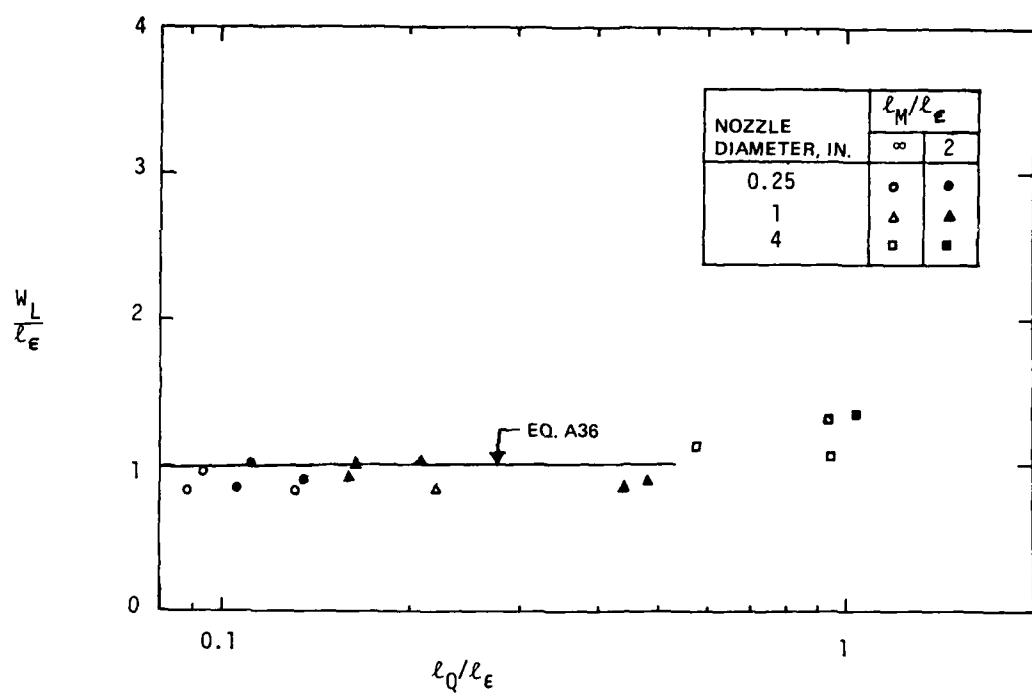
Figure A6. Experimental results, collapsed layer thickness of horizontal neutrally and slightly buoyant jets in linear stratification
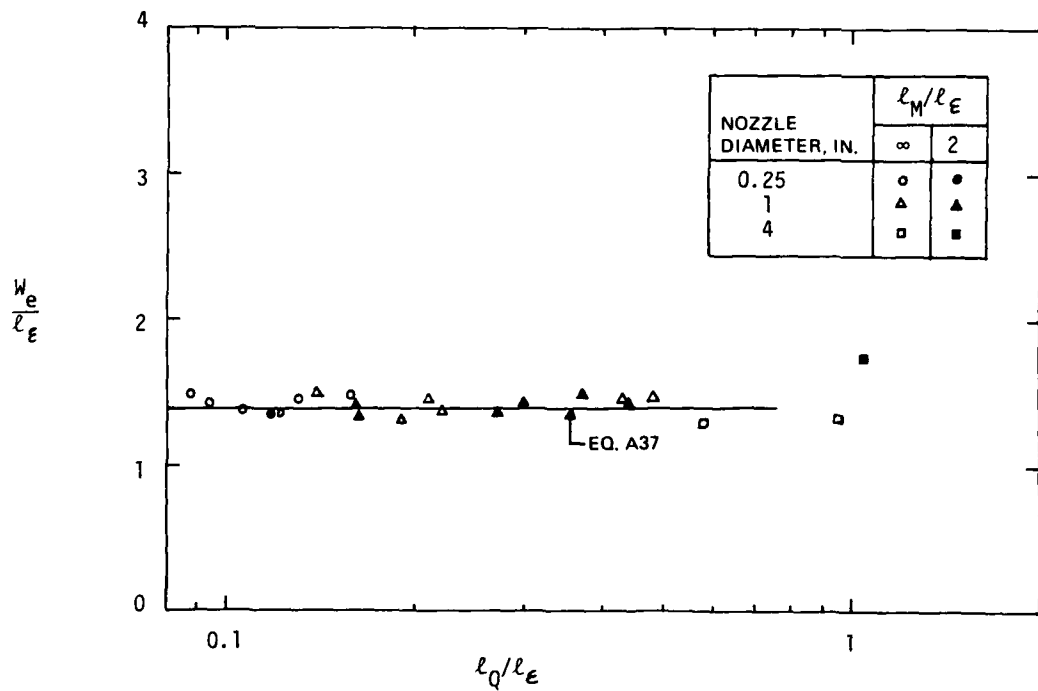
Figure A7. Experimental results, thickness of entrainment layer, horizontal neutrally and slightly buoyant jets in linear stratification
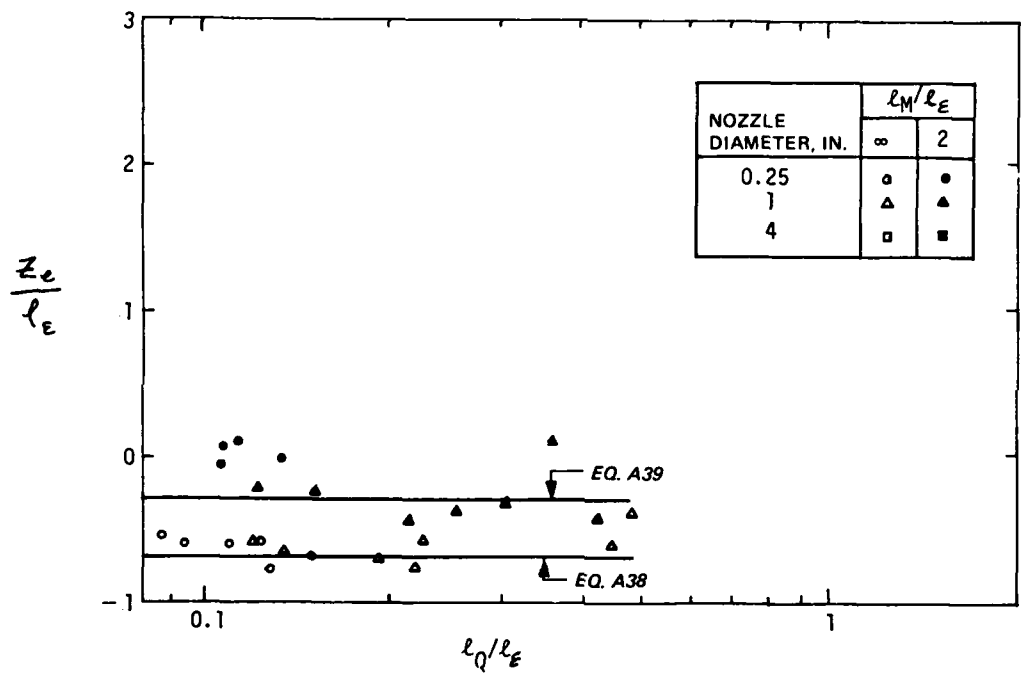
Figure A8. Experimental results, bottom location of entrainment layer caused by horizontal neutrally and slightly buoyant jets in linear stratification
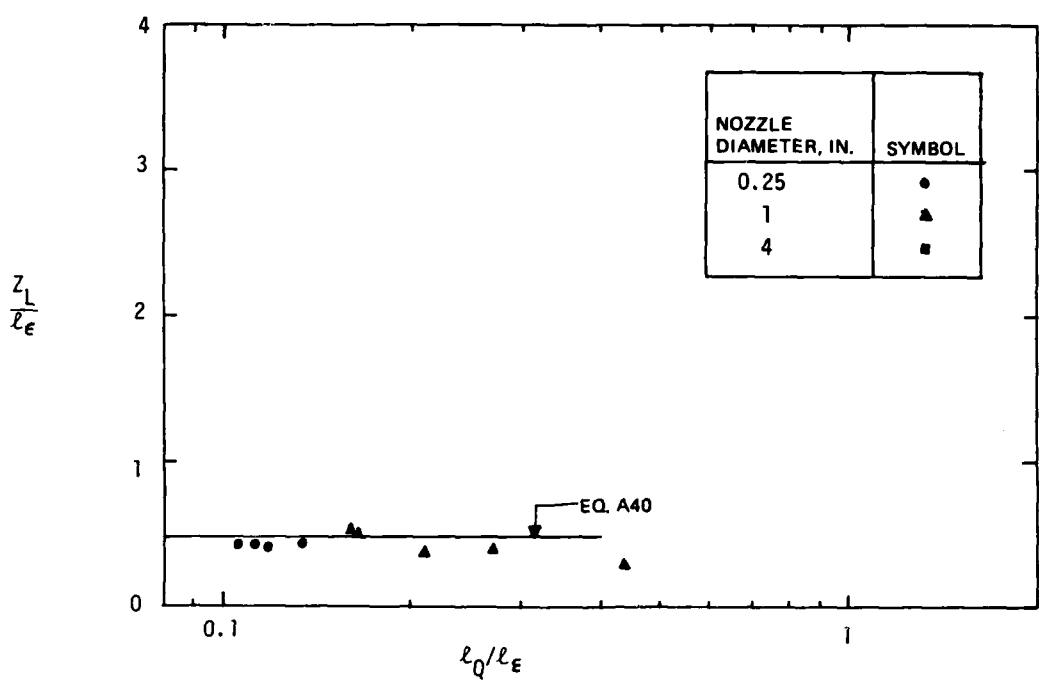
Figure A9. Experimental results for rise height of horizontal slightly buoyant ($\ell_M/\ell_\varepsilon = 2$) jets in linear stratification
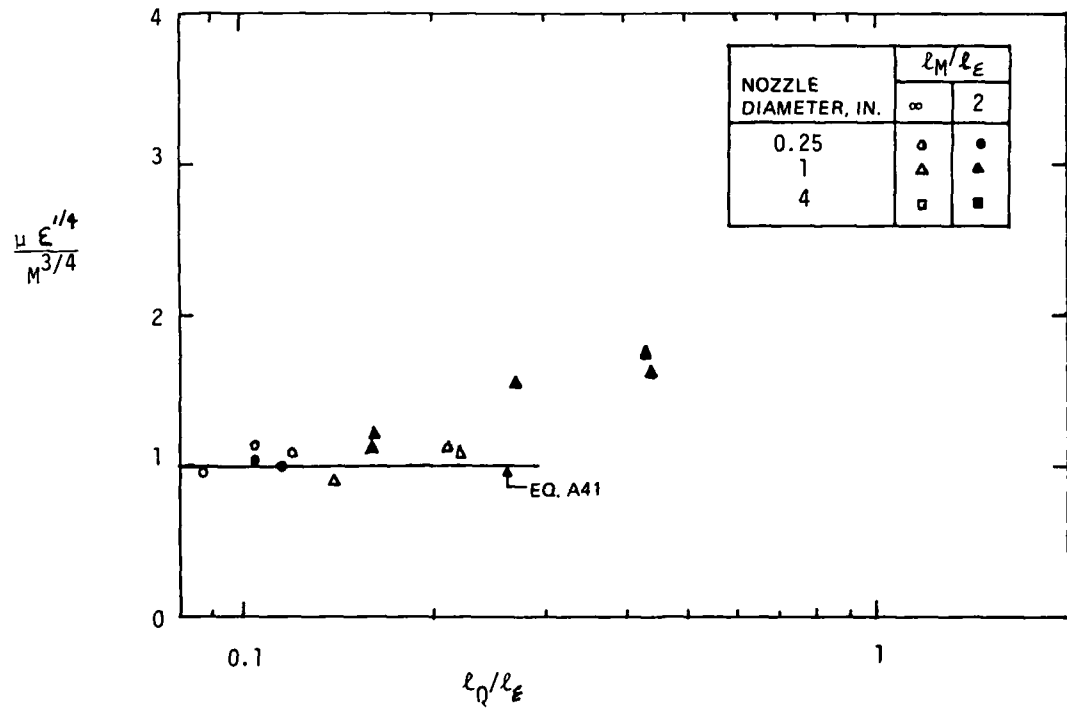
Figure A10. Experimental results for entrained volume flux of horizontal neutral and slightly buoyant jets in linear stratification
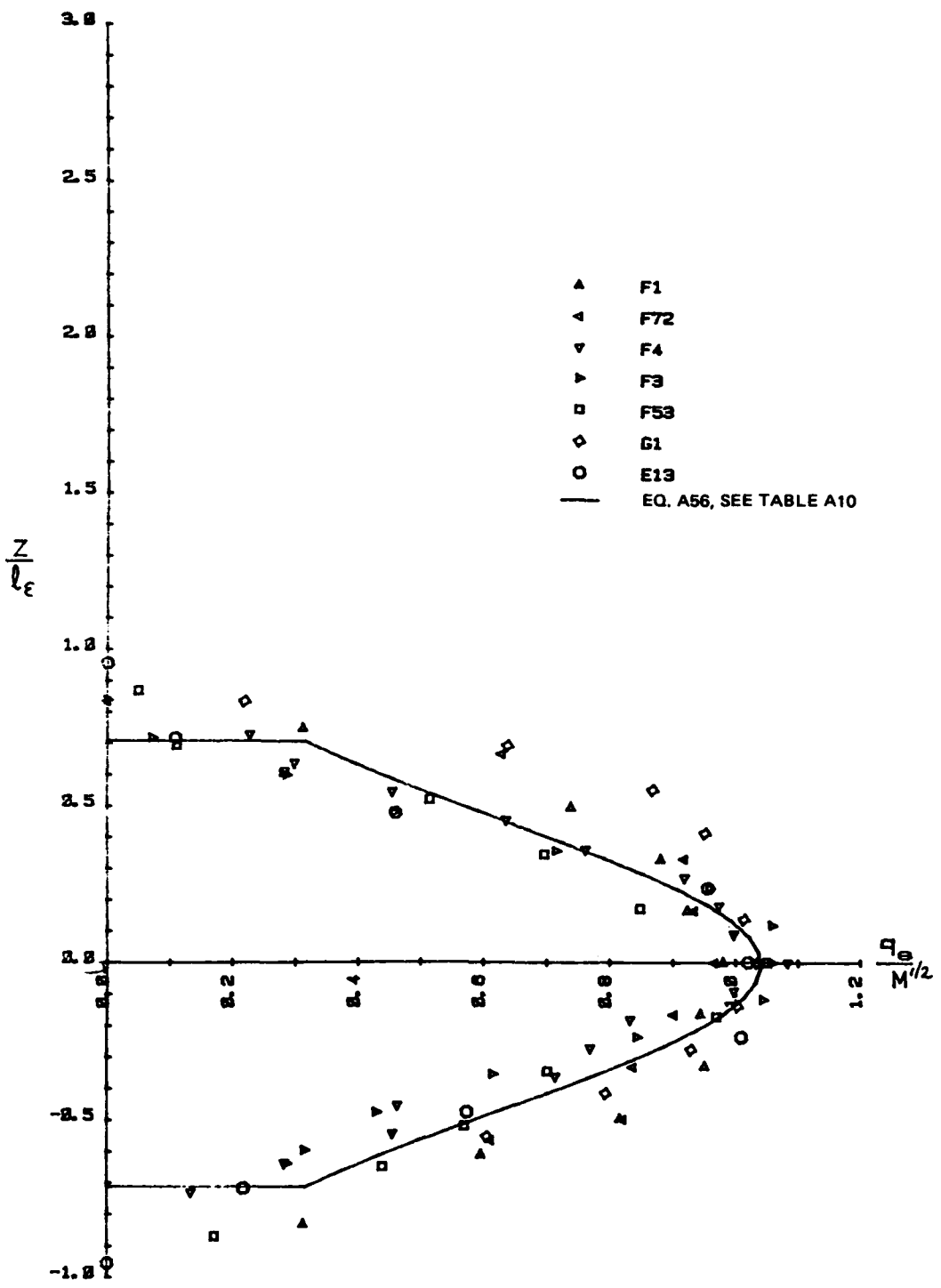
Figure A11. Distribution of entrained volume flux for horizontal nonbuoyant ($\ell_M/\ell_\varepsilon = \infty$) jets in linear stratification

A16
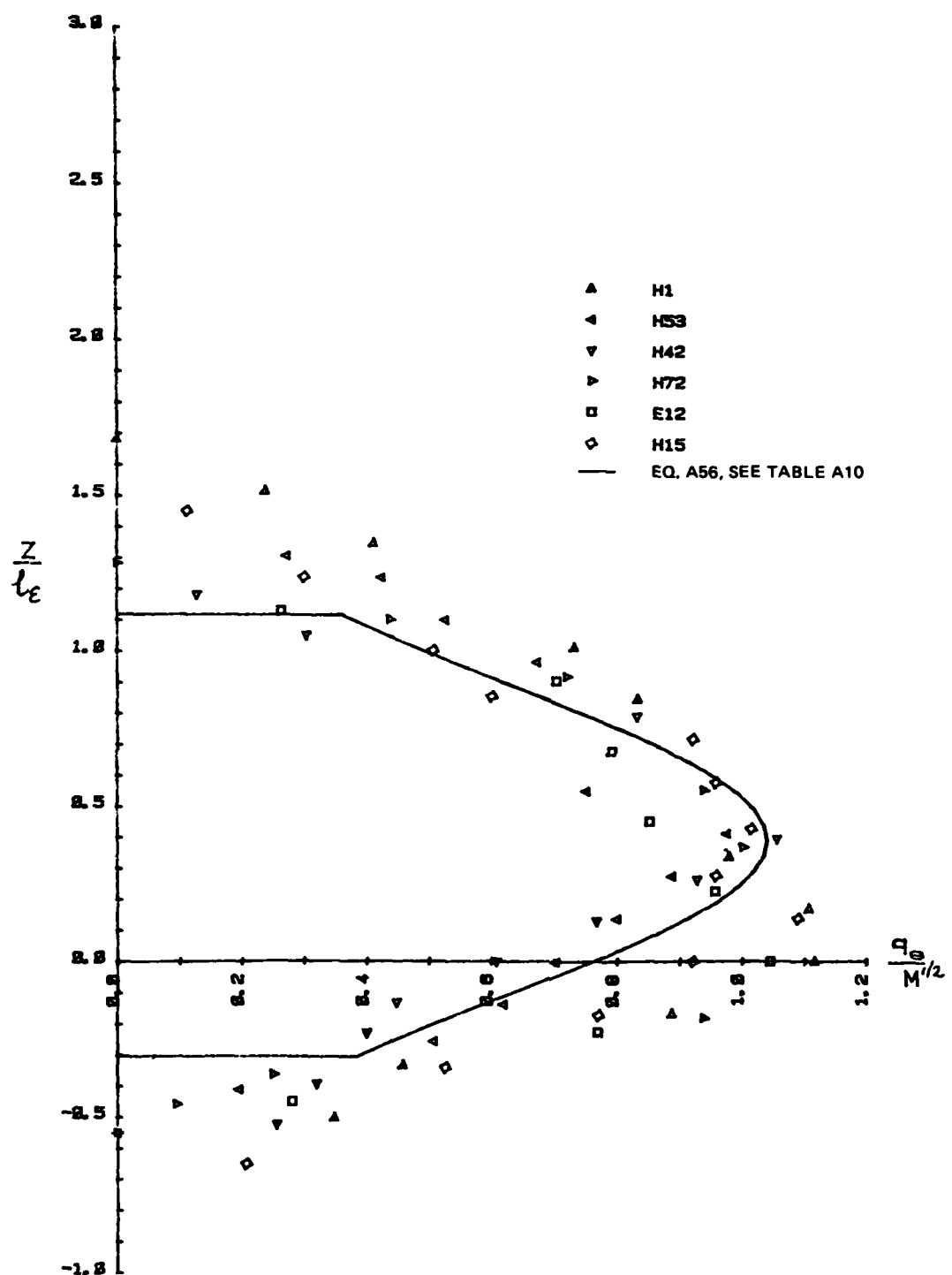
Figure A12. Distribution of entrained volume flux for horizontal slightly buoyant ($\ell_M/\ell_\varepsilon = 2$) jets in linear stratification

A17

results for volume flux (Figure A10) show a dependence on ℓ_Q , and these also approach a constant value for small ℓ_Q/ℓ_ε . This result is expected, since for distances from the origin much greater than ℓ_Q , the properties of a jet are dominated by the momentum flux M and become independent of the nozzle size (Fischer et al. 1979, Chap. 9).

24. Therefore, this series of experiments was conducted for a small nozzle size only, i.e., $\ell_Q/\ell_\varepsilon < 0.1$. Only the 0.25-in. (6.3-mm) nozzle was used. The angles of inclination θ were 22.5 deg and 45 deg, with buoyancies corresponding to $\ell_M/\ell_\varepsilon = \infty$ (nonbuoyant) and 2 (positively and negatively buoyant). The term $\ell_M/\ell_\varepsilon = -2$ denotes a negatively buoyant jet. The experimental parameters for all experiments are shown in Tables A3 and A4.

25. Photographs of typical jets are shown in Figures A13 and A14. Some of the jet characteristics, in particular the jet collapse and the rapid spreading after collapse, are similar to those for horizontal jets, as discussed in the previous section.

26. For this class of jets ℓ_Δ is again not a parameter, as there is no interfacial density jump. As previously discussed, the nozzle size is not a parameter, and so Equations A12, A15, and A18 become:

$$\frac{X_m}{\ell_\varepsilon}, \frac{W_L}{\ell_\varepsilon}, \frac{Z_L}{\ell_\varepsilon}, \frac{W_e}{\ell_\varepsilon}, \frac{Z_e}{\ell_\varepsilon}, \frac{W_m}{\ell_\varepsilon}, \frac{Z_m}{\ell_\varepsilon} = f\left(\frac{\ell_M}{\ell_\varepsilon}, \theta\right) \tag{A27}$$

$$\frac{\mu\varepsilon^{1/4}}{M^{3/4}} = f\left(\frac{\ell_M}{\ell_\varepsilon}, \theta\right) \tag{A28}$$

and

$$\frac{q_e}{M^{1/2}} = f\left(\frac{Z}{\ell_\varepsilon}, \frac{\ell_M}{\ell_\varepsilon}, \theta\right) \tag{A29}$$

The experimental results for these parameters are plotted in the form of Equations A27, A28, and A29 in Figures A15 through A27. These results are discussed further in paragraphs 30-37.
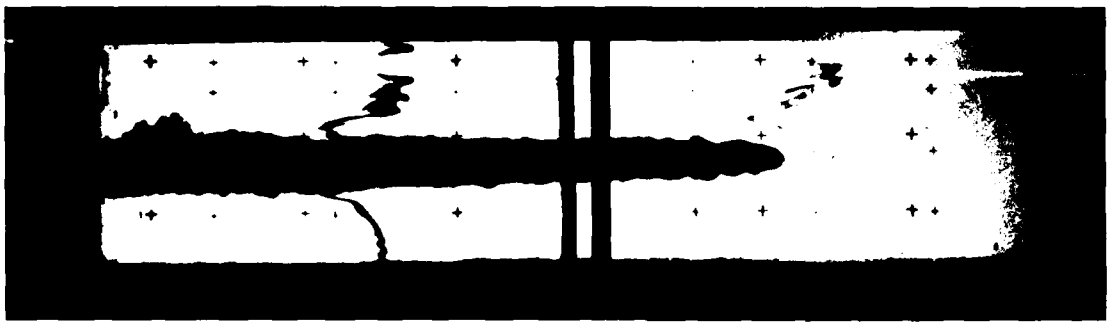
Figure A13. Side-view photograph of inclined jet (θ = 45 deg)
into linear stratification

Figure A14. Simultaneous overhead and side view (in mirror at top)
of inclined jet (θ = 45 deg) into linear stratification

A19
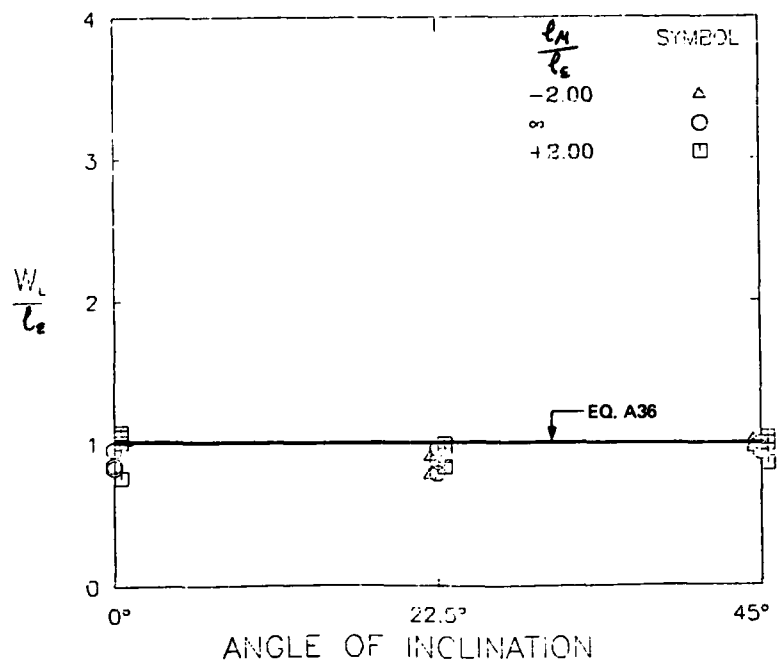
Figure A15. Experimental results for collapsed layer
thickness of inclined jets of slightly negative $(\ell_M/\ell_\varepsilon$
$= -2)$, neutral $(\ell_M/\ell_\varepsilon = \infty)$, and slightly positive buoy-
ancy $(\ell_M/\ell_\varepsilon = 2)$ into linear stratification
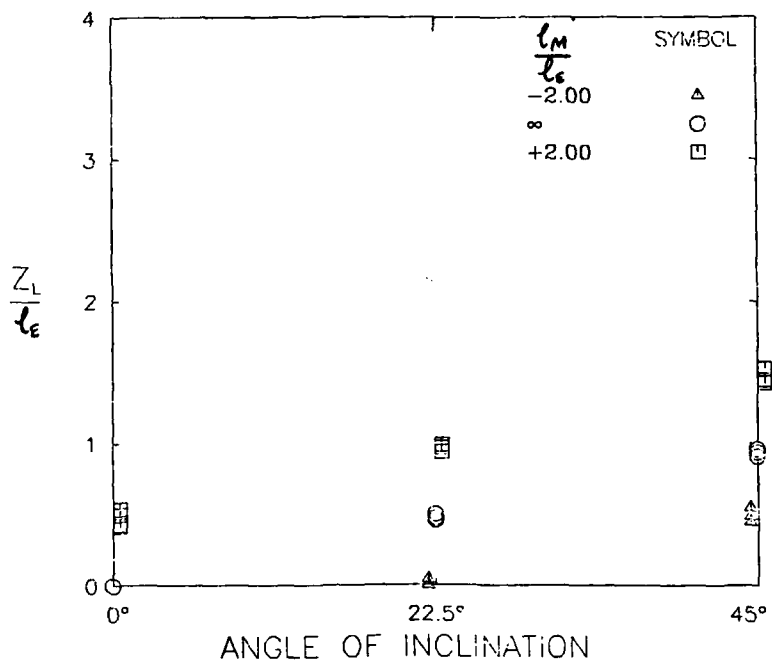
Figure A16. Experimental results for rise height of inclined jets of slightly negative ($\ell_M/\ell_\varepsilon = -2$), neutral ($\ell_M/\ell_\varepsilon = \infty$), and slightly positive buoyancy ($\ell_M/\ell_\varepsilon = 2$) into linear stratification

A21
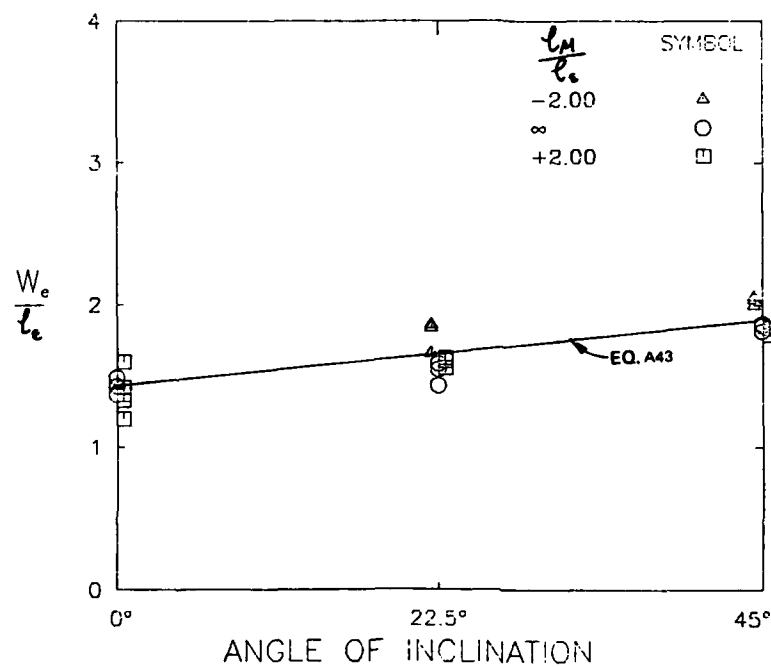
Figure A17. Experimental results for thickness of entrainment layer of inclined jets of slightly negative ($\ell_M/\ell_\varepsilon = -2$), neutral ($\ell_M/\ell_\varepsilon = \infty$), and slightly positive buoyancy ($\ell_M/\ell_\varepsilon = 2$) into

linear stratification

A22
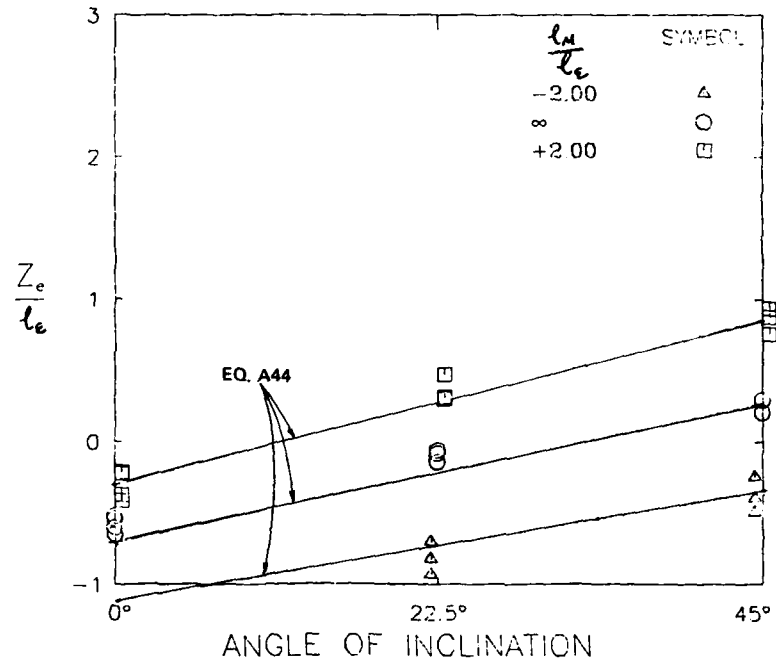
Figure A18. Experimental results for location of bottom of entrainment layers of inclined jets of slightly negative ($\ell_M/\ell_\varepsilon = -2$), neutral ($\ell_M/\ell_\varepsilon = \infty$), and slightly positive buoyancy ($\ell_M/\ell_\varepsilon = 2$) into linear stratification
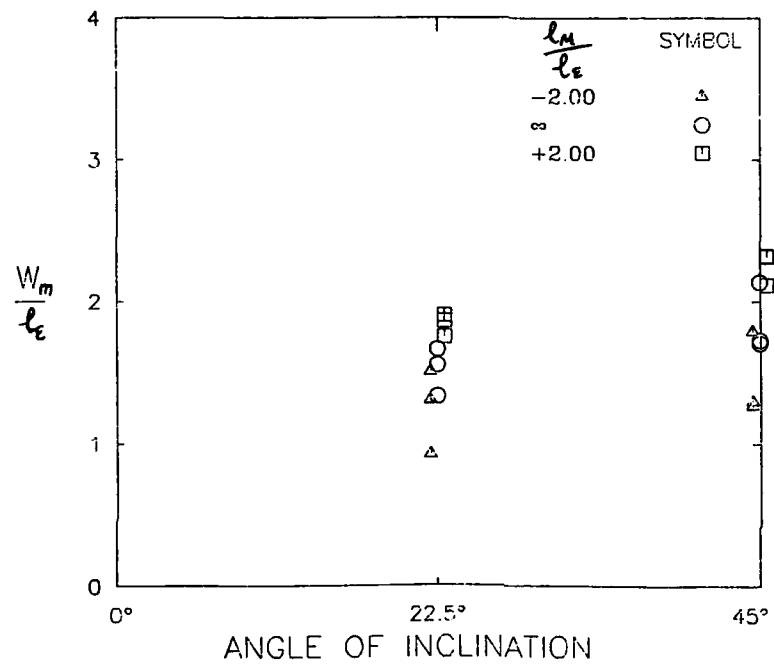
Figure A19. Experimental results for mixed layer thickness of inclined jets of slightly negative ($\ell_M/\ell_\varepsilon = -2$), neutral ($\ell_M/\ell_\varepsilon = \infty$), and slightly positive buoyancy ($\ell_M/\ell_\varepsilon = 2$) into linear stratification

A24
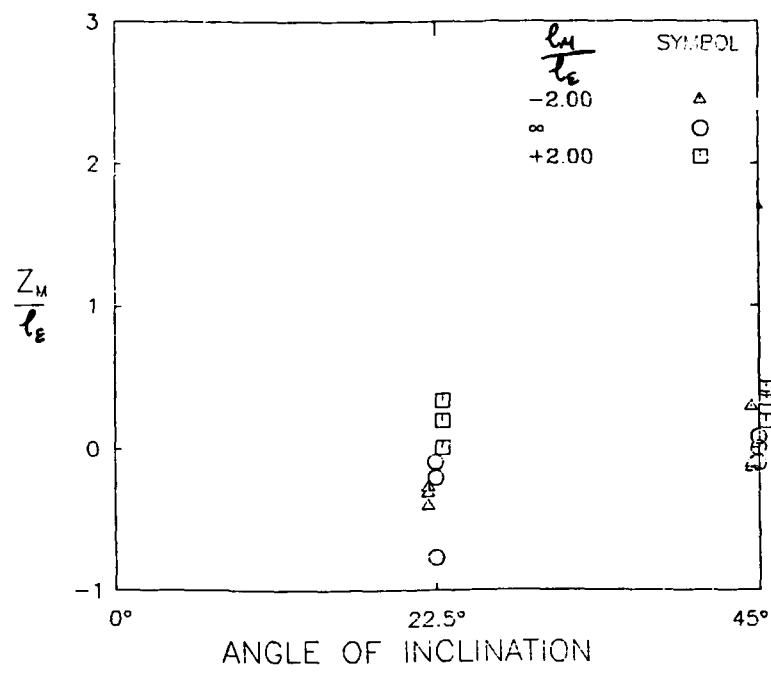
Figure A20. Experimental results for bottom of mixed layer of inclined jets of slightly negative $(\ell_M/\ell_\varepsilon = -2)$, neutral $(\ell_M/\ell_\varepsilon = \infty)$, and slightly positive buoyancy $(\ell_M/\ell_\varepsilon = 2)$ into linear stratification

A25
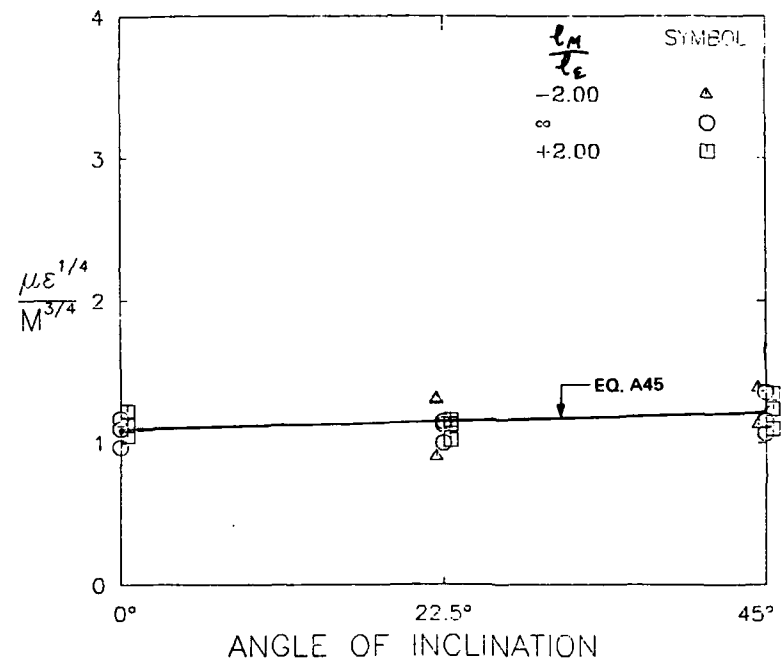
Figure A21. Experimental results for entrained volume flux of inclined jets of slightly negative ($\ell_M/\ell_\varepsilon = -2$), neutral ($\ell_M/\ell_\varepsilon = \infty$), and slightly positive buoyancy ($\ell_M/\ell_\varepsilon = 2$) into linear stratification
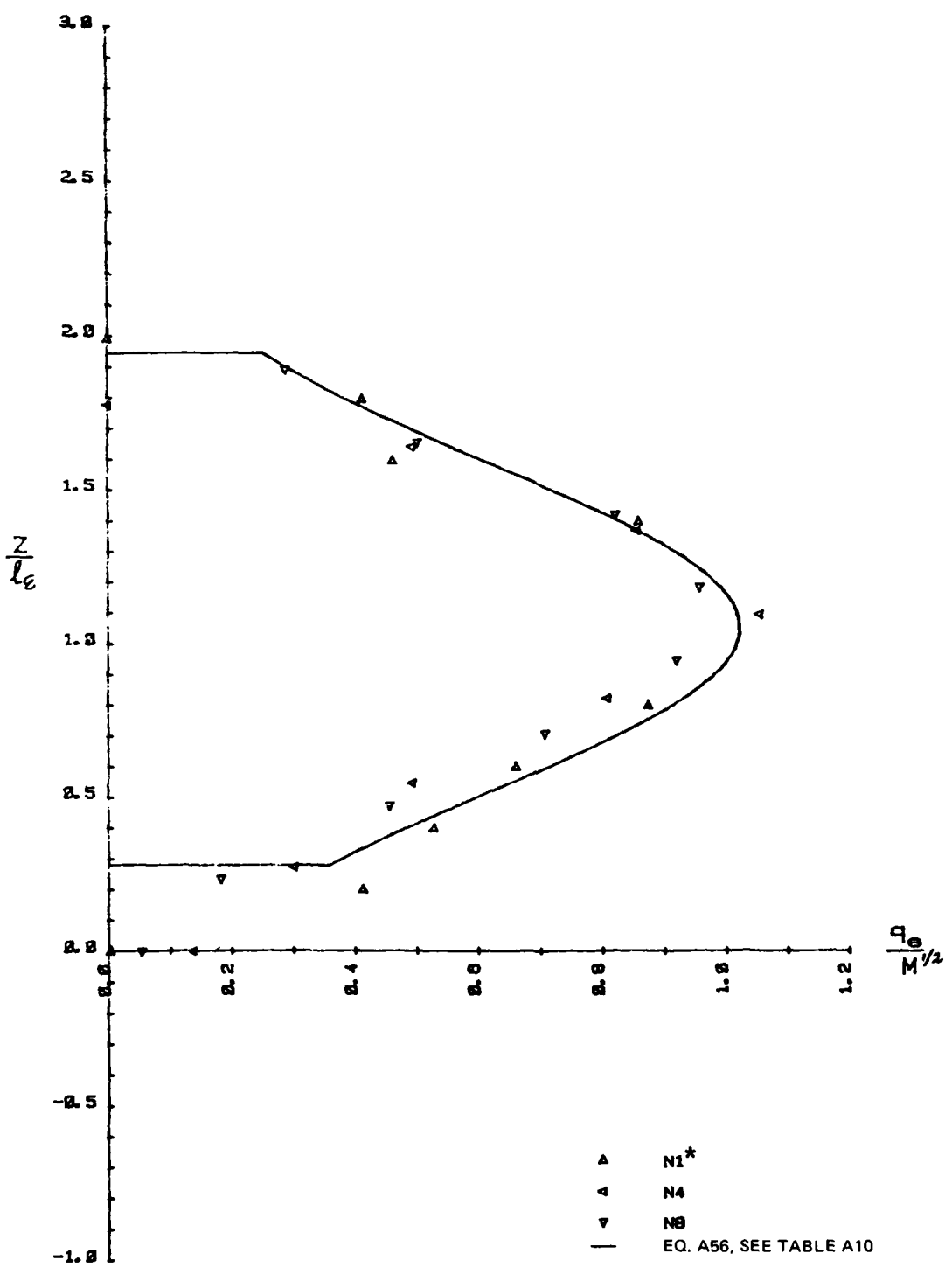
Figure A22. Distribution of entrained volume flux into inclined jet, θ = 22.5 deg, slightly buoyant ($\ell_M/\ell_\epsilon = 2$) (*Referenced to test conditions shown in data tables)

$\dfrac{Z}{\ell_\mathcal{E}}$

3.0

2.5

2.0

1.5

1.0

0.5

0.0

-0.5

-1.0

$\dfrac{q_e}{M^{1/2}}$

0.0 0.2 0.4 0.6 0.8 1.0 1.2

△   N3
◄   N6
▽   N7
—   EQ. A56, SEE TABLE A10
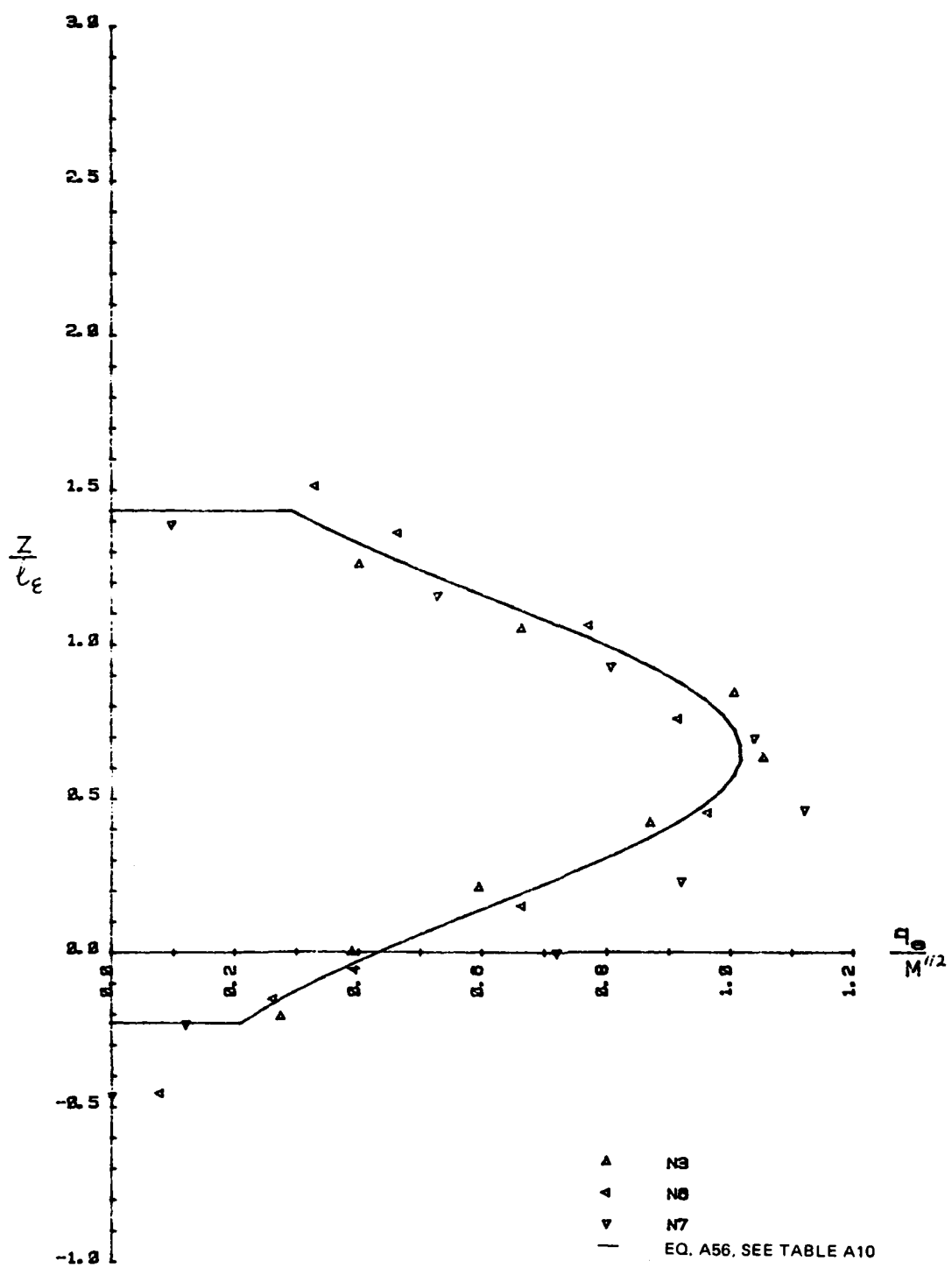
Figure A23.   Distribution of entrained volume flux into inclined jet, $\theta = 22.5$ deg, neutrally buoyant $(\ell_M/\ell_\mathcal{E} = \infty)$

A28
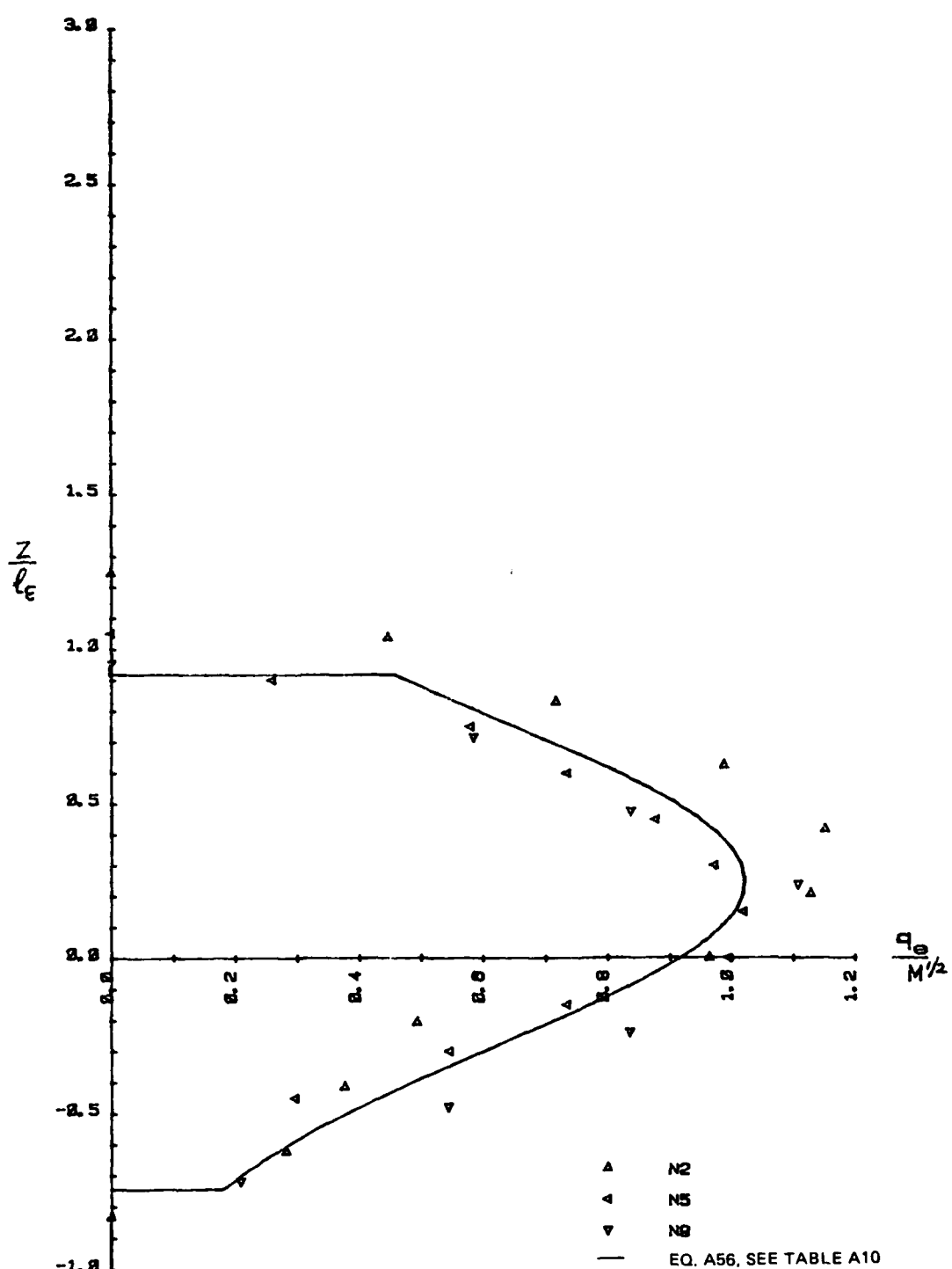
Figure A24. Distribution of entrained volume flux into inclined jet, $\theta = 22.5$ deg, slightly negative buoyancy ($\ell_M/\ell_\varepsilon = -2$)

$\dfrac{Z}{\ell_\varepsilon}$

3.8 —

2.5

2.8

1.5

1.8

2.5

2.8

-2.5

-1.8

$\dfrac{q_e}{M^{1/2}}$

8.8   8.2   8.4   8.6   8.8   1.8   1.2

▲   M1
◄   M5
▼   M7
—   EQ. A56, SEE TABLE A10
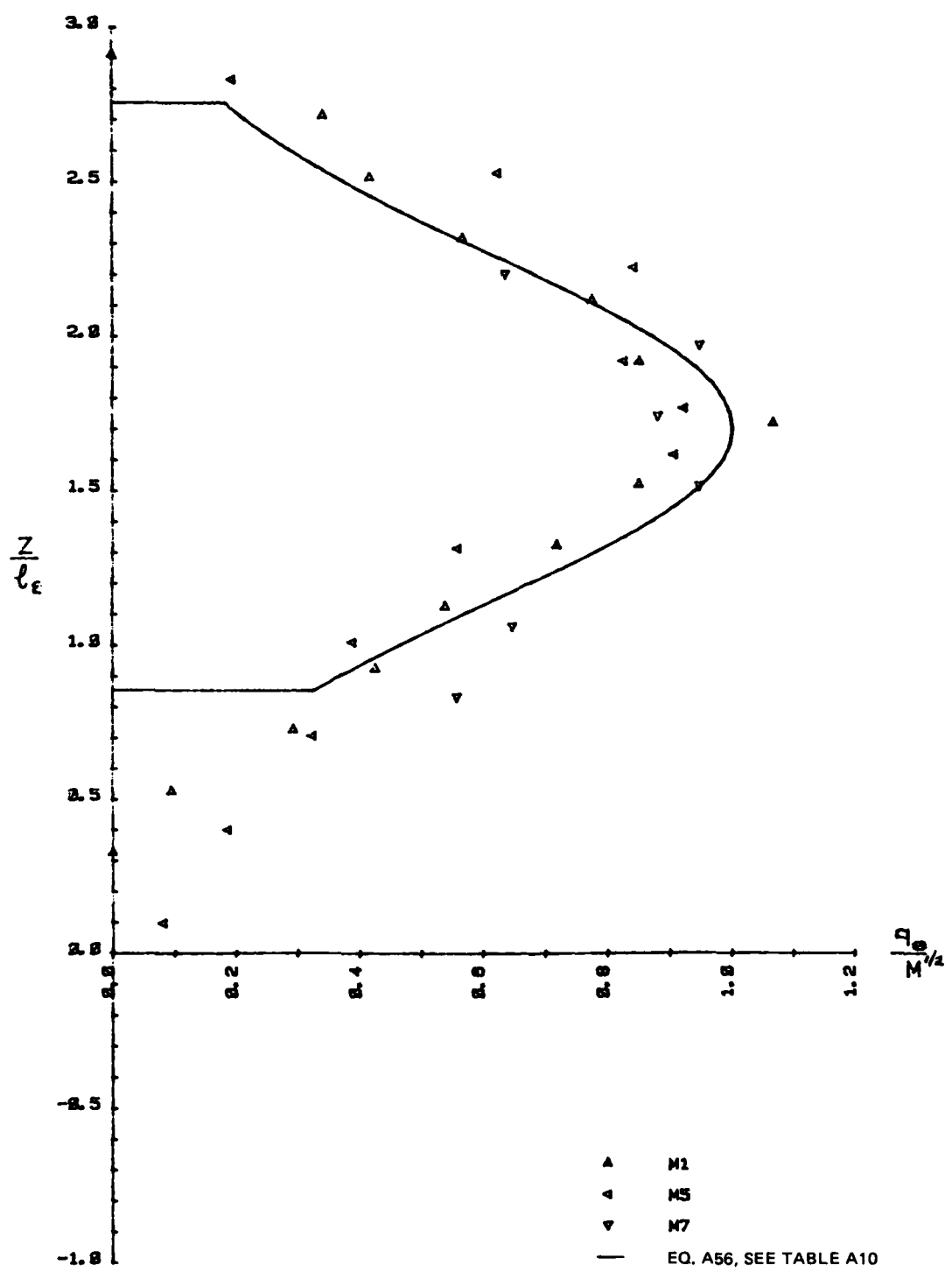
Figure A25.   Distribution of entrained volume flux into inclined jet,
θ = 45 deg, slightly buoyant $(\ell_M/\ell_\varepsilon = 2)$

A30
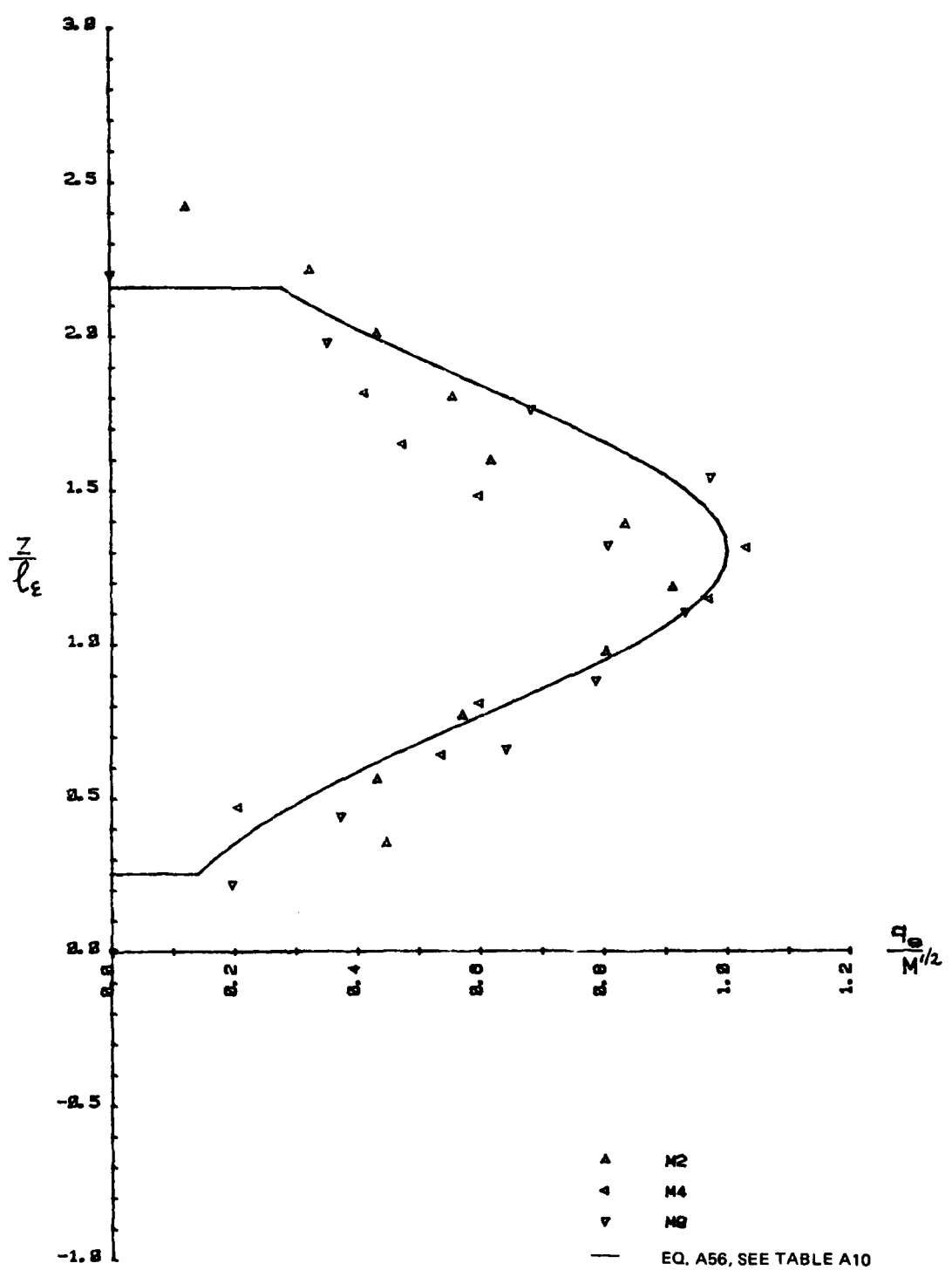
Figure A26. Distribution of entrained volume flux into inclined jet, θ = 45 deg, neutrally buoyant ($\ell_M/\ell_\varepsilon = \infty$)

A31
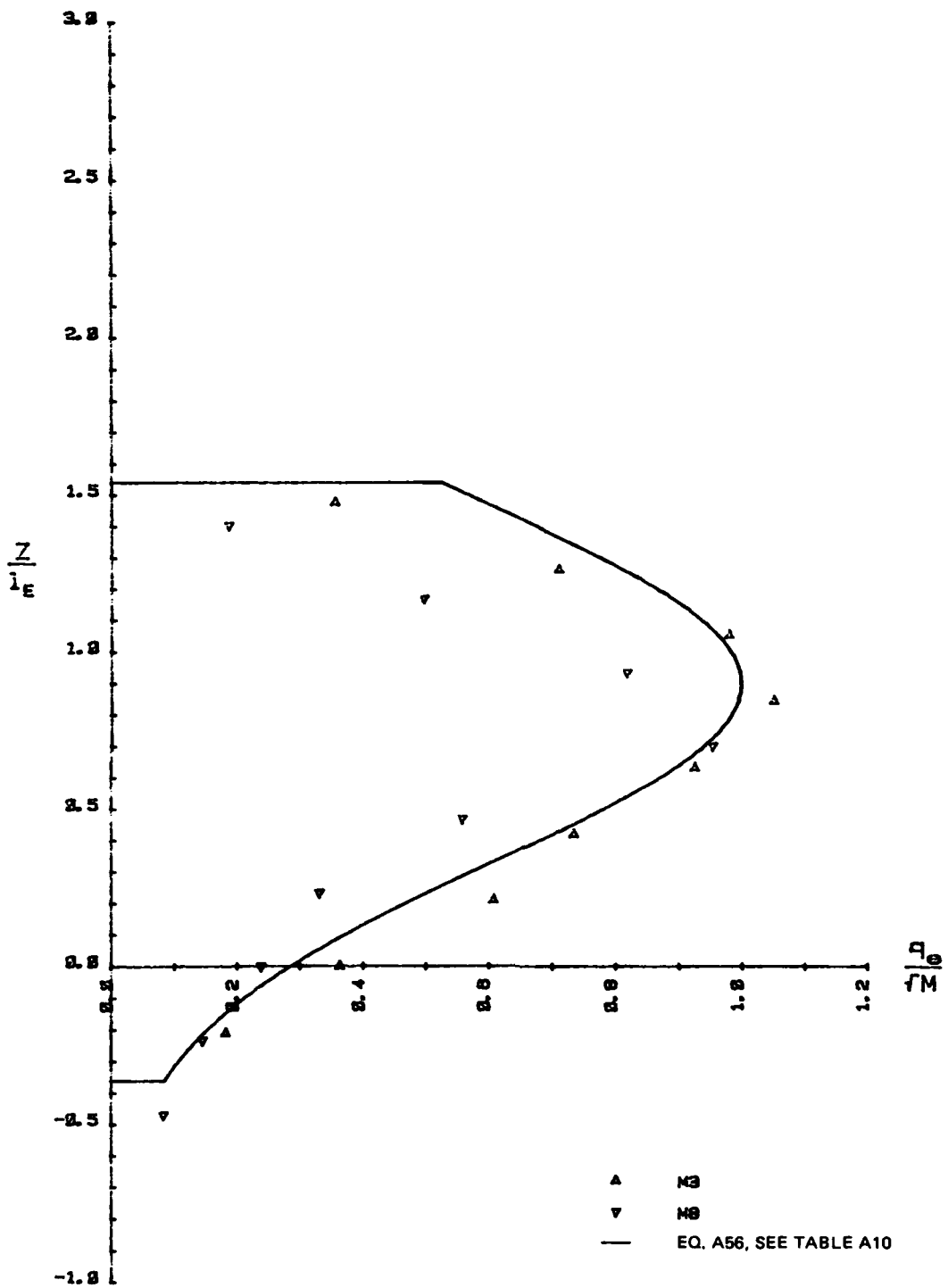
Figure A27. Distribution of entrained volume flux into inclined jet, θ = 45 deg, slightly negative buoyancy ($\ell_M/\ell_\varepsilon = -2$)

Horizontal nonbuoyant jets
into two-layer stratification

27. The form of the stratification for these experiments is as shown in Figure A1. A well-mixed upper layer overlies a linearly stratified lower layer. The layers are separated by a density jump of magnitude $\Delta\rho$. Only horizontal nonbuoyant jets were considered. As in the previous section, the 0.25-in. (6.3-mm) nozzle was used and $\ell_Q/\ell_\varepsilon < \sim 0.1$, so that effects of ℓ_Q could be neglected. Equations A12, A13, and A15 then become:

$$\frac{X_m}{\ell_\varepsilon}, \frac{W_L}{\ell_\varepsilon}, \frac{Z_L}{\ell_\varepsilon}, \frac{W_e}{\ell_\varepsilon}, \frac{Z_e}{\ell_\varepsilon}, \frac{W_m}{\ell_\varepsilon}, \frac{Z_m}{\ell_\varepsilon} = f\left(\frac{h}{\ell_\varepsilon}, \frac{h}{\ell_\Delta}\right) \tag{A30}$$

$$\text{stability} = f\left(\frac{h}{\ell_\varepsilon}, \frac{h}{\ell_\Delta}\right) \tag{A31}$$

and

$$\frac{\mu\varepsilon^{1/4}}{M^{3/4}} = f\ \frac{h}{\ell_\varepsilon}, \frac{h}{\ell_\Delta} \tag{A32}$$

Equation A18 becomes:

$$\frac{q_e}{M^{1/2}} = f\left(\frac{Z}{\ell_\varepsilon}, \frac{h}{\ell_\varepsilon}, \frac{h}{\ell_\Delta}\right) \tag{A33}$$

28. Parameters for all experiments are shown in Tables A5 and A6. Photographs of typical experiments are shown in Figures A28 and A29. In Figure A28, the jet is submerged well below the density jump, and the appearance of the jet is very similar to that in a continuous linear stratification, Figure A3. The jet in Figure A29 is closer t₁ the interface, the effect of which is to sharply suppress the turbulence there, causing a flattened top to the jet.
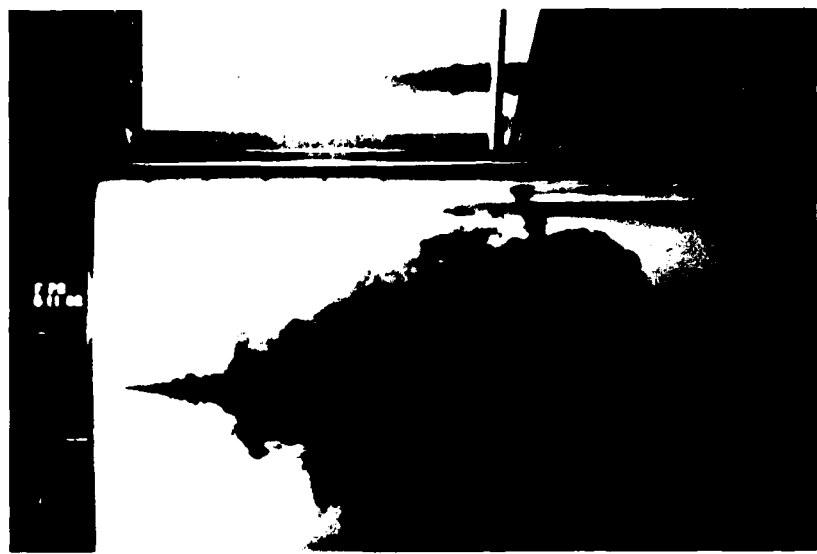
Figure A28. Simultaneous overhead and side view (in mirror at top) of horizontal nonbuoyant jet in two-layer stratification. Jet is well below interface.
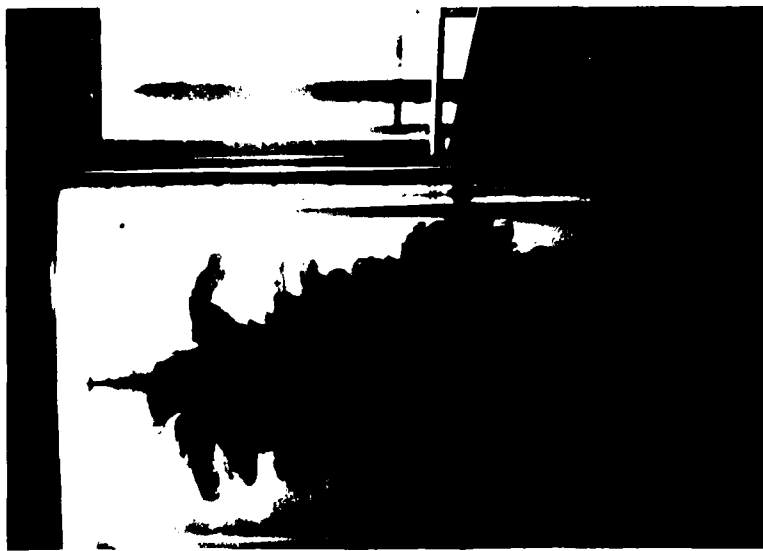
Figure A29. Simultaneous overhead and side view (in mirror at top) of horizontal nonbuoyant jet in two-layer stratification. Jet is near interface.

A34

29. Experimental results, presented in the form of Equations A30, A31, and A32, are given in Figures A30 through A36. The entrained flow distribution is shown in Figure A37 for jets far from the interface ($h/\ell_\varepsilon > 0.7$) and in Figure A38 for jets near the interface ($h/\ell_\varepsilon < 0.7$).

Discussion

30. A great deal of data were collected during the course of the three sets of experiments. In this section, only the results pertinent to the modeling of PS reservoirs will be discussed. Further discussion can be found in a number of journal articles prepared on these results (Roberts and Matthews 1984, for example).

31. Discussion of the analysis of the effects of inflow angle, source volume, momentum, and buoyancy fluxes, and ambient stratification parameters by dimensional and length scale arguments was presented in paragraphs 5-13. Perhaps the most important result is that the experiments confirmed these results. The effect of each parameter is summarized below, and then limited equations are presented to summarize the results. The discussion applies only to the range for which experiments were conducted; that is, high momentum, low buoyancy, for which $\ell_M/\ell_\varepsilon \geq 2$; $\ell_Q/\ell_\varepsilon < {\sim}1$.

32. The nozzle size ℓ_Q does not play a significant role, as expected. For volume flux, the results are independent of ℓ_Q for $\ell_Q/\ell_\varepsilon < 0.2$ (Figure A10). The effect on collapse width, entrainment width, entrainment layer location, buoyant jet rise height, and entrained volume flux distribution is even less, the results being independent of ℓ_Q for $\ell_Q/\ell_\varepsilon < {\sim}0.5$, as shown in Figures A6 through A9. For this reason, the effect of ℓ_Q was neglected in the subsequent experiments, series 2 and 3, where ℓ_Q/ℓ_ε was kept less than 0.1.

33. The dominant parameters for all experiments were the momentum flux M and the stratification parameter ε . The collapsed layer thickness (Figures A6, A15, and A30) depended only on M and ε . Other parameters are also primarily controlled by M and ε , although their values are slightly modified by the inclination angle and buoyancy. For

A35
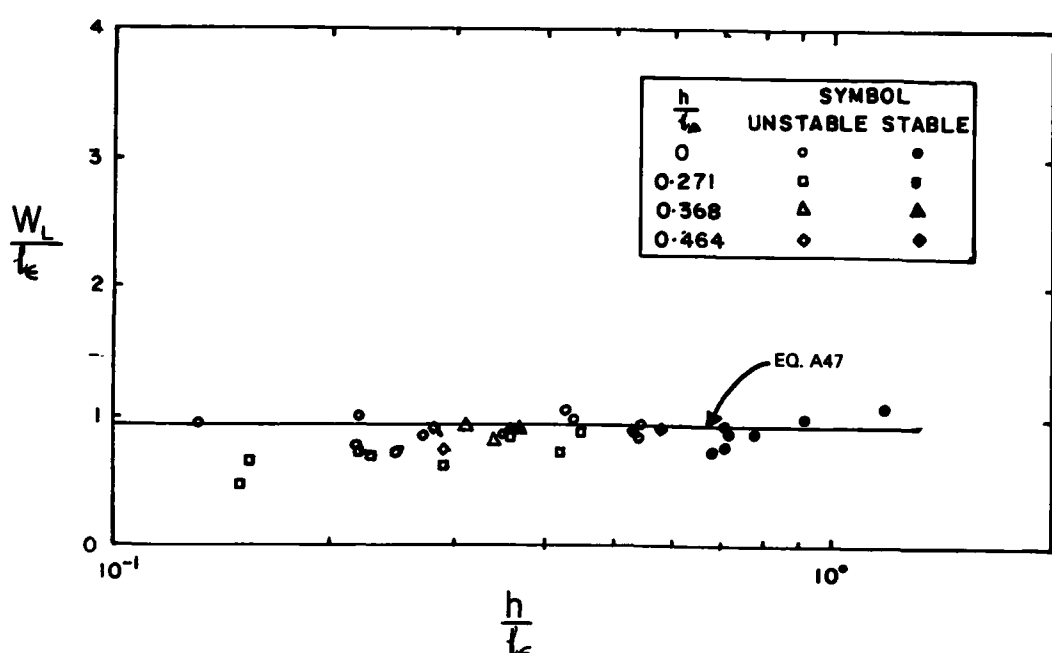
Figure A30. Experimental results for collapsed layer thickness of horizontal nonbuoyant jet into two-layer stratification
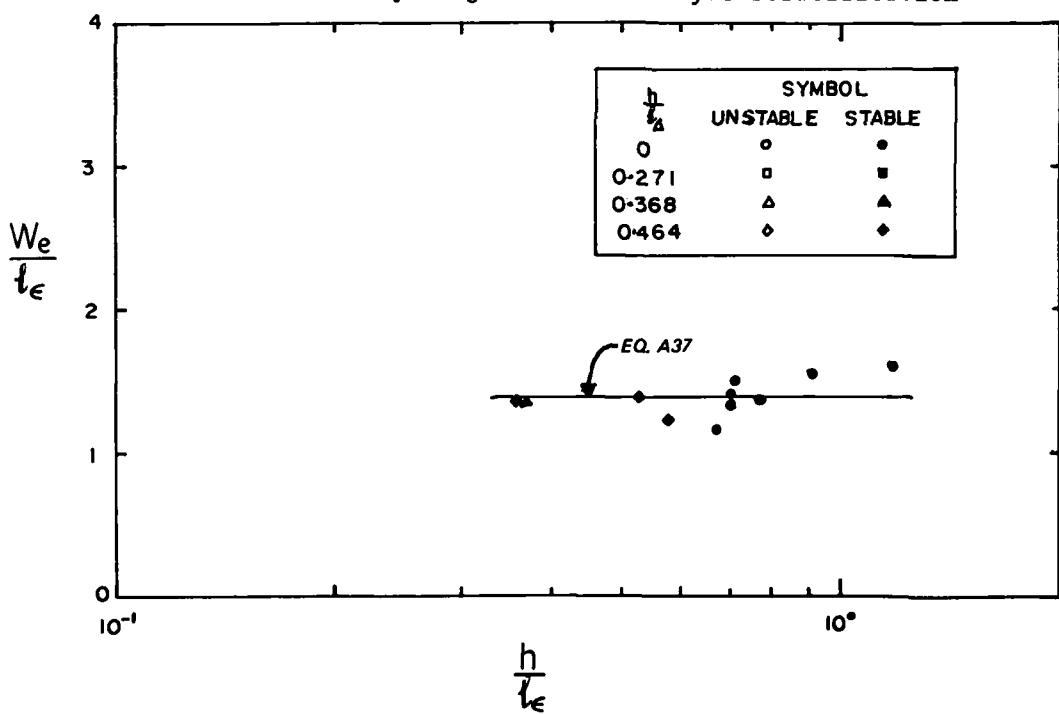
Figure A31. Experimental results for entrained layer thickness of horizontal nonbuoyant jet into two-layer stratification

A36
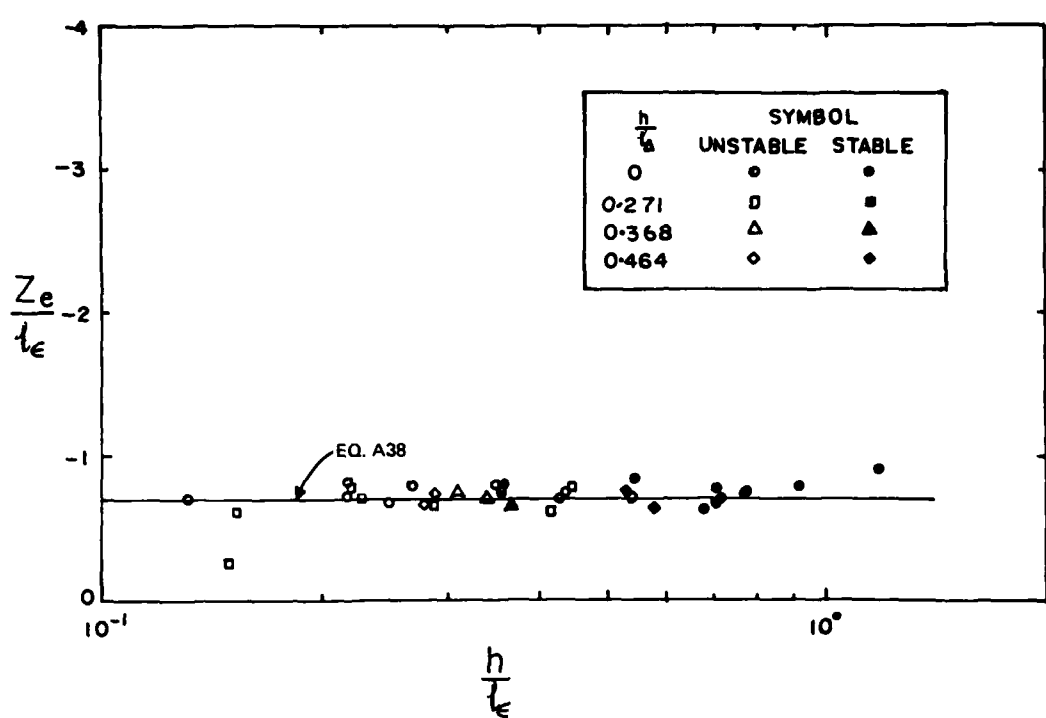
Figure A32.   Location of bottom of entrained layer thickness of horizontal nonbuoyant jet into two-layer stratification
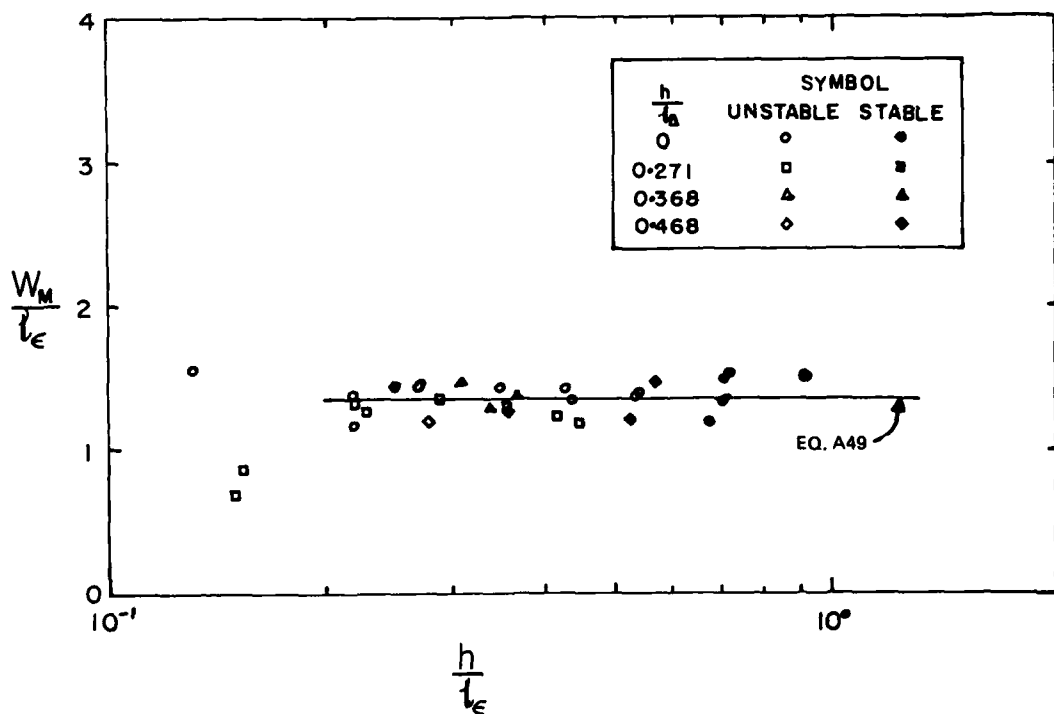
Figure A33.   Mixed layer thickness of horizontal nonbuoyant jet into two-layer stratification

A37
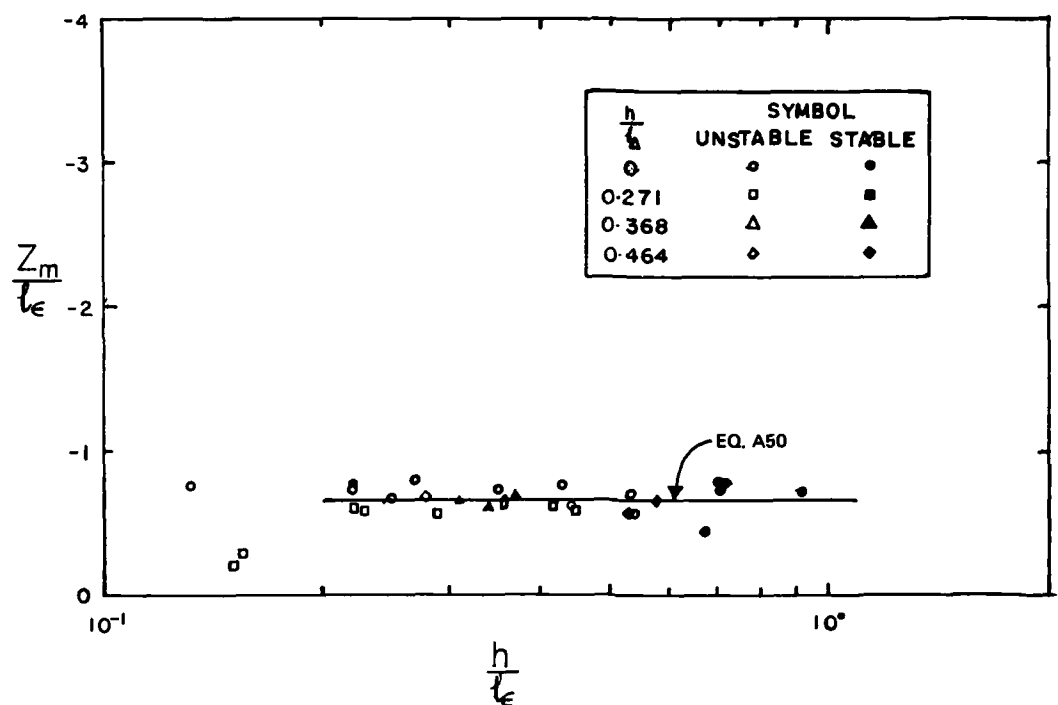
Figure A34.   Location of bottom of mixed layer of horizontal
nonbuoyant jet into two-layer stratification
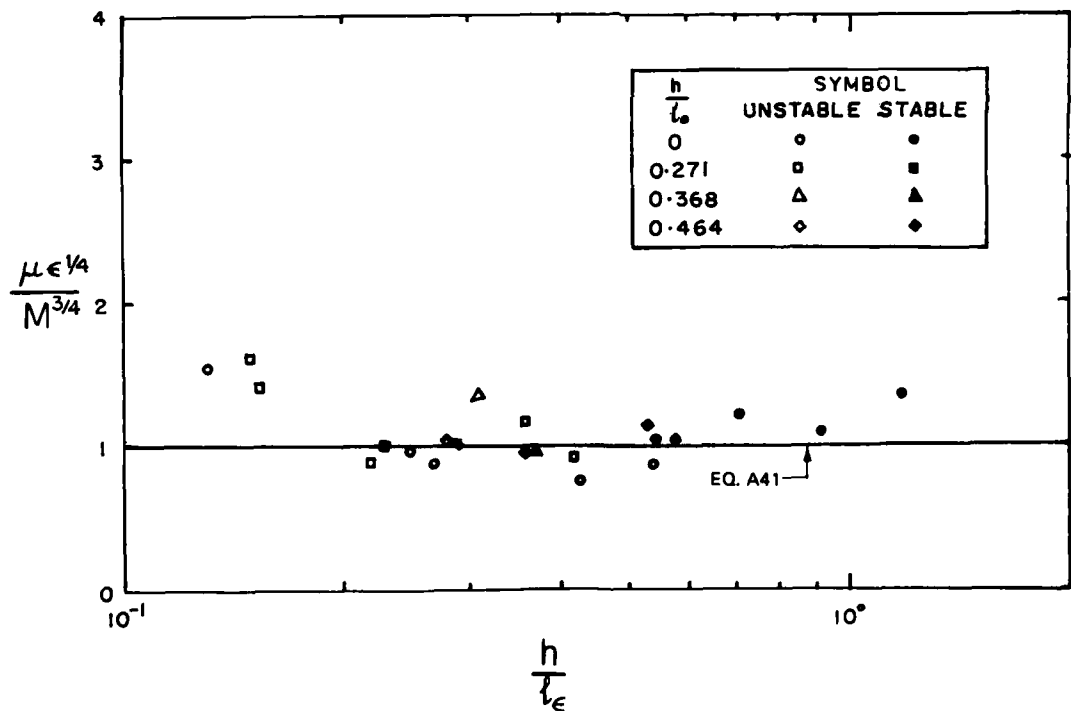
Figure A35.   Entrained volume flux of horizontal nonbuoyant
jet into two-layer stratification

A38
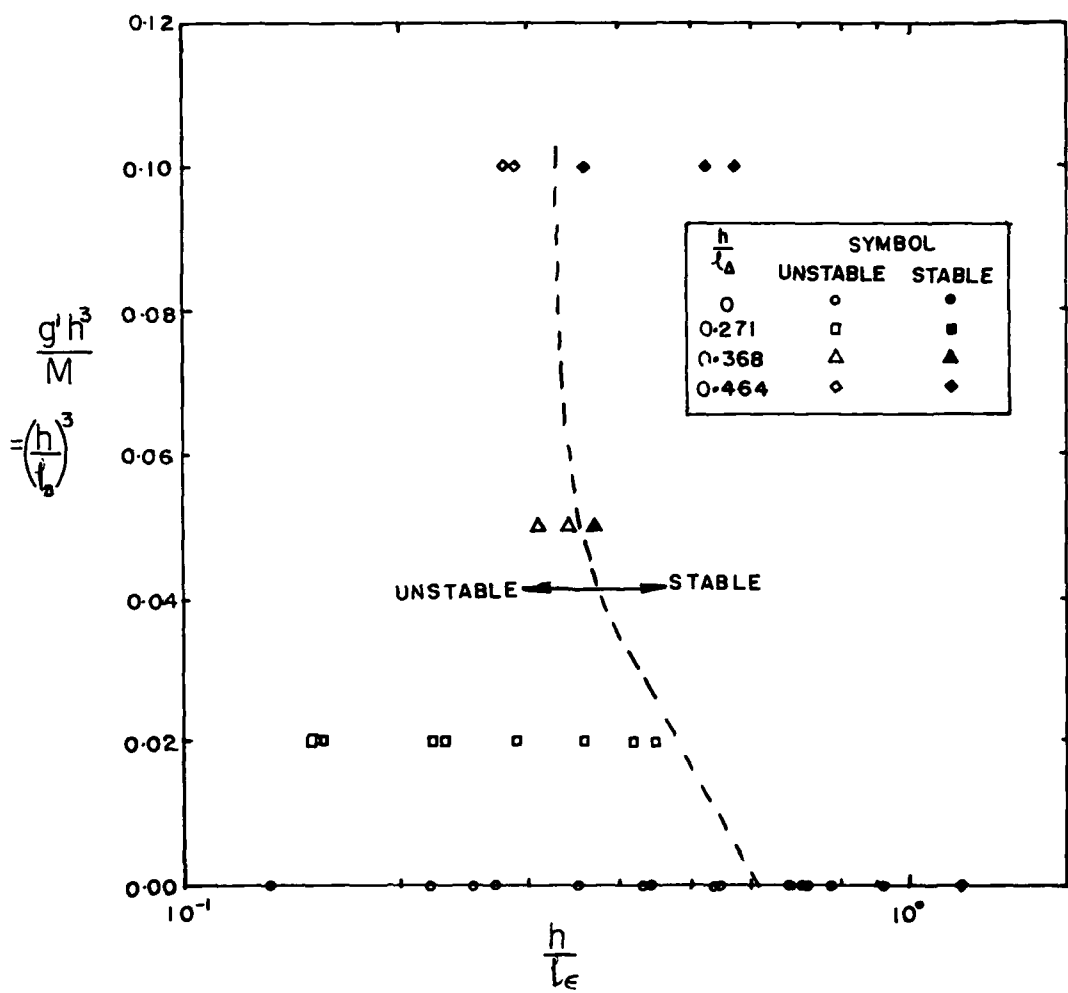
Figure A36. Stability of horizontal nonbuoyant jet into two-layer stratification. Stable signifies no entrainment through the density interface.

A39
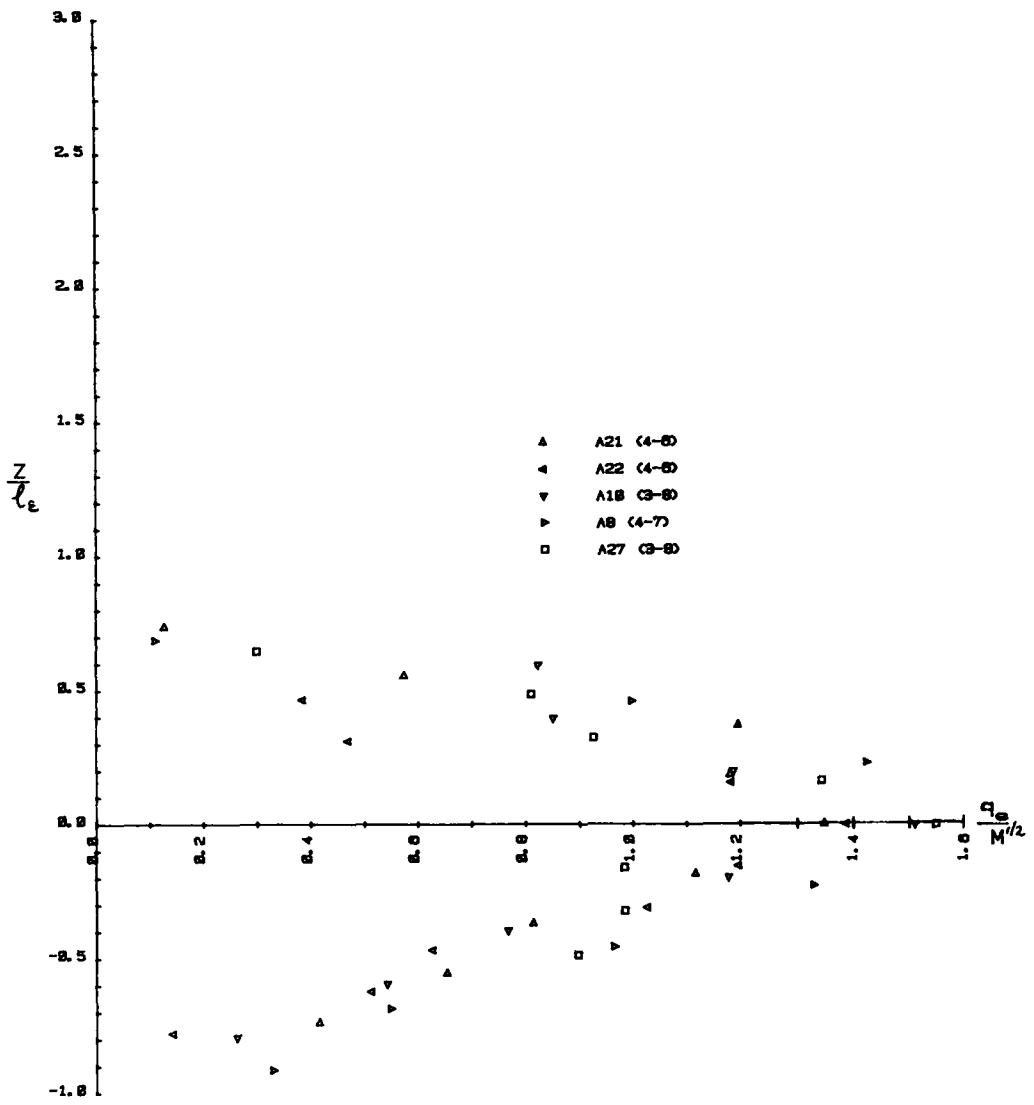
Figure A37. Distribution of entrained volume flux caused
by a horizontal nonbuoyant jet into two-layer stratifica-
tion. Jet far from interface ($h/\ell_\varepsilon > 0.7$).

A40
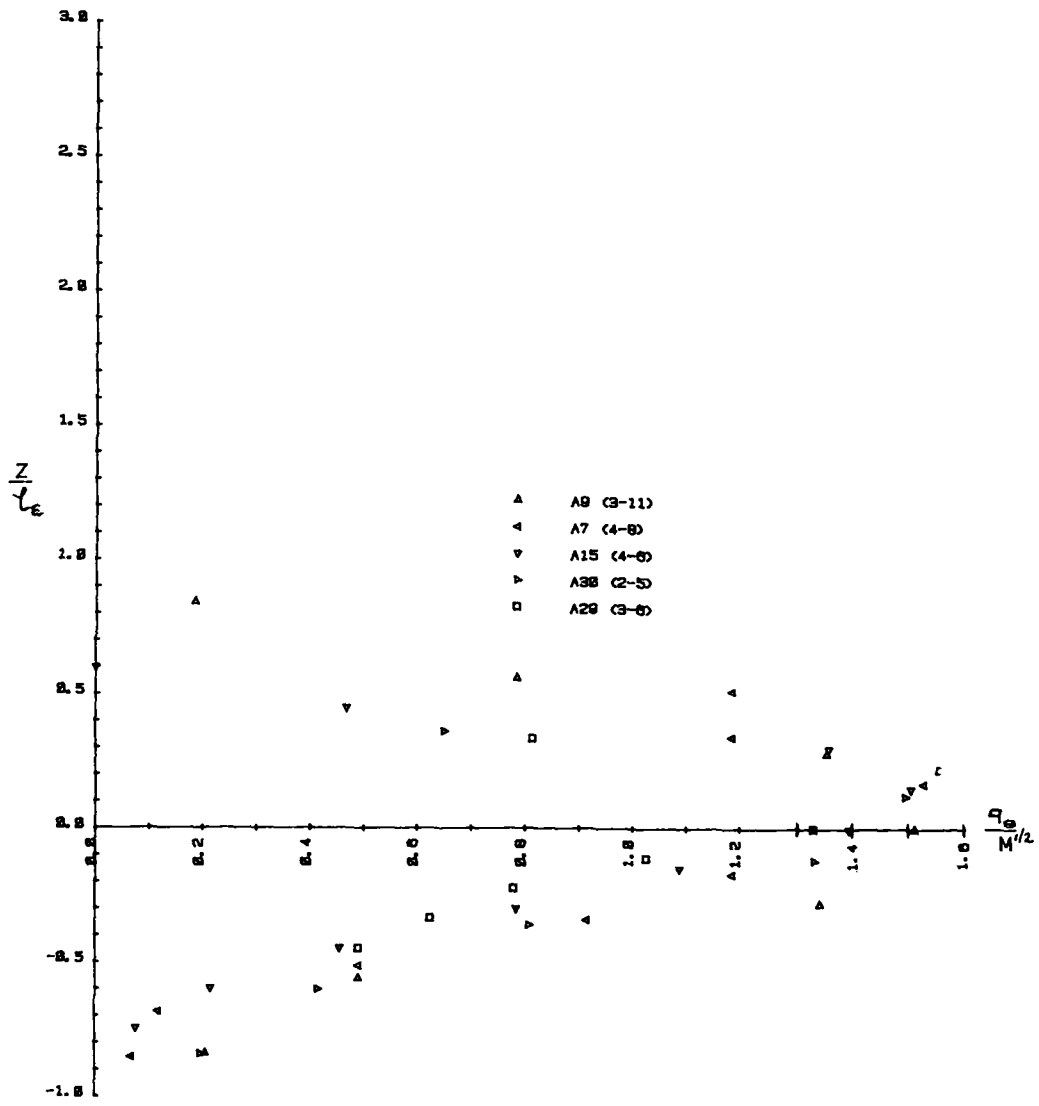
Figure A38. Distribution of entrained volume flux caused by a horizontal nonbuoyant jet into two-layer stratification. Jet near interface ($h/\ell_\varepsilon < 0.7$).

A41

example, the entrainment width and total volume flux are independent of buoyancy, but vary with the angle of the PS inflow (Figures A7, A10, A17, A21, A31, A35).

34. The effect of the buoyancy flux B is primarily on the rise height and the location of the entrainment layer bottom (Figures A8, A16, and A18). The effect of B on all other parameters can be neglected for $\ell_M/\ell_\varepsilon \geq 2$. The rise height and entrainment layer bottom are also affected by the angle of inflow θ, as shown in Figures A16 and A18. The thickness of the entrainment layer W_e is also affected by θ, becoming thicker as θ increases (Figure A17). The total volume flux also increases with θ (Figure A21), although the dependence is weak.

35. The presence of the interfacial density jump in the two-layer experiments (Figures A30-A35) does not affect the gross flow parameters significantly. The collapsed layer thickness is apparently reduced as the jet is moved near to the interface (Figure A30). One interesting effect is that the maximum value of the entrained volume flux distribution (Figures A37 and A38) does appear to be substantially increased over that in a continuous linear stratification. The reason for this is not presently known, but it may be caused by differing internal circulations and wave patterns. The scatter of the total volume flux results (Figure A35) makes it difficult to deduce definite conclusions on the effects of the interface on the entrained flow distribution.

36. With these observations, it is now possible to deduce limiting formulas for the equations presented in paragraphs 20-29. For example, Equation A12 for the entrainment layer thickness of a horizontal jet in a linear stratification is:

$$\frac{W_e}{\ell_\varepsilon} = f\left(\frac{\ell_Q}{\ell_\varepsilon}, \frac{\ell_M}{\ell_\varepsilon}\right) \tag{A34}$$

For $\ell_Q/\ell_\varepsilon \ll 1$, and neutrally buoyant, $\ell_M/\ell_\varepsilon = \infty$, Equation A34 becomes:

A42

$$\frac{W_e}{\ell_\varepsilon} = C_1 \qquad\qquad (A35)$$

where C_1 is an experimental constant. The results of Figure A7 suggest a value of 1.40 for C_1. Figure A7 also shows the value of C_1 to apply to slightly buoyant jets, $\ell_M/\ell_\varepsilon = 2$, and to be valid for values of ℓ_Q/ℓ_ε up to about 0.5. Therefore, Equation A35 can be written:

$$\frac{W_e}{\ell_\varepsilon} = 1.40 \text{ for } \frac{\ell_M}{\ell_\varepsilon} \geq 2 \;,\; \frac{\ell_Q}{\ell_\varepsilon} \leq 0.5 \qquad\qquad (A37)$$

37. Similar reasoning (see paragraph 36) can be applied to the other results given. The resulting formulas (Equations 36-50) are presented in Tables A7-A9, along with their range of limitation, and are plotted on the graphs where appropriate.

Entrained Volume Flux Distribution

38. The distribution of entrained volume flux with height is given in dimensionless form by Equations A18 and A19, and plotted in the previous sections. For the purpose of using these results for numerical modeling of entrainment in PS reservoirs, it is convenient to use empirical curves to describe this entrainment distribution. Consider first the horizontal, neutrally buoyant jet in linear stratification. Equations A18 and A19 for this case become:

$$\frac{q_e}{M^{1/2}} = f\left(\frac{Z}{\ell_\varepsilon}, \frac{\ell_Q}{\ell_\varepsilon}\right) \qquad\qquad (A51)$$

and

$$\frac{q_{em}}{M^{1/2}} = f\left(\frac{\ell_Q}{\ell_\varepsilon}\right) \qquad\qquad (A52)$$

A43

39. Following the arguments of paragraphs 30-37, the effect ℓ_Q/ℓ_ε can be neglected, if small. Thus, Equations A51 and A52 become:

$$\frac{q_e}{M^{1/2}} = f\left(\frac{Z}{\ell_\varepsilon}\right) \qquad (A53)$$

and

$$\frac{q_{em}}{M^{1/2}} = C_2 \qquad (A54)$$

where C_2 is an experimental constant. The distribution expressed by Equation A53 is shown in Figure A11, which suggests a value of 1.04 for C_2. We will now assume that the distribution of Equation A53 can be expressed approximately as Gaussian, i.e.:

$$\frac{q_e}{M^{1/2}} = \frac{q_{em}}{M^{1/2}} \exp\left[-\left(\frac{\eta}{b}\right)^2\right] \qquad (A55)$$

where $q_{em}/M^{1/2}$ is given by Equation A54, $\eta = Z/\ell_\varepsilon$, and b (see Equation A61) is characteristic of the entrainment width. Equation A55 is shown plotted in Figure A11 between the limits Z_e to $Z_e + W_e$ with a value of b of 0.65, and gives a good fit to the data.

40. To extend this distribution to the other cases, we also assume a Gaussian distribution not centered on the origin, i.e.:

$$\frac{q_e}{M^{1/2}} = \frac{q_{em}}{M^{1/2}} \exp\left[-\left(\frac{\eta - \eta_o}{b}\right)^2\right] \qquad (A56)$$

The task is to find the values of $q_{em}/M^{1/2}$, η_o, and b for all cases.

41. Based on the previous results, the rise height, represented by η_o; the entrainment width, represented by b; and $q_{em}/M^{1/2}$ would be expected to be primarily dependent on ℓ_M/ℓ_ε and θ, with the nozzle size ℓ_Q being of secondary importance. That is:

$$\frac{q_{em}}{M^{1/2}} \ , \ \eta_o \ , \ b = f\left(\frac{\ell_M}{\ell_\varepsilon} \ , \ \theta\right) \tag{A57}$$

42. Equation A56 must also satisfy the earlier constraints on the total volume flux, μ , when integrated between the lower and upper limits of the entrained volume flux distribution. That is:

$$Q_e = \int_{Z_e}^{Z_e + W_e} q_e \ dz \tag{A58}$$

On substituting Equations A8, A56, A6, and A22 into Equation A58, we obtain, after considerable manipulation:

$$\frac{\mu \varepsilon^{1/4}}{M^{3/4}} = \frac{\sqrt{\pi} \ q_{em}}{2M^{1/2}} \ b \ \left[erf\left(\frac{Z_\varepsilon/\ell_\varepsilon + W_\varepsilon/\ell_\varepsilon - \eta_o}{b}\right) \right.$$

$$\left. - erf\left(\frac{Z_e/\ell_\varepsilon - \eta_o}{b}\right) \right] + \frac{\ell_Q}{\ell_\varepsilon} \tag{A59}$$

which must be consistent with the earlier obtained values of total volume flux. The empirical formulas fitted to Equation A57, along with those used for W_e and Z_e are shown in Table A10.

43. The assumed entrained flow distribution Equation A56, with parameters computed from the equations given in Table A10, is plotted along with the experimental results in Figures A11-A12 and A22-A27. The assumed distribution gives a good fit in all cases. As a further check, the total volume flux was computed from Equation A59 and compared to the experimental results of Figures A10 and A21. The values computed in this way were from 7 to 11 percent higher than those measured directly. Considering the experimental errors involved, this is an acceptable fit.

Concluding Remarks

44. A great deal of experimental data were collected during this study, as summarized in this appendix. The results are presented in a form suitable for direct inclusion into a PS reservoir model. Of these results, many are of a fundamental nature, and the constants obtained are fundamental. These include the constants for nonbuoyant horizontal jets into linear stratification, with $\ell_Q/\ell_\varepsilon \ll 1$, for example: Equations A36, A37, A38, A41, and A42; and for buoyant jets with $\ell_M/\ell_\varepsilon = 2$, Equations A39 and A40.

45. The extension of the nonbuoyant results to buoyant jets and the other empirical formulas for inclined jets shown in Tables A7-A9 are approximations which the results show to be good ones. Finally, the fitted Gaussian curves to the entrained flow distribution and associated empirical formulas (Table A10) are also approximations which the results show to be good ones. These approximate formulas make the prediction of entrained volume distribution an easy task within the parameter range with which this study is concerned.

Table A1

Summary of Experimental Parameters for Horizontal Neutral and

Slightly Buoyant Jets in Linear Stratification

Run No.	Nozzle Diam, d cm	Discharge Rate, Q cm³/sec	Density Difference $\rho_a - \rho_\sigma$ σ_t	Stratification Parameter, ε sec⁻²	Entrainment Width, W_e cm	Location of Entrainment Bottom, Z_e cm	Collapsed Layer Thickness W_L cm	Rise Height Z_L cm	Total Volume Flux, μ cm³/sec
B10	0.635	7.57	0	1.17	5.21	-2.41	--	0	--
B11	0.635	11.0	0	1.14	6.22	-3.18	3.59	0	--
B12	0.635	16.4	0	0.646	7.11	-3.05	5.77	0	--
F1	0.635	18.7	0	1.40	7.24	-3.18	--	0	207
F7	2.54	50.5	-1.30	1.08	6.86	-1.80	4.27	-1.3	--
F72	2.54	69.4	0	1.25	7.67	-3.10	--	0	298
F52	2.54	265.0	1.30	0.760	15.2	-8.00	--	--	--
F4	2.54	104.0	0.30	0.180	14.2	-5.59	8.88	0	530
F3	2.54	240.0	0.07	0.180	23.6	-10.2	--	--	1540
F53	2.54	231.0	0	0.810	15.6	-8.13	14.9	0	1239
F32	2.54	360.0	0	0.231	22.4	-9.65	21.4	0	--
G1	0.635	23.3	2.2	1.04	9.45	-3.30	5.29	2.20	256
F8	10.2	278.0	0.13	0.117	20.8	--	12.6	5.19	--
F82	10.2	243.0	0.85	0.132	15.0	--	11.7	6.18	--
F91	10.2	741.0	0.04	0.113	20.1	--	17.6	2.17	--
F10	10.2	770.0	0.32	0.899	12.5	--	10.3	1.37	--
H1	0.635	18.7	15.9	1.44	6.35	0.0	4.02	2.24	185
H53	2.54	353.0	16.3	0.676	18.3	-3.05	13.9	7.47	2642
H4	2.54	102.0	2.06	0.161	17.0	-4.32	11.1	4.27	--
H42	2.54	120.0	1.45	0.068	20.3	-3.05	15.5	7.70	862
H72	2.54	66.2	3.70	1.21	7.37	-2.16	5.35	1.60	250
D1	0.635	15.8	14.5	1.21	8.00	-0.25	5.10	2.23	--
D2	0.635	11.0	13.5	1.25	6.86	0.13	3.72	1.86	--
E12	0.635	14.5	15.4	1.30	6.43	0.51	2.17	1.95	123
E13	0.635	13.6	0	1.28	6.22	-2.54	--	0	128
H15	2.54	138.0	5.65	0.799	11.3	-3.05	8.68	3.51	789
H16	2.54	69.4	4.47	0.712	9.02	0.64	--	--	--
H17	2.54	105.0	4.41	0.664	10.9	-2.29	--	--	--
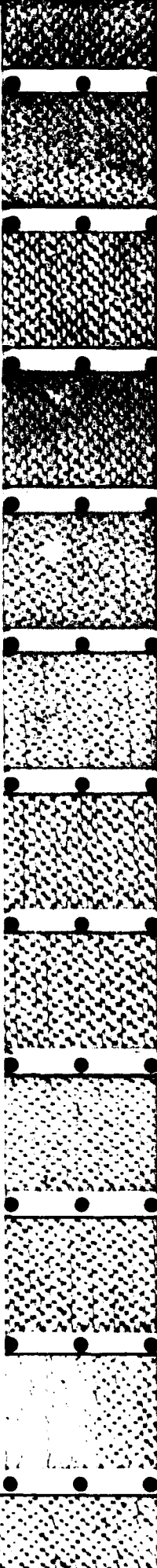
Table A2

Summary of Length Scales and Dimensionless Ratios for Horizontal Neutral

and Slightly Buoyant Jets in Linear Stratification

Run No.	ℓ_Q cm	ℓ_ε cm	ℓ_M cm	$\frac{\ell_Q}{\ell_\varepsilon}$	$\frac{\ell_M}{\ell_\varepsilon}$	$\frac{w_e}{\ell_\varepsilon}$	$\frac{z_e}{\ell_\varepsilon}$	$\frac{w_L}{\ell_\varepsilon}$	$\frac{z_L}{\ell_\varepsilon}$	$\frac{\mu\varepsilon^{1/4}}{M^{3/4}}$	Reynolds No. (ud/ν)*
B10	0.563	3.53	∞	0.159	∞	1.48	-0.68	--	0	--	1514
B11	0.563	4.29	∞	0.131	∞	1.45	-0.74	0.84	0	--	2200
B12	0.563	6.02	∞	0.094	∞	1.43	-0.59	0.96	0	--	3280
F1	0.563	5.30	∞	0.106	∞	1.37	-0.60	--	0	1.17	3740
F7	2.25	4.65	13.2	0.454	2.84	1.47	-0.39	0.92	-0.28	--	2525
F72	2.25	5.25	∞	0.429	∞	1.46	-0.59	--	0	1.84	3470
F52	2.25	11.6	69.5	0.194	5.99	1.31	-0.69	--	--	--	13250
F4	2.25	10.4	56.9	0.216	5.47	1.37	-0.54	0.85	0	1.10	5200
F3	2.25	15.8	270.0	0.142	17.1	1.49	-0.65	--	--	0.91	12000
F53	2.25	10.7	∞	0.210	∞	1.46	-0.76	1.39	0	1.13	11550
F32	2.25	18.2	∞	0.124	26.4	1.23	-0.53	1.18	0	--	18000
G1	0.563	6.36	38.1	0.088	6.0	1.49	-0.52	0.83	0.35	0.97	4660
F8	9.00	9.49	28.9	0.948	3.05	2.19	--	1.32	0.55	--	3460
F82	9.00	8.62	9.85	1.04	1.14	1.74	--	1.35	0.72	--	3030
F91	9.00	15.6	139.0	0.577	8.91	1.29	--	1.13	0.14	--	9230
F10	9.00	9.50	51.7	0.947	5.44	1.32	--	1.08	0.14	--	9590
H1	0.563	5.27	11.3	0.106	2.15	1.20	0.06	0.85	0.43	1.06	3740
H53	2.25	13.8	26.4	0.163	1.91	1.33	-0.22	1.01	0.54	1.22	17650
H4	2.25	10.6	21.2	0.212	2.00	1.60	-0.41	1.05	0.40	--	5100
H42	2.25	14.3	29.5	0.157	2.06	1.42	-0.21	1.08	0.54	1.13	6000
H72	2.25	5.17	10.3	0.435	1.99	1.43	-0.42	1.03	0.31	1.64	3310
D1	0.563	5.04	9.94	0.112	1.97	1.59	-0.05	1.01	0.44	--	3160
D2	0.563	4.18	7.19	0.135	1.72	1.64	0.03	0.89	0.44	--	2200
E12	0.563	4.76	8.89	0.118	1.87	1.35	0.11	0.46	0.41	1.00	2900
E13	0.563	4.61	∞	0.122	∞	1.35	-0.55	--	0	1.15	2720
H15	2.25	8.26	17.4	0.272	2.11	1.37	-0.37	1.05	0.42	1.55	6900
H16	2.25	6.04	9.88	0.373	1.64	1.49	0.11	--	--	--	3470
H17	2.25	7.56	15.0	0.298	1.98	1.44	-0.30	--	--	--	5250

* u = nozzle velocity; d = nozzle diameter.
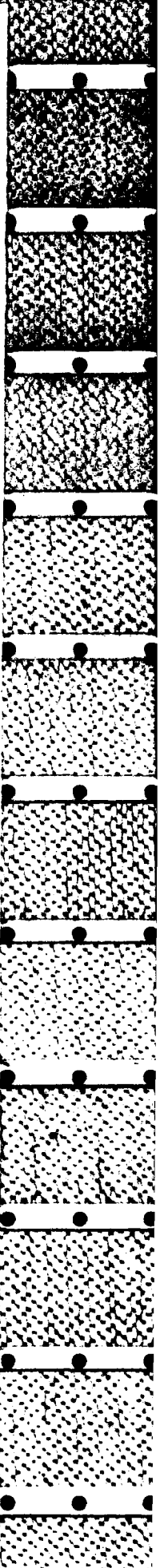
Table A3

Summary of Experimental Parameters for Inclined Buoyant and

Nonbuoyant Jets into Linear Stratification

Run No.	Angle, θ deg	Stratification Parameter, ε sec^{-2}	Discharge Rate, Q cm^3/sec	Density Difference $\rho_a - \rho_o$ σ_t	Entrainment Width, W_e cm	Location of Entrainment Bottom, Z_e cm	Collapsed Layer Thickness W_L cm	Rise Height Z_L cm	Mixed Layer Thickness W_m cm	Location of Mixed Layer Bottom, Z_m cm	Total Volume Flux, μ cm^3/sec
N1	22.5	0.829	25.2	19.7	11.3	2.21	5.88	6.82	13.3	0.0	365
N2	22.5	0.820	22.9	-17.4	11.1	-4.70	5.22	0	7.62	-1.91	358
N3	22.5	0.838	22.9	-0.17	10.4	-0.51	6.42	3.07	8.89	-0.64	273
N4	22.5	0.250	22.1	11.9	15.9	4.72	10.2	10.1	17.8	1.91	537
N5	22.5	0.233	23.3	-9.47	17.0	-7.59	7.20	-0.41	12.1	-3.81	347
N6	22.5	0.250	23.2	0	14.5	-1.30	7.22	4.55	14.6	-1.91	433
N7	22.5	1.25	23.3	-0.1	8.53	-0.36	5.21	2.81	8.89	-1.91	270
N8	22.5	1.43	22.9	22.5	9.5	1.75	5.35	5.48	10.8	1.91	269
N9	22.5	1.38	21.8	-21.3	10.7	-5.36	5.21	0	8.89	-4.45	289
M1	45	0.857	24.5	19.0	12.3	6.02	5.86	9.92	15.9	1.27	404
M2	45	0.889	23.2	0.1	12.4	1.96	6.63	5.94	11.4	0	372
M3	45	0.904	22.6	-18.3	13.4	-2.54	6.23	3.20	8.26	1.91	365
M4	45	0.333	21.6	0.09	15.1	2.41	7.69	7.83	14.0	0.64	334
M5	45	0.299	25.1	11.1	16.7	8.51	9.38	13.8	21.0	3.18	444
M6	45	0.297	24.1	-10.7	17.8	-2.16	8.69	4.92	15.9	-1.27	668
M7	45	1.23	22.5	20.8	11.1	4.57	5.99	8.56	12.8	2.54	298
M8	45	1.29	22.0	-21.0	12.0	-2.90	5.96	2.65	7.62	-0.64	260
M9	45	1.20	23.8	-0.1	11.4	1.30	5.96	5.85	13.3	-0.64	308

Table A4

Summary of Length Scales and Dimensionless Ratios for Inclined Buoyant

and Nonbuoyant Jets into Linear Stratification

Run No.	ℓ_ϵ cm	ℓ_M cm	$\dfrac{\ell_Q}{\ell_\epsilon}$	$\dfrac{\ell_M}{\ell_\epsilon}$	$\dfrac{W_e}{\ell_\epsilon}$	$\dfrac{Z_e}{\ell_\epsilon}$	$\dfrac{W_L}{\ell_\epsilon}$	$\dfrac{Z_L}{\ell_\epsilon}$	$\dfrac{W_m}{\ell_\epsilon}$	$\dfrac{Z_m}{\ell_\epsilon}$	$\dfrac{\mu\epsilon^{1/4}}{M^{3/4}}$	Reynolds No. (ud/ν)*
N1	7.02	13.8	0.08	1.97	1.61	0.31	0.84	0.97	1.90	0.0	1.16	5065
N2	6.70	-13.3	0.08	-1.98	1.66	-0.70	0.78	0	0.92	-0.28	1.31	4600
N3	6.67	-136.0	0.08	∞	1.55	-0.08	0.96	0.46	1.33	-0.10	1.01	4600
N4	10.2	20.2	0.06	1.70	1.56	0.47	1.00	0.99	1.75	0.19	1.03	5825
N5	9.27	-18.3	0.06	-1.97	1.84	-0.82	0.78	-0.04	1.30	-0.41	0.90	4685
N6	9.08	∞	0.06	∞	1.59	-0.14	0.80	0.50	1.61	-0.21	1.16	4660
N7	5.94	-171.0	0.10	∞	1.44	-0.06	0.88	0.47	1.50	-0.32	1.15	4470
N8	5.83	11.8	0.10	2.02	1.63	0.30	0.92	0.94	1.86	0.33	1.13	4600
N9	5.74	11.4	0.10	-1.99	1.86	-0.93	0.91	0	1.55	-0.77	1.30	4379
M1	6.85	13.7	0.08	1.98	1.79	0.88	0.86	1.45	2.32	0.19	1.36	4910
M2	6.61	178.0	0.09	∞	1.87	0.30	1.00	0.91	1.73	0	1.36	4660
M3	6.50	-12.8	0.09	-1.97	2.06	-0.39	0.96	0.49	1.27	0.29	1.40	4530
M4	8.15	172.0	0.07	∞	1.86	0.30	0.94	0.96	1.71	0.08	1.07	4330
M5	9.03	18.1	0.06	2.00	1.84	0.94	1.04	1.53	2.32	0.35	1.10	5040
M6	8.86	-17.7	0.06	-2.00	2.00	-0.24	0.98	0.55	1.79	-0.14	1.76	4840
M7	5.99	12.0	0.09	2.01	1.84	0.76	1.00	1.43	2.12	0.42	1.25	4510
M8	5.87	-11.8	0.10	-2.00	2.04	-0.49	1.02	0.45	1.30	-0.11	1.13	4420
M9	6.22	∞	0.09	∞	1.82	0.21	0.96	0.94	2.14	-0.10	1.17	4790

* u = nozzle velocity; d = nozzle diameter.

Table A5

Summary of Experimental Parameters for Horizontal

Nonbuoyant Jets into Two-Layer Stratification

Run No.	Discharge Depth, h (cm)	Stratification Parameter, ε (sec⁻²)	Jet Flow Rate, Q (cm³/sec)	Interfacial Density Jump, Δρ (σt)	Entrainment Width, We (cm)	Location of Entrainment Bottom, Ze (cm)	Collapsed Layer Thickness, WL (cm)	Mixed Layer Thickness, Wm (cm)	Location of Mixed Layer Bottom, Zm (cm)	Total Collapsed Jet Volume Flux, μ (cm³/sec)
A3	3.81	0.964	97.2	11.0	16.6	-8.6	8.2	17.8	-7.6	1050
A4	4.32	1.010	59.9	2.8	12.1	-6.4	7.5	12.7	-6.4	1030
A6	1.27	0.672	32.8	33.0	∞	-2.3	4.0	5.7	-1.9	730
A7	5.59	1.452	63.1	7.7	12.0	-6.3	8.7	14.0	-6.4	1150
A8	5.08	1.552	36.3	0.0	9.7	-4.8	5.4	10.8	-5.1	--
A9	4.01	1.600	24.6	0.0	6.9	-3.7	4.4	7.0	-2.5	--
A10	6.00	1.660	49.8	0.0	12.5	-5.9	7.3	12.7	-6.4	--
A11	3.11	1.660	36.6	2.8	∞	-5.4	6.9	9.5	-4.5	--
A14	2.90	0.220	26.9	9.4	11.4	-7.4	7.5	--	--	490
A15	5.80	0.350	40.4	2.7	15.3	-8.5	9.9	13.3	-6.4	910
FPO	1.59	1.080	30.3	15.1	∞	-9.4	5.3	9.5	-4.5	320
A16	4.95	1.178	50.5	0.0	∞	-7.8	8.6	12.7	-5.1	870
A17	1.28	0.732	32.5	33.9	∞	-5.1	5.3	7.0	-2.5	708
A18	3.36	1.315	55.5	5.3	∞	-7.0	7.8	12.1	-5.7	1080
A19	2.92	1.600	29.7	2.2	∞	-5.1	5.7	7.6	-3.8	--
A20	5.54	0.440	38.5	0.0	∞	-7.3	8.6	14.0	-7.0	610
A21	9.75	0.350	21.8	0.0	12.9	-7.3	8.6	--	--	430
A22	8.89	0.360	31.5	0.0	15.0	-7.6	9.6	14.6	-7.0	570
A23	1.65	0.387	20.5	0.0	∞	-6.4	5.9	8.9	-5.7	--
A24	6.09	0.301	18.8	0.0	10.7	-5.9	6.8	--	--	--
A25	3.56	0.400	37.9	0.0	∞	-8.3	8.8	14.6	-7.6	970
A26	5.46	0.398	56.2	0.0	∞	-9.0	13.1	17.8	-9.5	400
A27	5.72	0.369	22.4	0.0	11.4	-6.4	7.5	10.8	-6.4	580
A28	2.79	0.377	35.9	0.0	∞	-8.3	8.8	14.6	-8.3	950
A29	4.32	0.326	46.1	8.6	16.3	-9.6	10.5	15.2	-7.6	820
A30	4.12	0.355	41.0	3.8	14.9	-7.3	9.9	15.2	-7.6	810
A31	2.43	1.549	42.9	20.4	10.3	-5.9	7.3	11.4	-5.1	980
A32	2.85	0.774	51.1	36.4	∞	-6.7	9.3	12.1	-7.0	--
A33	3.15	1.652	63.1	20.6	∞	-6.7	7.5	12.1	-5.7	1190
A34	2.79	1.660	69.4	0.0	∞	-7.6	7.9	15.9	-7.6	360
A35	0.762	1.470	22.6	0.0	∞	-4.1	5.4	8.9	-4.5	730
A36	3.05	0.327	60.6	0.0	∞	-10.2	13.6	19.1	-10.2	950
A13	2.71	0.330	44.2	6.2	14.6	-8.3	7.9	14.6	-7.0	

Table A6

Summary of Length Scales and Dimensionless Ratios for Horizontal

Nonbuoyant Jets into Two-Layer Stratification

Run No.	$\dfrac{\ell_\Delta}{\text{cm}}$	$\dfrac{\ell_\varepsilon}{\text{cm}}$	$\dfrac{\ell_Q}{\ell_\varepsilon}$	$\dfrac{h}{\ell_\varepsilon}$	$\dfrac{h}{\ell_\Delta}$	$\dfrac{W_e}{\ell_\varepsilon}$	$\dfrac{Z_e}{\ell_\varepsilon}$	$\dfrac{W_L}{\ell_\varepsilon}$	$\dfrac{W_m}{\ell_\varepsilon}$	$\dfrac{Z_m}{\ell_\varepsilon}$	$\dfrac{\mu\varepsilon^{1/4}}{M^{3/4}}$	Stable(s) or Unstable(u)
A3	14.1	13.3	0.05	0.29	0.27	1.25	-0.65	0.62	1.34	-0.57	0.46	u
A4	16.1	10.3	0.05	0.42	0.27	1.17	-0.62	0.72	1.23	-0.62	0.94	u
A6	4.8	8.4	0.07	0.15	0.27	∞	-0.27	0.47	0.68	-0.23	1.63	u
A7	11.9	9.6	0.06	0.58	0.47	1.24	-0.65	0.90	1.49	-0.66	1.06	s
A8	∞	7.2	0.08	0.71	0	1.34	-0.67	0.76	1.50	-0.71	--	s
A9	∞	5.9	0.10	0.68	0	1.17	-0.63	0.73	1.19	-0.43	--	s
A10	∞	8.3	0.07	0.72	0	1.50	-0.72	0.88	1.53	-0.77	--	s
A11	11.6	7.1	0.08	0.44	0.27	∞	-0.76	0.97	1.34	-0.63	--	u
A14	6.1	10.1	0.06	0.29	0.47	1.13	-0.74	0.75	--	--	1.02	u
A15	12.6	11.0	0.05	0.53	0.46	1.39	-0.77	0.90	1.21	-0.58	1.16	s
FPO	5.8	7.2	0.08	0.22	0.27	∞	-0.81	0.73	1.32	-0.62	0.91	s
A16	∞	9.1	0.06	0.55	0	∞	-0.85	0.95	1.40	-0.56	1.06	u
A17	4.7	8.2	0.07	0.15	0.27	∞	-0.62	0.64	0.85	-0.31	1.43	u
A18	12.4	9.3	0.06	0.36	0.27	∞	-0.75	0.84	1.30	-0.62	1.18	u
A19	10.3	6.5	0.09	0.45	0.28	∞	-0.79	0.88	1.18	-0.59	--	u
A20	∞	10.2	0.06	0.54	0	∞	-0.72	0.84	1.37	-0.69	0.88	u
A21	∞	8.0	0.07	1.19	0	1.60	-0.91	1.07	--	--	1.37	u
A22	∞	9.7	0.06	0.92	0	1.55	-0.79	0.99	1.51	-0.72	1.11	s
A23	∞	7.7	0.07	0.22	0	∞	-0.83	0.77	1.16	-0.75	--	s
A24	∞	7.8	0.07	0.78	0	1.37	-0.76	0.87	--	--	--	u
A25	∞	10.2	0.06	0.35	0	∞	-0.81	0.87	1.43	-0.75	0.77	s
A26	∞	12.6	0.04	0.43	0	∞	-0.71	1.04	1.41	-0.76	1.23	u
A27	∞	8.1	0.07	0.71	0	1.41	-0.78	0.93	1.33	-0.78	0.89	u
A28	∞	10.2	0.06	0.27	0	∞	-0.81	0.86	1.43	-0.81	0.97	s
A29	9.3	12.0	0.05	0.36	0.47	1.36	-0.80	0.88	1.27	-0.64	0.98	s
A30	11.3	11.1	0.07	0.37	0.37	1.35	-0.66	0.89	1.38	-0.69	1.36	u
A31	6.7	7.8	0.07	0.31	0.36	1.31	-0.75	0.93	1.46	-0.65	1.06	u
A32	6.2	10.2	0.06	0.28	0.46	∞	-0.66	0.92	1.19	-0.69	--	s
A33	8.6	9.3	0.06	0.34	0.37	∞	-0.71	0.81	1.29	-0.61	--	u
A34	∞	11.1	0.05	0.25	0	∞	-0.69	0.71	1.43	-0.69	0.98	u
A35	∞	5.8	0.10	0.13	0	∞	-0.72	0.95	1.55	-0.77	1.55	u
A36	∞	13.7	0.04	0.22	0	∞	-0.74	0.99	1.39	-0.74	0.49	u
A13	10.1	11.7	0.05	0.23	0.27	1.25	-0.71	0.68	1.25	-0.60	1.03	u

Note: $\ell_Q = 0.56$ cm.

Table A7

Summary of Empirical Equations for Horizontal Neutrally and
Slightly Buoyant Jets into Linear Stratification

Parameter	Equation	Equation No.	Figure No.	Range of Validity
Collapsed layer thickness	$\dfrac{W_L}{\ell_\epsilon} = 1.0$	A36	A6	$\dfrac{\ell_Q}{\ell_\epsilon} \leq 0.4$; $\left\|\dfrac{\ell_M}{\ell_\epsilon}\right\| \geq 2$
Entrainment width	$\dfrac{W_e}{\ell_\epsilon} = 1.4$	A37	A7	$\dfrac{\ell_Q}{\ell_\epsilon} \leq 0.5$; $\left\|\dfrac{\ell_M}{\ell_\epsilon}\right\| \geq 1$
Entrainment bottom	$\dfrac{Z_e}{\ell_\epsilon} = -0.70$	A38	A8	$\dfrac{\ell_Q}{\ell_\epsilon} \leq 0.4$; $\dfrac{\ell_M}{\ell_\epsilon} = 8$
Entrainment bottom	$\dfrac{Z_e}{\ell_\epsilon} = -0.30$	A39	A8	$\dfrac{\ell_Q}{\ell_\epsilon} \leq 0.4$; $\dfrac{\ell_M}{\ell_\epsilon} = 2$
Rise height for buoyant jets	$\dfrac{Z_L}{\ell_\epsilon} = 0.50$	A40	A9	$\dfrac{\ell_Q}{\ell_\epsilon} \leq 0.5$; $\dfrac{\ell_M}{\ell_\epsilon} = 2$
Volume flux	$\dfrac{\mu \epsilon^{1/4}}{\epsilon^{3/4}} = 1.0$	A41	A10	$\dfrac{\ell_Q}{\ell_\epsilon} \leq 0.4$; $\left\|\dfrac{\ell_M}{\ell_\epsilon}\right\| \geq 2$
Maximum of entrained volume flux distribution	$\dfrac{q_{em}}{M^{1/2}} = 1.04$	A42	A11,A12'	$\dfrac{\ell_Q}{\ell_\epsilon} \leq 0.4$; $\left\|\dfrac{\ell_M}{\ell_\epsilon}\right\| \geq 2$

Table A8

Summary of Empirical Equations for Inclined Positively and
Negatively Buoyant Jets into Linear Stratification

Parameter	Equation	Equation No.	Figure No.	Range of Validity
Collapsed layer thickness	$\dfrac{w_L}{\ell_\epsilon} = 1.0$	A36	A15	$\dfrac{\ell_Q}{\ell_\epsilon} \leq 0.4^*$; $\left\|\dfrac{\ell_M}{\ell_\epsilon}\right\| \geq 2$; $0 \leq \theta \leq 45°$
Entrainment width	$\dfrac{w_e}{\ell_\epsilon} = 1.42 + 1.07 \times 10^{-2}\,\theta$	A43	A17	$\dfrac{\ell_Q}{\ell_\epsilon} \leq 0.4^*$; $\left\|\dfrac{\ell_M}{\ell_\epsilon}\right\| \geq 2$; $0 \leq \theta \leq 45°$
Entrainment bottom	$\dfrac{z_e}{\ell_\epsilon} = -0.71 + 0.82\left(\dfrac{\ell_M}{\ell_\epsilon}\right)^{-1} + \left[2.13 \times 10^{-2} + 8.17 \times 10^{-3}\left(\dfrac{\ell_M}{\ell_\epsilon}\right)^{-1}\right]\theta$	A44	A18	$\dfrac{\ell_Q}{\ell_\epsilon} \leq 0.4^*$; $\left\|\dfrac{\ell_M}{\ell_\epsilon}\right\| \geq 2$; $0 \leq \theta \leq 45°$
Volume flux	$\dfrac{\mu\epsilon^{1/4}}{M^{3/4}} = 1.06 + 3.56 \times 10^{-3}\theta$	A45	A21	$\dfrac{\ell_Q}{\ell_\epsilon} \leq 0.2^*$; $\left\|\dfrac{\ell_M}{\ell_\epsilon}\right\| \geq 2$; $0 \leq \theta \leq 45°$
Maximum of entrained volume flux distribution	$\dfrac{q_{em}}{M^{1/2}} = 1.04 - 0.04\left(\dfrac{\theta}{45}\right)$	A46	A22,A23 A24,A25, A26,A27	$\dfrac{\ell_Q}{\ell_\epsilon} \leq 0.4^*$; $\left\|\dfrac{\ell_M}{\ell_\epsilon}\right\| \geq 2$; $0 \leq \theta \leq 45°$

Note: θ is in degrees.
* Experiments were done only for $\ell_Q/\ell_\epsilon < 0.1$. Range given is probable limit based on series 1 experiments.
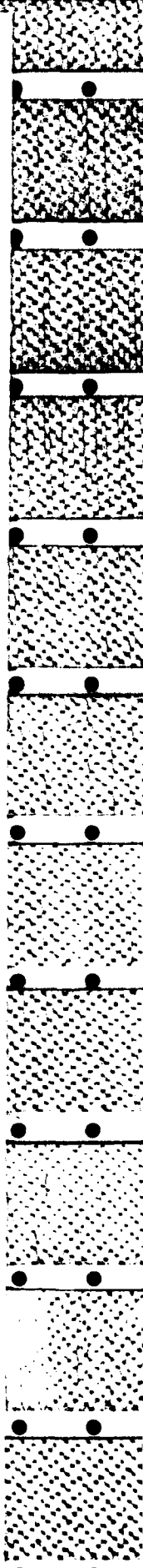
Table A9

Summary of Empirical Equations for Horizontal Nonbuoyant

Jets into Two-Layer Stratifications

Parameter	Equation	Equation No.	Figure No.	Range of Validity
Collapsed layer thickness	$\dfrac{W_L}{\ell_\epsilon} = 0.92$	A47	A30	$\dfrac{\ell_Q}{\ell_\epsilon} \leq 0.4^*$; $\dfrac{\ell_M}{\ell_\epsilon}^{**}$
Entrainment width	$\dfrac{W_e}{\ell_\epsilon} = 1.4$	A37	A31	$\dfrac{\ell_Q}{\ell_\epsilon} \leq 0.4^*$; $\dfrac{\ell_M}{\ell_\epsilon}^{**}$
Entrainment bottom	$\dfrac{Z_e}{\ell_\epsilon} = -0.70$	A38	A32	$\dfrac{\ell_Q}{\ell_\epsilon} \leq 0.4^*$; $\dfrac{\ell_M}{\ell_\epsilon}^{**}$
Volume flux	$\dfrac{\mu \epsilon^{1/4}}{M^{3/4}} = 1.00$	A41	A35	$\dfrac{\ell_Q}{\ell_\epsilon} \leq 0.2$; $\dfrac{\ell_M}{\ell_\epsilon}^{**}$
Maximum of entrained volume flux distribution	$\dfrac{q_{em}}{M^{1/2}} = 1.4$	A48	A37,A38	$\dfrac{\ell_Q}{\ell_\epsilon} \leq 0.4^*$; $\dfrac{\ell_M}{\ell_\epsilon}^{**}$
Mixed layer thickness	$\dfrac{W_m}{\ell_\epsilon} = 1.35$	A49	A33	$\dfrac{\ell_Q}{\ell_\epsilon} \leq 0.4^*$; $\dfrac{\ell_M}{\ell_\epsilon}^{**}$
Mixed layer bottom	$\dfrac{Z_m}{\ell_\epsilon} = -0.66$	A50	A34	$\dfrac{\ell_Q}{\ell_\epsilon} \leq 0.4^*$; $\dfrac{\ell_M}{\ell_\epsilon}^{**}$

* Experiments were done only for $\ell_Q/\ell_\epsilon < 0.1$. Range given is probable limit based on series 1 experiments.

** Experiments were done only for neutrally buoyant jets, i.e. $\ell_M/\ell_\epsilon = \infty$. Probable range of validity is $\left| \ell_M/\ell_\epsilon \right| \gtrsim 2$.
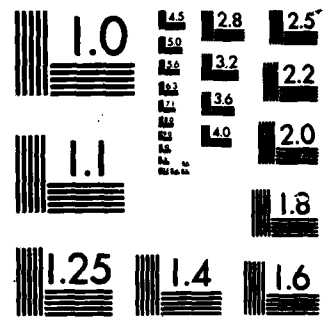
MICROCOPY RESOLUTION TEST CHART
NATIONAL BUREAU OF STANDARDS-1963-A

Table A10

Summary of Empirical Equations Used to Describe

Entrained Volume Flux Distribution*,**,†

Parameter	Equation	Equation
Entrainment layer width	A43	$\dfrac{w_e}{\ell_\epsilon} = 1.42 + 1.07 \times 10^{-2}\,\theta$
Entrainment layer bottom	A44	$\dfrac{z_e}{\ell_\epsilon} = -0.71 + 0.82\left(\dfrac{\ell_M}{\ell_\epsilon}\right)^{-1} + \left[2.13 \times 10^{-2} + 8.7 \times 10^{-3}\left(\dfrac{\ell_M}{\ell_\epsilon}\right)^{-1}\right]\theta$
Height of entrainment layer maximum	A60	$\eta_o = 0.8\left(\dfrac{\ell_M}{\ell_\epsilon}\right)^{-1} + 1.3\,\dfrac{\theta}{45}$
Entrainment layer variance	A61	$b = 0.65 + 0.1\left|\dfrac{\ell_M}{\ell_\epsilon}\right|^{-1} + 0.1\left(\dfrac{\theta}{45}\right)$
Entrained flow rate maximum	A62	$\dfrac{q_{em}}{M^{1/2}} = 1.04 - 0.04\left(\dfrac{\theta}{45}\right)$

* Range of applicability: $\ell_Q/\ell_\epsilon \leq 0.5$; $\ell_M/\ell_\epsilon \geq 2$; $0 \leq \theta \leq 45°$.

** θ in degrees.

† $q_e/M^{1/2} = q_{em}/M^{1/2} \exp\left[-(\eta - \eta_o)^2/b^2\right]$ (A56, bis)
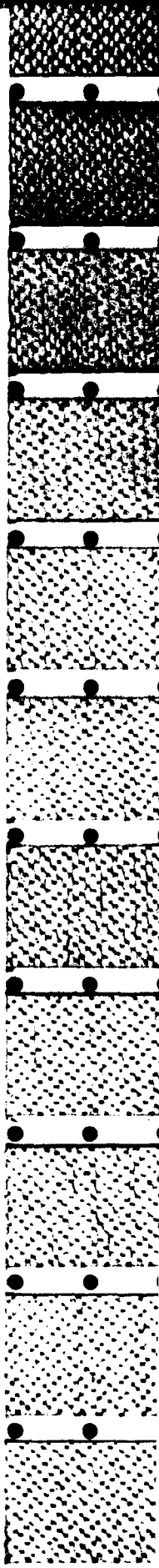
APPENDIX B: COMPARISON OF PRESENT EXPERIMENTS WITH THE PREDICTIONS OF FAN AND BROOKS

Introduction

1. By the use of integral equation models, Fan and Brooks (1969)* have produced predictions of the behavior of buoyant round jets in a linearly stratified environment. Their model is described in Appendix C. The relationship of these predictions to the present work is discussed in this appendix.

2. Fan and Brooks expressed their results in terms of different parameters than those used here. The conversion between their parameters and the length scales used in this study is presented in paragraphs 3-13 of this appendix. A comparison of one of the experiments with values predicted by Fan and Brooks is given in paragraphs 14-15, and unified diagrams for jet volume flux which incorporate the results of both Fan and Brooks and the present experiments are given in paragraphs 16-20. Concluding remarks are presented in paragraphs 21-22.

Parameter Conversion

3. Fan and Brooks expressed their results as:

$$\xi_t, \eta_t, \mu_t = f(m_o, \mu_o) \tag{B1}$$

where ξ_t, η_t, and μ_t are terminal rise height, horizontal distance, and volume flux parameters, and m_o and μ_o are source momentum and volume flux parameters defined by:

$$\xi_t = \frac{z_t}{\delta d} \tag{B2}$$

---

* Bibliographic information is given in the References section of the main text, p 35.

B1

$$\eta_t = \frac{X_m - 6.2d}{\delta d} \tag{B3}$$

$$\delta = \frac{m_o^{1/4}}{2\sqrt{2}\alpha\mu_o} \tag{B4}$$

$$\mu_t = \frac{(1 + \lambda^2)}{2\lambda^2} \mu_o S_t \tag{B5}$$

$$m_o = \frac{(1 + \lambda^2)F^2}{4\lambda^4 T} \tag{B6}$$

$$\mu_o = \frac{\left(1 + \lambda^2\right)^{5/8} F^{1/4}}{2\alpha^{1/2}\lambda^{3/2}T^{5/8}} \tag{B7}$$

where X_m and Z_t are the x and z coordinates of the jet at its terminal height (X_m and Z_t are equivalent to Fan and Brooks' X_t' and Y_t'). The term λ is a form of the turbulent Schmidt number, a constant, and α is the entrainment coefficient, also assumed constant. The term S_t is the terminal center-line dilution and δ is a scale factor; F is a densimetric Froude number:

$$F = \frac{u}{\sqrt{g \dfrac{\Delta\rho_o}{\rho_a} d}} \tag{B8}$$

and T is a stratification parameter:

$$T = \frac{\Delta\rho_o}{d\left(-\dfrac{d\rho}{dz}\right)} \tag{B9}$$

where $\Delta\rho_o = \rho_a - \rho_o$, ρ_o is the source density, ρ_a is the ambient density at the elevation of the source, u is the jet velocity, and d is the nozzle diameter.

B2

4. The problem is to express m_o, μ_o, ξ_t, η_t, and μ_t in terms of the variables ℓ_M/ℓ_ϵ and $\ell_Q \ell_\epsilon$. We begin by writing Equations B6 and B7 as:

$$m_o = K_1 F^2 T^{-1} \tag{B10}$$

and

$$\mu_o = K_2 F^{1/4} T^{-5/8} \tag{B11}$$

where

$$K_1 = \frac{(1 + \lambda^2)}{4\lambda^4} \tag{B12}$$

and

$$K_2 = \frac{\left(1 + \lambda^2\right)^{5/8}}{2\alpha^{1/2}\lambda^{3/2}} \tag{B13}$$

5. Now, from Equations A1 through A8:

$$\frac{\ell_Q}{\ell_\epsilon} = \frac{\epsilon^{1/4}Q}{M^{3/4}} = \left(\frac{\pi}{4}\right)^{1/4} g^{1/4} \rho_a^{-1/4} \left(-\frac{d\rho}{dz}\right)^{1/4} d^{1/2} u^{-1/2} \tag{B14}$$

and

$$\frac{\ell_M}{\ell_\epsilon} = \frac{\epsilon^{1/4}M^{1/2}}{B^{1/2}} = g^{-1/4} \rho_a^{1/4} \left(-\frac{d\rho}{dz}\right)^{1/4} u^{1/2} (\Delta\rho_o)^{-1/2} \tag{B15}$$

6. We now combine Equations B10 and B11 as:

$$\mu_o m_o^{-3/8} = \left(K_2 F^{1/4} T^{-5/8}\right)\left(K_1 F^2 T^{-1}\right)^{-3/8}$$

$$\tag{B16}$$

$$= K_2 K_1^{-3/8} F^{-1/2} T^{-1/4}$$

B3

and substitute Equations B8 and B9 in Equation B16 to yield:

$$\mu_o m_o^{-3/8} = K_2 K_1^{-3/8} g^{1/4} \rho_a^{-1/4} \left(- \frac{d\rho}{dz}\right)^{1/4} d^{1/2} u^{-1/2} \tag{B17}$$

7. Similarly, Equation B10 can be written:

$$m_o^{1/4} = \left(K_1 F^2 T^{-1}\right)^{1/4}$$

$$= K_1^{1/4} F^{1/2} T^{-1/4}$$

$$= K_1^{1/4} g^{-1/4} \rho_a^{1/4} \left(- \frac{d\rho}{dz}\right)^{1/4} u^{1/2} \left(\Delta\rho_o\right)^{-1/2} \tag{B18}$$

8. Comparison of Equation B14 with B17 and Equation B15 with B18 yields:

$$\frac{\ell_Q}{\ell_\varepsilon} = \left(\frac{\pi}{4}\right)^{1/4} \frac{K_1^{3/8}}{K_2} \mu_o m_o^{-3/8} \tag{B19}$$

and

$$\frac{\ell_M}{\ell_\varepsilon} = K_1^{-1/4} m_o^{1/4} \tag{B20}$$

9. To complete the conversions between Fan and Brooks' parameters and our length scales, values of K_1 and K_2 are required. These are given in Fischer et al. (1979), pp 325 and 371, as:

$$\alpha = 0.0535 \pm 0.0025 \quad \text{for jets} \tag{B21}$$
$$\alpha = 0.0833 \pm 0.0042 \quad \text{for plumes} \tag{B22}$$

and

$$\lambda = 1.2 \quad\quad\quad\quad \text{for jets and plumes} \tag{B23}$$

10. Substituting the mean values from Equations B21 and B22 into Equations B12 and B13 and rewriting Equations B19 and B20:

$$\frac{\ell_Q}{\ell_\epsilon} = 0.208\mu_o m_o^{-3/8} \quad \text{for jets} \tag{B24}$$

$$\frac{\ell_Q}{\ell_\epsilon} = 0.259\mu_o m_o^{-3/8} \quad \text{for plumes} \tag{B25}$$

$$\frac{\ell_M}{\ell_\epsilon} = 1.35 m_o^{1/4} \quad \text{for jets and plumes} \tag{B26}$$

$$\delta = 6.61 m_o^{1/4}\mu_o^{-1} \quad \text{for jets} \tag{B27}$$

$$\delta = 4.24 m_o^{1/4}\mu_o^{-1} \quad \text{for plumes} \tag{B28}$$

The terminal center-line dilution becomes

$$S_t = \frac{2\lambda^2}{1+\lambda^2}\frac{\mu_t}{\mu_o} = 1.17\frac{\mu_t}{\mu_o} \quad \text{for jets and plumes} \tag{B29}$$

and the terminal average dilution S_{at} is

$$S_{at} = 2\frac{\mu_t}{\mu_o} \tag{B30}$$

11. Volume flux relationships can now be obtained by noting that the average dilution is equal to the volume flux ratio, thus:

$$S_{at} = \frac{\mu}{Q} \tag{B31}$$

where μ is the total volume flux in jet after collapse (our notation, not Fan and Brooks'; note that their μ_t and μ_o are nondimensional volume flux parameters). The parameter $\mu\epsilon^{1/4}/M^{3/4}$ can then be

B5

written; by combining Equations B30, B31, B24, B25, A6, and A8 we obtain:

$$\frac{\mu\varepsilon^{1/4}}{M^{3/4}} = 0.416\mu_t m_o^{-3/8} \text{ for jets} \tag{B32}$$

and

$$\frac{\mu\varepsilon^{1/4}}{M^{3/4}} = 0.518\mu_t m_o^{-3/8} \text{ for plumes} \tag{B33}$$

12. The thickness of the jet at collapse W_L can be estimated by assuming

$$W_L = 2 w_t \tag{B34}$$

where w_t is the terminal half-width of the jet defined by two standard deviations from the mean of the assumed Gaussian distributions. From Fan and Brooks' Equation 73:

$$w_t = \delta\tilde{w}_t d = \delta 2 \sqrt{2} \ \alpha\mu_t m_o^{-1/4} d \tag{B35}$$

for horizontal jets (when $h_o = m_o$). Combining Equations B21, B22, B34, and B35 yields:

$$W_L = 0.303\delta\mu_t m_o^{-1/4} d \quad \text{for jets} \tag{B36}$$

and

$$W_L = 0.471\delta\mu_t m_o^{-1/4} d \quad \text{for plumes} \tag{B37}$$

13. The range of parameters for which solutions are given by Fan and Brooks is:

$$0.001 < \mu_o < 1$$

$$0.0006 < m_o < 6$$

which corresponds (using Equations B24-B26) to:

$$1.06 \times 10^{-4} < \frac{\ell_Q}{\ell_\epsilon} < 4.18$$

and

$$0.21 < \frac{\ell_M}{\ell_\epsilon} < 2.1$$

Example

14. For an example, we compare the results of Experiment E12 (see Tables A1 and A2) with the predictions of Fan and Brooks. For this experiment:

$$\frac{\ell_Q}{\ell_\epsilon} = 0.118 \qquad \frac{\ell_M}{\ell_\epsilon} = 1.87$$

Using Equations B2, B3, B24-B30, B36, B37, and Fan and Brooks' Figures 14, 15, and 16, we can evaluate all parameters and compare them with the experimental results as shown in Table B1.

15. As would be expected, the results for this high momentum jet show better agreement with the predictions based on jet coefficients than on plume coefficients. It would not be expected that Fan and Brooks' predictions would be very close to the present results as their model was not intended for application to low-buoyancy jets. Nevertheless, the comparisons shown in Table B1 suggest an encouraging consistency between their approach and ours.

B7

Total Volume Flux

16. By combining the predictions of Fan and Brooks with the present experimental results, we can now predict the volume flux, or dilution, of a horizontal buoyant jet over the whole parameter range, from momentum-dominated neutrally buoyant to buoyancy-dominated with negligible momentum. For linear stratification with no momentum flux, and $\theta = 0$ deg, Equation A15 becomes:

$$\frac{\mu \varepsilon^{1/4}}{M^{3/4}} = f\left(\frac{\ell_Q}{\ell_\varepsilon}, \frac{\ell_M}{\ell_\varepsilon}\right) \tag{B38}$$

The volume flux predictions given in Fan and Brooks' Figure 16 were converted to the form of Equation B38 using Equations B24, B26, and B32, and were combined with the present results (Figure A10) as shown in Figure B1.

17. The results clearly demonstrate the asymptotic behavior discussed in Appendix A. That is, as the nozzle size becomes small such that $\ell_Q/\ell_\varepsilon \ll 1$, the results become independent of ℓ_Q/ℓ_ε. Equation B38 then becomes:

$$\frac{\mu \varepsilon^{1/4}}{M^{3/4}} = f\left(\frac{\ell_M}{\ell_\varepsilon}\right) \tag{B39}$$

The asymptotic solution to Equation B39 for a buoyancy-dominated flow, i.e., a pure plume, can also be simply decided. In this case:

$$\mu = f(B, \varepsilon) \tag{B40}$$

which, following dimensional analysis becomes:

$$\mu = C_5 B^{3/4} \varepsilon^{-5/8} \tag{B41}$$

where C_5 is an experimental constant. Equation B41 can be written in
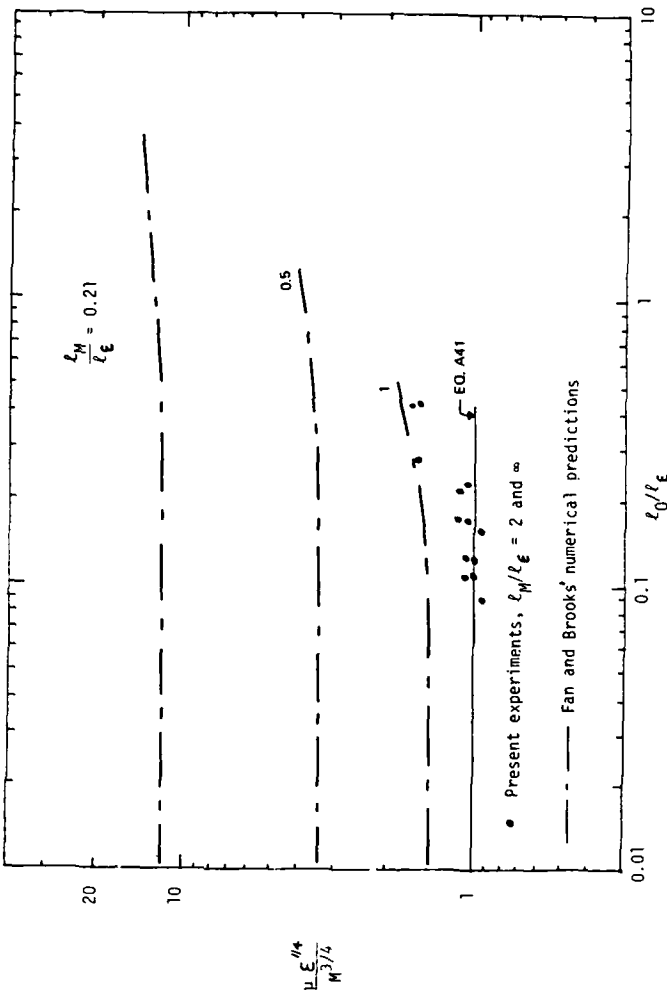
Figure B1. Comparison of present results with numerical predictions of Fan and Brooks using a jet entrainment coefficient

B9

the present notation of Equation B39 by combining it with Equations A7 and A8 to yield:

$$\frac{\mu\varepsilon^{1/4}}{M^{3/4}} = C_5 \left(\frac{\ell_M}{\ell_\varepsilon}\right)^{-3/2} \tag{B42}$$

18. Although C_5 is a fundamental constant, we only have Fan and Brooks' numerical predictions from which to estimate its value. Using Figure B1, we would arrive at an estimate of C_5 of 1.1; thus Equation B42 becomes:

$$\frac{\mu\varepsilon^{1/4}}{M^{3/4}} = 1.1\left(\frac{\ell_M}{\ell_\varepsilon}\right)^{-3/2} \tag{B43}$$

Figure B1 was derived using a jet entrainment coefficient, however, and a plume entrainment coefficient is higher than that of a jet. Therefore, the derivation of Figure B1 was repeated, using a plume entrainment coefficient, $\alpha = 0.0833$, as recommended by Fischer et al. (1979), to yield a value of $C_5 = 1.4$. Therefore, Equation B42 becomes:

$$\frac{\mu\varepsilon^{1/4}}{M^{3/4}} = 1.4 \left(\frac{\ell_M}{\ell_\varepsilon}\right)^{-3/2} \quad \text{for } \frac{\ell_M}{\ell_\varepsilon} \ll 1 \tag{B44}$$

19. The results can now be plotted in the form of Equation B39 to predict the behavior of horizontal round buoyant jets of small nozzle size over the whole parameter range, from momentum- to buoyancy-dominated. This is done in Figure B2, where the present experimental results (Figure A10, for $\ell_Q/\ell_\varepsilon < 0.2$) and the asymptotic solutions for a pure jet (Equation A41) and a pure plume (Equation B44) are also shown. Predictions from Fan and Brooks' model (Figure B1) and the plume solution

B10
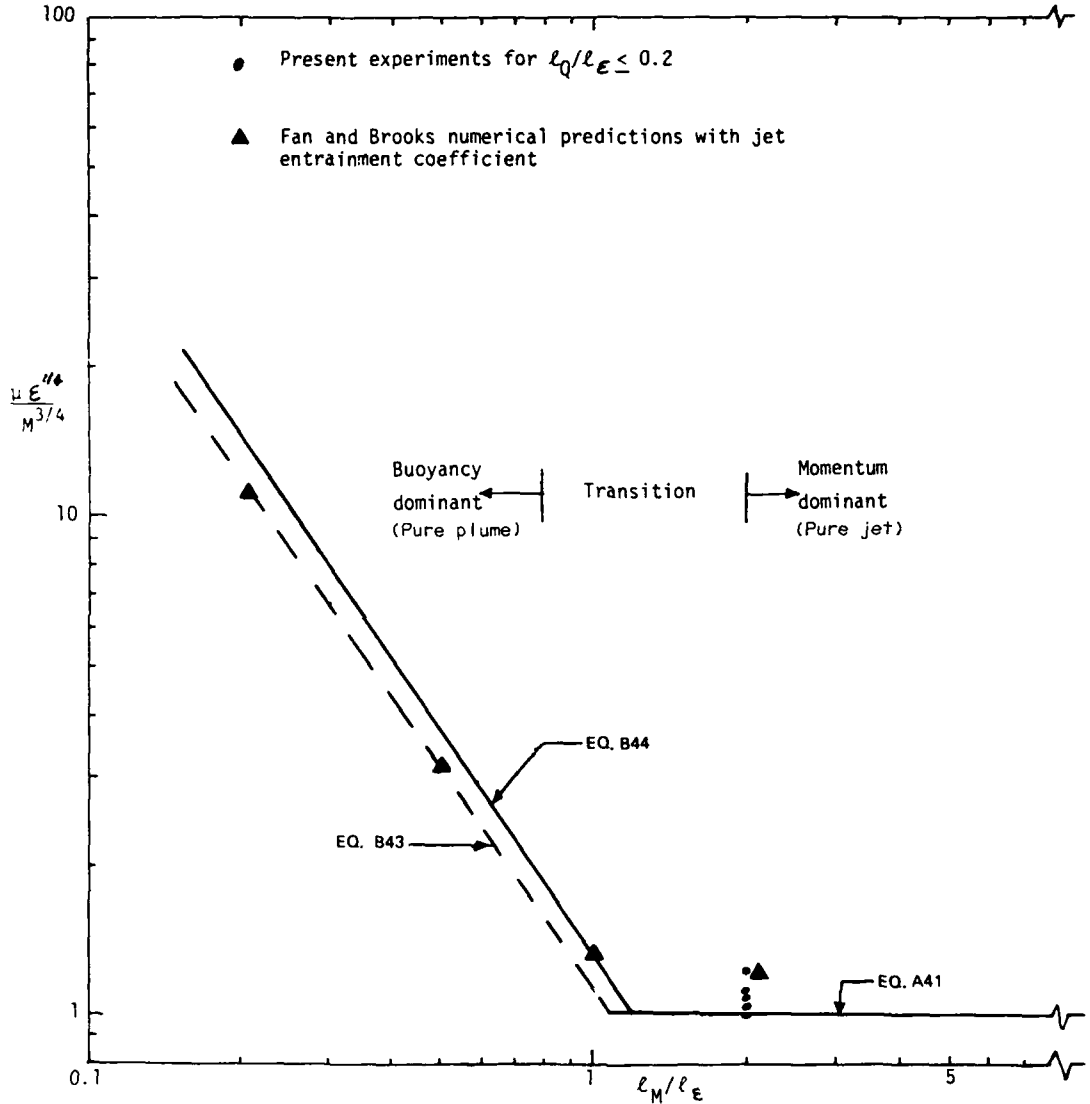
Figure B2. Terminal volume flux of horizontal round buoyant jets in linear stratification, for which $\ell_Q \ll \ell_M$ and $\ell_Q \ll \ell_\varepsilon$

B11

(Equation B43), both using the jet entrainment coefficient, are also shown. A better approach to the numerical modeling would be to use a variable entrainment coefficient dependent on local conditions, as recommended by List and Imberger (1973). This refinement would hardly affect the present discussion, however.

20. The predictions of Fan and Brooks appear to be consistent with the present results. The deviation at ℓ_M/ℓ_ε 2 is probably caused by the breakdown of the assumptions of the Fan and Brooks model for weakly buoyant jets. The results of Figure B2 suggest that, for ℓ_Q $\ll \ell_M$ and ℓ_ε, the flow is plumelike for $\ell_M/\ell_\varepsilon < {\sim}0.8$ and jetlike for $\ell_M/\ell_\varepsilon > {\sim}2$. In between, both momentum and buoyancy influence the flow. If the nozzle is large enough that ℓ_Q is not much smaller than ℓ_M or ℓ_ε, then Figure B1 should be used.

Concluding Remarks

21. Discussion of the present problem in terms of competing length scales is seen to be very convenient. In cases in which the source volume, buoyancy, and momentum are all important, all the length scales expressed by Equations A6, A7, and A8 should be considered. The effect of the nozzle geometry is confined to a distance of several nozzle diameters from the source, however, and is frequently of secondary importance compared to the other length scales.

22. The present experimental and theoretical results of Appendixes A and B show this clearly. If $\ell_Q \ll \ell_M$ and ℓ_ε, the length of the potential core of the jet is much less than the collapse length. The jet can then be analyzed as if generated by a point source of momentum only. Even for larger values of ℓ_Q/ℓ_ε, the results are not sensitive to ℓ_Q/ℓ_ε, with only the volume flux parameter μ showing much variation.

B12

Table B1

Comparison of Fan and Brooks' Predictions

with Experiment E12

	Jet Coefficients	Plume Coefficients	Experimental Results
m_o	3.68	3.68	--
μ_o	0.925	0.743	--
δ	9.90	7.90	--
ξ_t	0.6	0.6	--
η_t	2.9	3.0	--
μ_t	5.5	5.5	--
Z_t (cm)	3.8	3.0	2.0
X_m (cm)	14.3	11.1	14.3*
S_t	7.0	8.7	--
S_{at}	11.9	14.8	8.5
W_L	7.6	9.4	5.1

* Computed as $3\ell_\varepsilon$.

B13

APPENDIX C: INTEGRAL BUOYANT JET MODEL OF FAN AND BROOKS

1. The integral model used for strongly buoyant jets in subroutine SBJET is based on the model RBJ presented in Koh and Fan (1970). The material in this appendix is extracted from their report. Note that the notation is slightly different from that followed in the rest of this report. The model of Koh and Fan allows for the merging of individual round buoyant jets to a two-dimensional flow similar to that issuing from a slot jet. As SBJET may in the future be extended to apply to merging jets, the round and slot flow formulations are presented below.

2. Consider a jet oriented at angle θ_o to the horizontal issuing fluid of density ρ_1 and temperature T_1 into an ambient of density stratification $\rho_a(y)$ and temperature stratification $T_a(y)$. Let Q_1 be the discharge, M_1 the momentum flux, F_1 the density deficiency flux, and G_1 the temperature deficiency flux at the source. Figure C1 illustrates the general behavior of such a jet. The bending of the jet path is a result of the fact that the discharge is buoyant. Define u^* as the velocity, T^* as the temperature, and ρ^* as the density of the buoyant jet flow. Since the ambient is motionless, u^* is assumed to be along the jet path. Let s be the coordinate along the jet path, A-plane be the plane perpendicular to the jet path, and θ the angle of the jet path with respect to horizontal. We now define the volume flux Q , momentum flux M , density deficiency flux F , and temperature deficiency flux G along the jet trajectory as:

$$Q = \int_A u^* dA \tag{C1}$$

$$M = \frac{M'}{\rho_o} = \frac{1}{\rho_o} \int_A u^{*2} \rho^* dA \approx \int_A u^{*2} dA \tag{C2}$$

$$F = \int_A (\rho_a - \rho^*) u^* dA \tag{C3}$$

C1
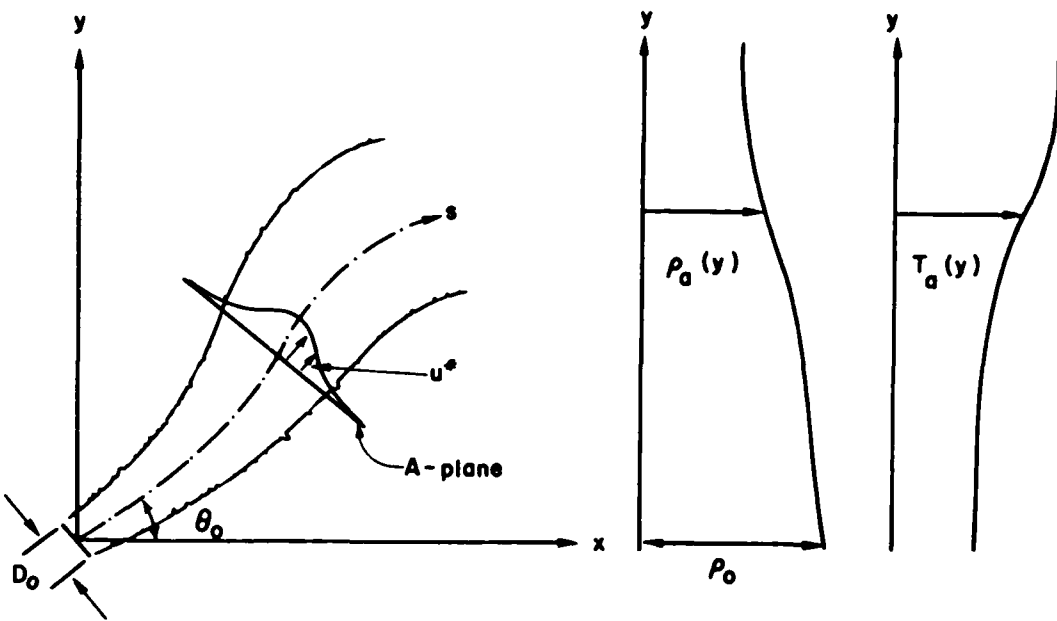
Figure C1. Definition diagram for integral model
of round buoyant jets

$$G = \int_A (T_a - T^*) \, u^* dA \qquad (C4)$$

Note that M' is the true momentum flux while M is the kinematic momentum flux.

3. We note that in the vertical direction, a buoyancy force exists due to the density difference between the jet fluid and the ambient fluid tending to bend the jet. This force f is

$$f = g \int_A (\rho_a - \rho^*) dA \qquad (C5)$$

4. The conservation equations can now be written in terms of these variables. The conservation of mass equation is

C2

$$\frac{dQ}{ds} = E \qquad (C6)$$

or

$$\Delta Q = E\Delta S$$

where E is the rate of entrainment of ambient fluid. Note that, strictly speaking, since the density is variable, we should really have, instead of Equation C6

$$\frac{d}{ds} \left[\int u^* \rho^* dA \right] = E\rho_a \qquad (C7)$$

However, all density differences are small, and we may approximate Equation C7 by C6. The variable ΔQ is equivalent to Q_{ep} (see Equation 11, main text).

    5. The conservation of horizontal momentum flux is

$$\frac{d(M \cos \theta)}{ds} = 0 \qquad (C8)$$

For the vertical momentum, we must include the buoyancy force. Thus,

$$\frac{d}{ds} (M' \sin \theta) = f \qquad (C9)$$

The conservation of density deficiency flux equation reads

$$\frac{d}{ds} \left[\int_A u^* (\rho_0 - \rho^*) dA \right] = E(\rho_0 - \rho_a) \qquad (C10)$$

where ρ_0 is a reference density (e.g., $\rho_0 = \rho_a (0)$). Equation C10 can be written

$$\frac{d}{ds} \left[\int_A u^* (\rho_0 - \rho_a) dA + \int_A u^* (\rho_a - \rho^*) dA \right] = E(\rho_0 - \rho_a)$$

C3

or

$$(\rho_o - \rho_a) \frac{dQ}{ds} + Q\left(-\frac{d\rho_a}{ds}\right) + \frac{dF}{ds} = E(\rho_o - \rho_a) \qquad (C11)$$

Using Equation C6 we finally have

$$\frac{dF}{ds} = \frac{d\rho_a}{ds} Q \qquad (C12)$$

Similarly, the conservation of temperature deficiency flux equation reads

$$\frac{d}{ds}\left[\int_A u^*(T_o - T^*)dA\right] = E(T_o - T_a) \qquad (C13)$$

which reduces, with Equation C6, to

$$\frac{dG}{ds} = \frac{dT_a}{ds} Q \qquad (C14)$$

6. Equations C6, C8, C9, C12, and C14 constitute five equations for the five unknowns Q, M, θ, F, G, as functions of s, once we can express E and f in terms of known quantities or these unknowns. To do this, we will make two more assumptions. First, we shall assume similarity of the shapes of the velocity profile, temperature deficiency profile, and density deficiency profile in the plane A. In particular, it will be assumed that the profiles are Gaussian. Thus, in the two-dimensional case (slot jet) we assume

$$u^*(s,\eta) = u(s)e^{-\eta^2/b^2(s)} \qquad (C15)$$

$$\rho_a - \rho^*(s,\eta) = \left[\rho_a - \rho(s)\right] e^{-\eta^2/\lambda_s^2 b^2} \qquad (C16)$$

C4

$$T_a - T^*(s,\eta) = \left[T_a - T(s) \right] e^{-\eta^2/\lambda_s^2 b^2} \qquad (C17)$$

where $u(s)$, $\rho(s)$, and $T(s)$ are the values along the jet center line. The term η is the coordinate normal to s , $b(s)$ is the characteristic jet width, and λ_s is a turbulent Schmidt number for the two-dimensional case (2-D). Similarly, in the axisymmetric case, we take

$$u^*(s,r) = u(s) e^{-r^2/b^2} \qquad (C18)$$

$$\rho_a - \rho^*(s,r) = \left[\rho_a - \rho(s) \right] e^{-r^2/\lambda_r^2 b^2} \qquad (C19)$$

$$T_a - T^*(s,r) = \left[T_a - T(s) \right] e^{-r^2/\lambda_r^2 b^2} \qquad (C20)$$

where r is the radius normal to the s coordinate.

7. Secondly, we shall assume that the entrainment function E is proportional to the jet characteristic velocity u and the jet boundary ($2\pi b$ or $2L$ for the axisymmetric and 2-D case, respectively) and that the proportionality constant is α (α_r for round jet and α_s for slot jet). Substituting these expressions into the definitions for Q , M , F , G , and f (Equations C1-C5) will give Q , M , F , G , and f expressed in terms of the quantities u , ρ , T , and b . For example, substituting Equation C15 into C1 gives

$$Q = L \int_{-\infty}^{\infty} u(s) e^{-\eta^2/b^2} d\eta$$

where L is the length of the 2-D slot jet. Thus,

$$Q = Lub \int_{-\infty}^{\infty} e^{-\xi^2} d\xi = \sqrt{\pi} ubL$$

C5

8. Similarly, substituting Equations C15 and C16 into Equation C3 gives

$$F = L \int_{-\infty}^{\infty} u e^{-\eta^2/\lambda_s^2 b^2 - \eta^2/b^2} (\rho_a - \rho) d\eta$$

$$= Lu(\rho_a - \rho) \int_{-\infty}^{\infty} e^{-(\eta^2/b^2)(1/\lambda_s^2 + 1)} d\eta$$

$$= Lu(\rho_a - \rho) b \sqrt{\frac{\lambda_s^2 \pi}{1 + \lambda_s^2}}$$

In this fashion, Table C1 may be constructed.

Table C1

Definition of Variables, Buoyant Jet Model

Variable	For Round Jet	For Slot Jet of Length L
Volume Flux Q	$\pi u b^2$	$\sqrt{\pi} u b L$
Momentum Flux $M = \dfrac{M'}{\rho_o}$	$\dfrac{\pi u^2 b^2}{2}$	$\sqrt{\dfrac{\pi}{2}} u^2 b L$
Density Deficiency Flux F	$\dfrac{\lambda_r^2}{1 + \lambda_r^2} \pi u b^2 (\rho_a - \rho)$	$\sqrt{\dfrac{\pi \lambda_s^2}{1 + \lambda_s^2}} u b (\rho_a - \rho) L$

(Continued)

C6

Table C1 (Concluded)

Variable	For Round Jet	For Slot Jet of Length L
Temperature Deficiency Flux G	$\dfrac{\lambda_r^2}{1 + \lambda_r^2}\, \pi ub^2(T_a - T)$	$\sqrt{\dfrac{\pi \lambda_s^2}{1 + \lambda_s^2}}\, ub(T_a - T)L$
Buoyancy Force f	$\pi \lambda_r^2 b^2 (\rho_a - \rho)g$	$\sqrt{\pi}\lambda_s bLg(\rho_a - \rho)$
Entrainment Function E	$2\pi \alpha_r ub$	$2\alpha_s uL$

9.   Table C1 gives the transformation from the variables u , b , etc., to the variables Q , M , etc.   (The inverse transformation is given in Table C2. Moreover, it is possible to express E and f now in terms of Q , M , etc., as shown in Table C3.)

10.   The problem of the mixing processes involved for a row of round buoyant jets spaced a distance L_p apart is now considered. Initially, the jets are separate round jets. However, after a while, they begin to merge and form more nearly a two-dimensional slot jet. Thus, in the calculations, it is necessary to provide a criterion whereby the round jet analysis is switched to that for a slot jet. Two such criteria are proposed. We assume that transition occurs when the width of the round jet becomes equal to the jet spacing. This shall be designated transition 1. Referring to Table C2, this occurs when

$$\frac{Q2\sqrt{2}}{\sqrt{2\pi M}} = L_p \quad \text{or} \quad \frac{Q}{\sqrt{M}} = L_p \frac{\sqrt{\pi}}{2} = 0.885 L_p \qquad (C21)$$

where the "jet width" is taken as $2\sqrt{2}b$.

C7

Table C2
Inverse Transformation of Variables, Buoyant Jet Model

Variable	Round Jet	Slot Jet
Center-line Velocity u	$\dfrac{2M}{Q}$	$\dfrac{\sqrt{2}\,M}{Q}$
Nominal Half-Width b	$\dfrac{Q}{\sqrt{2\pi M}}$	$\dfrac{Q^2}{\sqrt{2\pi}\,LM}$
Density Deficiency $\rho_a - \rho$	$\dfrac{1 + \lambda_r^2}{\lambda_r^2}\,F/Q$	$\sqrt{\dfrac{1 + \lambda_s^2}{\lambda_s^2}}\;F/Q$
Dilution Ratio S	$\dfrac{Q}{Q_1}$	$\dfrac{Q}{Q_1}$
Temperature Deficiency $T_a - T$	$\dfrac{1 + \lambda_r^2}{\lambda_r^2}\,G/Q$	$\sqrt{\dfrac{1 + \lambda_s^2}{\lambda_s^2}}\;G/Q$

Table C3
Expression of Terms E and f , Buoyant Jet Model

Variables	Round Jet	Slot Jet
E	$2\sqrt{2\pi}\,\alpha_r\,\sqrt{M}$	$\dfrac{2\sqrt{2}\,\alpha_s\,LM}{Q}$
f	$\dfrac{1 + \lambda_r^2}{2M}\,gQF$	$\dfrac{\sqrt{1 + \lambda_s^2}\;QgF}{\sqrt{2}\,M}$

11. It should be noted that the independent variable of integration is s , the distance along the jet path. However, the ambient conditions ρ_a and T_a are usually given only as functions of y . Thus, the following two equations are needed to allow conversion between s and x, y :

$$\frac{dx}{ds} = \cos \theta \qquad (C22)$$

$$\frac{dy}{ds} = \sin \theta \qquad (C23)$$

The system of Equations C6, C8, C9, C12, C14, C22, and C23 constitute seven ordinary differential equations for the seven unknowns, Q, M, θ, F, G, x, and y as a function of s. These equations may be solved given the initial values of the unknowns at $s = 0$.

12. The initial conditions are given by the source conditions, namely, u_o, the jet velocity; D_o, the jet diameter; T_1, the jet temperature; ρ_1, the jet density; and θ_o, the jet discharge angle. However, since the formulation is in terms of the flux quantities Q, M, F, and G, these jet characteristics must be converted to initial values in these variables. Moreover, it is well known that there exists a zone of flow establishment extending a few jet diameters during which the top-hat profiles of velocity, density deficiency, and temperature excess change gradually to Gaussian form (Figure C2). In this formulation, we shall start the integration from the beginning of the zone of established flow. Thus, it is necessary to relate the jet characteristics to the flux quantities at this point. Albertson et al. (1950), in their experimental investigations on the round jet, found that the zone of flow establishment extends a distance of 6.2 jet diameters. Equating the momentum flux at the beginning and end of the zone of flow establishment, assuming that the buoyancy force is negligible in such a short region, we get (see Table C1 for M and round jet)

$$\frac{\pi}{4} D_o^2 u_o^2 = \int_0^\infty u^{*2} 2\pi r dr = \frac{\pi b_o^2 u_o^2}{2}$$

where b_o is the jet half-width and u equals u_o at the end of the zone of flow establishment.

13. Thus, the initial value for Q is

$$Q_1 = \pi b_o^2 u_o = \frac{\pi}{2} D_o^2 u_o$$

C9
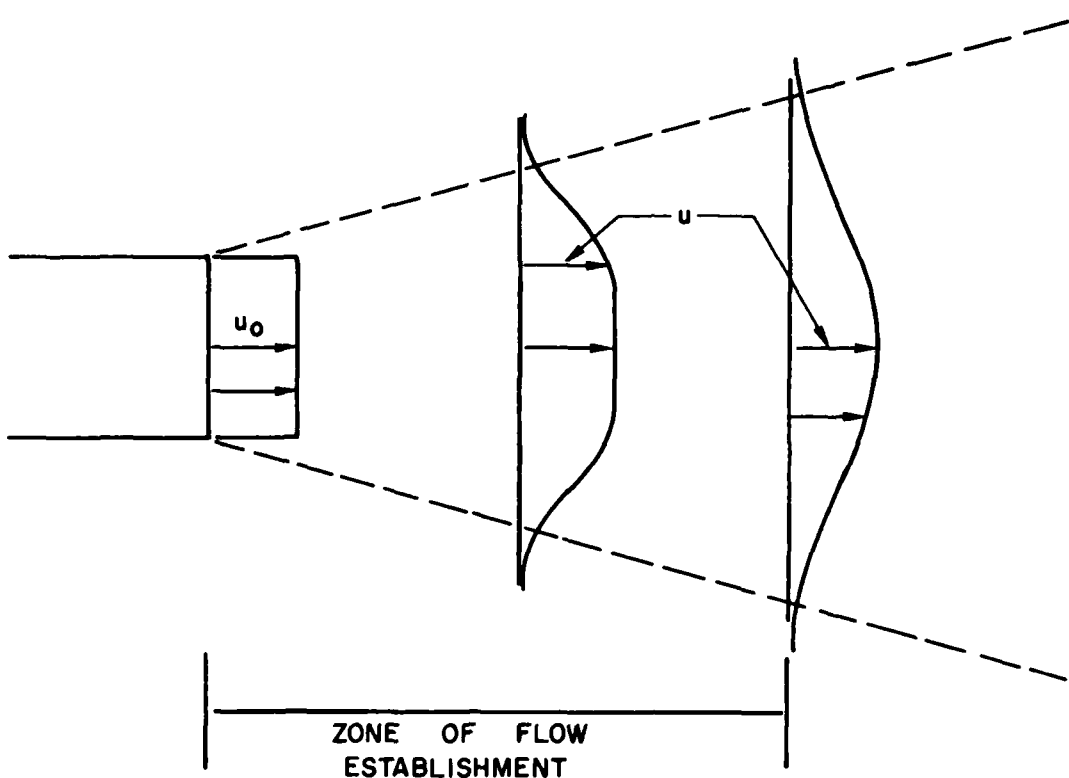
Figure C2. Zone of flow establishment in a submerged jet

In other words, the volume flux at the beginning of the zone of established flow is twice that at the source.

14. By assuming further that the ambient density is uniform in the zone of flow establishment, we may equate the density deficiency flux at the beginning and end of this zone to get

$$\frac{\pi}{4} D_o^2 u_o (\rho_a - \rho_1) = \int_0^\infty u^* (\rho_a - \rho^*) \, 2\pi r dr$$

$$= \frac{\lambda_r^2}{1 + \lambda_r^2} \pi b_o^2 u_o (\rho_a - \rho)$$

C10

Thus, the initial value for F is

$$F_1 = \frac{\pi}{4} D_o^2 u_o (\rho_a - \rho_1)$$

However, the center-line density deficiency is

$$\rho_a - \rho = \frac{1 + \lambda_r^2}{2\lambda_r^2} (\rho_a - \rho_1)$$

Similarly,

$$G_1 = \frac{\pi}{4} D_o^2 u_o (T_a - T_1)$$

and the center-line temperature excess is

$$T_a - T = \frac{1 + \lambda_r^2}{2\lambda_r^2} (T_a - T_1)$$

15. The equations presented above are solved numerically by the program RBJ (subroutine SBJET). The method of solution is to first obtain the initial conditions (Q_1, M_1, F_1, G_1) from the given source characteristics. Then the Equations C6, C8, C9, C12, C14, C22, and C23 are integrated with E and f as given by those for the round jet (column 2, Table C3). When transition is reached, given by Equation C21, one simply continues the solution but with E and f as given by those for the slot jet (column 3, Table C3). The results obtained are then converted from the variables Q, M, F, G, etc., to the physical variables u, ρ, T, and W, the jet width that is taken to be 2 2b. The conversion is effected by the relations in Table C2.

16. The input to the program consists of the following:

u_o = jet velocity

D_o = jet diameter

T_1 = jet temperature

C11

ρ_1 = jet density, gm/cm^3

θ_o = jet discharge angle with respect to horizontal, deg

d_j = jet discharge depth

L_p = jet spacing

α_r = entrainment coefficient for a round jet

α_s = entrainment coefficient for a slot jet

λ_r = spreading ratio for a round jet

λ_s = spreading ratio for a slot jet

g = gravitational acceleration

END

FILMED

3-86

DTIC